ABSTRACT

Title of Dissertation: PHYSICS BASED MODELING AND CONTROL OF REACTIVE EXTRUSION

Paul F. Elkouss, Doctor of Philosophy, 2004

Dissertation directed by: Professor David Bigio
Department of Mechanical Engineering

Kinematic modeling has been shown to be important for the understanding and control of co-rotating twin screw extruders. The residence time distribution (RTD) is often used to characterize the steady-state behavior of an extrusion process. Due to the complex rheological behavior of polymer flow in the extruder, few have felt that the RTD would be independent of changes in operating conditions for the same screw configuration. To investigate, we are asserting that resident distributions could be independent of operating conditions for certain types of polymers. Four different polymers, two polyethylenes and two polypropylenes, were processed on the same 30mm Werner and Pfleiderer co-rotating twin-screw extruder (CoTSE) equipped with reflectance optical probes to compare their RTD's. Additionally, each material was tested to determine its complex viscosity, to better understand the phenomena involved.

Using physically motivated models to control reactive extrusion processes is attractive because of the flexibility and robustness it could provide. This thesis uses residence distribution analyses to characterize the material flow through a co-rotating twin-screw extruder. Furthermore, we examine the applicability of residence distributions as the basis for kinematic modeling of the extrusion process. This demonstration of using a steady-state model - the residence distribution - as a basis for kinematic behavior is unique. The signals have been deconvoluted to kinematically characterize the flow in the different regions of the extruder, such as the melting, mixing and metering zones. Studies of step changes have shown that the steady state value of extrudate viscosity is dependent on the peroxide concentration, volume mixing, and on the residence time from the specific throughput. This data has also provided plant models of the peroxide initiated degradation reaction using system identification techniques. Although a specific example of vis-breaking of polypropylene is studied, the techniques are general. A proportional and integral controller (PI) with a Smith predictor was used to track set point changes and regulate the viscosity.

PHYSICS BASED MODELING AND CONTROL OF REACTIVE EXTRUSION

by

Paul F. Elkouss

Dissertation submitted to the Faculty of the Graduate School of the
University of Maryland, College Park in partial fulfillment
of the requirements for the degree of
Doctor of Philosophy
2004

Advisory Committee:

Professor David Bigio, Chairman/Advisor
Professor Robert M. Briber
Professor Hugh Bruck
Professor Dimitrios Hristu-Varsakelis
Professor Srinivasan R. Raghavan

DEDICATION

To my wife and family.

ACKNOWLEDGEMENTS

This would not have been possible without the support of many people. Many thanks to my wife, Mayah, and my family for their love and gentle prodding. The research would not have been possible without the generosity of Mark Wetzel in sharing his facilities and also for elucidating difficult concepts. I also thank my committee for giving their time and wisdom. I would especially like to thank David Bigio for his direction and insight in so many areas.

TABLE OF CONTENTS

List of Tables **ix**

List of Figures **xi**

1 Introduction **1**

2 Background **5**

2.1 Residence Distribution 5

2.2 Extruder Modeling 7

2.3 Vis-Breaking of Polypropylene 8

2.4 Controls Modeling 9

2.5 Warped Time Models 10

2.6 Closed Loop Control 12

2.7 Summary 14

3 Proposed Research **17**

3.1 Proposed Research 17

3.2 Investigative Work 20

4 Experimental **22**

4.1 Introduction 22

4.2 Experimental Facilities 23
4.3 Operating Conditions and Techniques 23

5 Residence Distribution Analysis 29
5.1 Introduction 29
5.2 Data Processing 29
5.3 Interpretation of Data 33
5.3.1 RTD Data 33
5.3.2 RVD Data 35
5.3.3 RRD Data 36
5.4 Summary 37

6 Steady State Analysis 38
6.1 Introduction 38
6.2 Data Processing 38
6.3 Initial Analysis 39
6.3.1 Exploratory Regressions 40
6.4 Best Subset Regression 40
6.5 Regression Analysis for Predictive Viscosity 42
6.5.1 Second Polypropylene 46
6.6 Conclusion 49

7 System Identification 50
7.1 Introduction 50
7.2 MatLAB System ID 51
7.2.1 MatLAB Code 51
7.2.2 Results 51

7.2.3 Analysis of Results and Summary 62
7.3 Conclusion 63

8 New Residence Distribution Model 64
8.1 Derivation 64
8.2 RTD Deconvolution Technique 66
8.2.1 Coupled Regions 66
8.3 RTD Characterization Results 67
8.4 Conclusion 75

9 Residence Distribution and Rheology 76
9.1 Introduction 76
9.2 Experiment Setup 77
9.3 Results 79
9.4 Dimensionless Numbers 98
9.5 Conclusions 109

10 Warp Time Analysis 111
10.1 Introduction 111
10.2 Derivation 112
10.2.1 General Equation Derivation 112
10.2.2 Transformation of Independent Variables 113
10.2.3 Constant Stretching 113
10.2.4 Exponential Stretching 115
10.2.5 Logarithmic Stretching 116
10.3 Kinetic Model of Reaction 117
10.4 Proposed Simulation Technique 119

11 Closed Loop Regulation of Polypropylene **121**

11.1 Introduction 121

11.2 experimental setup 122

11.3 Control Results 123

11.3.1 Open Loop Experiments 123

11.4 Gain Functions 126

11.5 Closed Loop Experiments 127

11.5.1 Improvement of Controller 152

11.6 Conclusion 157

12 Conclusions **158**

13 Future Work **161**

A Residence Distribution Figures **163**

A.1 Residence Time Distribution 163

A.2 Residence Volume Distribution 170

A.3 Residence Rotation Distribution 176

B Steady State Analysis **182**

B.1 Subset Regressions 182

B.2 Regression Analysis 184

C System Identification **186**

D Signal Deconvolution **191**

D.1 Curve Functions 191

D.2 Deconvolution 195

E LabVIEW Virtual Instrument **198**

F Warp Time Simulation Code **203**

F.1 Main Code 203

F.2 Supporting Code 205

BIBLIOGRAPHY **216**

INDEX **220**

LIST OF TABLES

4.1 Operating Conditions of RxD Analysis KF6100 25

4.2 Operating Conditions of Viscosity Tests KF6100 26

4.3 Operating Conditions of RxD Analysis PDC1277 27

4.4 Operating Conditions of Viscosity Tests PDC1277 28

5.1 Mean Residence Times 34

5.2 Parameters for mean residence time. 34

5.3 Experimental Screw Constants 36

6.1 Best Subset Regression 41

6.2 Regression Analysis Coefficient Significance 42

6.3 Analysis of Variance 43

6.4 Regression Analysis Coefficient Significance for PDC1277 46

6.5 Analysis of Variance for PDC1277 46

7.1 System Identification Results for $Q = 30pph$ and $N = 210rpm$. . . 52

7.2 System Identification Results for $Q = 30pph$ and $N = 160rpm$. . . 54

7.3 System Identification Results for $Q = 30pph$ and $N = 320rpm$. . . 56

7.4 System Identification Results for $Q = 40pph$ and $N = 210rpm$. . . 58

7.5 System Identification Results for $Q = 20pph$ and $N = 210rpm$. . . 60

7.6 Some System Identification Results 62

8.1 Time delays and first order time shape factors. 69
8.2 Volume delays and first order volume shape factors. 70
8.3 Revolution delays and first order revolution shape factors. 71
8.4 Means of different shape factors. 74

9.1 KF6100 fits to Equation 2.9. 92
9.2 PDC1277 fits to Equation 2.9. 93
9.3 HDPE6018 fits to Equation 2.9. 94
9.4 HDPE6060 fits to Equation 2.9. 95
9.5 Mean volume shape factors. 95
9.6 Dominant relaxation times. 103
9.7 Deborah and Weissenberg numbers for the different polymers. . . 105

11.1 Melt flow indices of different polypropylenes. 122
11.2 Open loop peak and rise times and gain and phase margins. . . . 143
11.3 Closed loop peak and rise times and gain and phase margins. . . . 144
11.4 Closed loop conditions with gross disturbances. 149

B.1 Preliminary Best Subset Regression 182
B.2 Preliminary Best Subset Regression 183
B.3 Preliminary Best Subset Regression 183
B.4 Preliminary Best Subset Regression 184
B.5 Preliminary Regression Analysis Coefficient Significance 185
B.6 Preliminary Analysis of Variance 185

LIST OF FIGURES

2.1 Nominal and closed loop frequency response. 11

3.1 Diagram of Research Plan 18

4.1 Experimental screw design. 23

5.1 *RTD* data with Equation 5.1 31

6.1 Normal probability plot of the residuals for KF6100. 44

6.2 Residuals versus the fitted values for KF6100. 45

6.3 Normal probability plot of the residuals for PDC1277. 47

6.4 Residuals versus the fitted values for PDC1277. 48

7.1 Bode plot for $Q = 30pph$ and $N = 210rpm$. 53

7.2 Bode plot for $Q = 30pph$ and $N = 160rpm$. 55

7.3 Bode plot for $Q = 30pph$ and $N = 320rpm$. 57

7.4 Bode plot for $Q = 40pph$ and $N = 210rpm$. 59

7.5 Bode plot for $Q = 20pph$ and $N = 210rpm$. 61

8.1 Model fits with Equation 8.2. 68

8.2 Comparison of RTD data and model fits. 72

9.1 RTD's for KF6100 80

9.2 RTD's for PDC1277 81
9.3 RTD's for HDPE6018 82
9.4 RTD's for HDPE6060 83
9.5 RVD's for KF6100 84
9.6 RVD's for PDC1277 85
9.7 RVD's for HDPE6018 86
9.8 RVD's for HDPE6060 87
9.9 RRD's for KF6100 88
9.10 RRD's for PDC1277 89
9.11 RRD's for HDPE6018 90
9.12 RRD's for HDPE6060 91
9.13 c vs. N for KF6100 96
9.14 Mean number of rotations versus inverse of specific throughput. . 97
9.15 Storage and loss moduli for polyethylene samples. 98
9.16 Storage and loss moduli for polypropylene samples. 99
9.17 The Loss moduli plotted against the Storage moduli. 100
9.18 Viscosities of polypropylenes and polyethylenes. 101
9.19 Comparison of viscosity curves. 102
9.20 Volume domain shape factors vs. N_{We}. 106
9.21 N_{De} vs. Q 107
9.22 N_{We} vs. N 108

11.1 Open loop peroxide step change at $2.98mL/s$ and $2.33rps$. 124
11.2 Bode plot for figure 11.1. 125
11.3 Comparison of equations 11.3 and 11.4. 128
11.4 Closed loop tracking, $K_c = 0.11$ and $K_i = 0.18min$. 130

11.5 Bode plot for figure 11.4. 131
11.6 Closed loop tracking, $K_c = 0.1$ and $K_i = 0.18min$. 132
11.7 Bode plot for figure 11.6. 133
11.8 Closed loop tracking, $K_c = 0.1$ and $K_i = 0.18min$. 134
11.9 Bode plot for figure 11.8. 135
11.10Closed loop tracking, $K_c = 0.1$ and $K_i = 0.18min$. 136
11.11Bode plot for figure 11.10. 137
11.12Closed loop tracking, $K_c = 0.1$ and $K_i = 0.18min$. 138
11.13Bode plot for figure 11.12. 139
11.14Closed loop tracking, $K_c = 0.1$ and $K_i = 0.18min$. 140
11.15Bode plot for figure 11.14. 141
11.16Closed loop regulation, $K_c = 0.1$ and $K_i = 0.18min$. 146
11.17Bode plot for figure 11.16. 147
11.18Closed loop regulation, $K_c = 0.1$ and $K_i = 0.18min$. 148
11.19Bode plot for figure 11.18. 149
11.20Closed loop tracking, $K_c = 0.1$ and $K_i = 0.18min$. 150
11.21Bode plot for figure 11.20. 151
11.22Normalized open loop step response. 153
11.23Proportional controller step response. 154
11.24Proportional Integral controller step response. 155
11.25Proportional Integral Derivative controller step response. 156

A.1 RTD Probe 1. 164
A.2 RTD Probe 2. 165
A.3 RTD Probe 3. 166
A.4 RTD mixing zone. 167

A.5 RTD metering zone. 168
A.6 RTD mixing and metering zones. 169
A.7 RVD Probe 1. 170
A.8 RVD Probe 2. 171
A.9 RVD Probe 3. 172
A.10 RVD mixing zone. 173
A.11 RVD metering zone. 174
A.12 RVD mixing and metering zones. 175
A.13 RRD Probe 1. 176
A.14 RRD Probe 2. 177
A.15 RRD Probe 3. 178
A.16 RRD mixing zone. 179
A.17 RRD metering zone. 180
A.18 RRD mixing and metering zones. 181

E.1 LabVIEW front panel. 198
E.2 LabVIEW back panel. 199
E.3 LabVIEW back panel. 199
E.4 LabVIEW back panel subpanel. 199
E.5 LabVIEW back panel subpanels. 200
E.6 LabVIEW back panel subpanels. 201
E.7 LabVIEW back panel subpanels. 201
E.8 LabVIEW back panel. 202

Chapter 1

Introduction

Manufacturing of polymers is moving from creating a new material for each use to blending different polymers to create an alloy with the desired material properties [1]. Extruders are the continuous processing device that provide the multiple steps of melting, pumping, mixing and forming that allows for the formation of the desired blends.

Most industrial blending processes use an open loop control model and experience to design the process. The extruder screw is typically designed using rules of thumb. Periodic testing is used to determine the quality of the extrudate. This type of quality control can lead to waste from infrequent testing, as well as poor uniformity. These operations do not account for disturbances in the feed rate, screw speed, and the fed materials. Most importantly, there is a lack of physical insight to be derived from these procedures.

To have more assurance of producing the desired material, closed loop control techniques, where the quality of the output influences the parameters affecting the process, are necessary to achieve this. Process modeling, simulation, and sensing are all important to creating a successful closed loop control scheme. The process variables that can be controlled in an extrusion process are feed

material selection, feed material throughput (Q), screw design, screw speed (N), and barrel temperature. Sensors can be used to measure properties of the process such as the die pressure. Studies have dealt with control of extrusion processes using these parameters [1–5].

Polymers such as polypropylene are typically made in large quantity for sale to plastics compounders. Although they are sold in many different grades to satisfy many different market niches, a compounder can be limited by availability when selecting their feed stock. The macroscopic properties of materials are a function of their chemical make-up. For polymers, attributes such as molecular weight distribution, and monomer structure can have great effect. After the polymer is made, it would be difficult to change its constituent polymers, but there exist processes that can change the molecular weight by modifying the polymer chain [6]. Polymers such as polypropylene can be modified to have different molecular weights by using peroxide to cut the polymer chain. With such processes, the polymer reactant is modified. The polymers are produced in a distribution of molecular weights, and not all molecules are affected equally. The different molecular weight distribution imply different material properties such as viscosity [7]. This process can be used to create different materials from a single type of feed, or to regulate the properties of the extrudate by the addition of peroxide to regulate the extrudate's molecular weight.

Models have been proposed to describe the peroxide initiated degradation of polypropylene [6, 7]. Control schemes have also been proposed to regulate to quality of extrudate [2, 3]. These schemes have been mainly empirical. Although the control schemes have the goal of regulating polymer molecular weight, the molecular weight is not easily measurable, as it must be done off-line. The melt

viscosity is a function of the molecular weight distributions and it is much more facile to measure, and on-line analysis can be performed [1, 4, 5], allowing closed loop control to be applied to the process.

Due to the importance of reactive extrusion, a physics based model of the reactive extrusion system was created, and implemented. To better understand the kinematics of the extruder it was necessary to characterize the process dynamics by acquiring residence time distributions and viscosity step changes. The residence time distributions were recorded as impulse responses to tracer feeds, and were used to kinematically characterize the steady-state process within the extruder. These responses were characterized using models that were functions of the screw geometry. Due to the nature of the melt flow within the extruder, the screw was modeled as a series of stirred tank reactors with transport delays. Three such stirred tank reactors represent the screw used, matching the three zones of melting, mixing, and pumping. Chapter 5 shows a model where the three zones are modeled with three repeated roots, while Chapter 8 shows a model with unique roots for each of the zones.

Viscosity step changes were determined (Chapter 6) and used to determine the relationship between the peroxide additive used for the reaction, and the melt viscosity. This step response data was also used to determine the kinematic contribution of the viscometer to the process (Chapter 8). The viscometer possessed a relatively large measurement delay which makes simple classical control schemes impractical to implement. This delay necessitates the use of a Smith predictor or another similar predictive controller.

Chapter 3 discusses the goal of the research. After a process has been characterized, it becomes possible to design a controller to regulate the process. With

this knowledge, a proportional and integral (PI) controller with a Smith predictor was used to track set point changes in melt viscosity (Chapter 11). It was also used to regulate the melt viscosity and was successful in maintaining product quality in spite of some large perturbations to the system.

During the experimentation to control the reactive extrusion process, residence time distributions were recorded for different materials. The data have shown that, for the same extruder at the same conditions, two different materials could give behave very similarly, kinematically (Figures 9.3 and 9.4). In order to investigate this (Chapter 9), data from experiments to characterize the Residence Time Distributions from various experiments on the same machine, but with different materials: two different viscosities of polypropylene, and two different viscosities of polyethylene were used. The complex viscosities of the materials were studied to help explain the results of the residence distribution studies. The Weissenberg number proved to predict the similarities and differences of the distributions as the operating conditions varied.

Chapter 2

Background

2.1 Residence Distribution

The distribution of how much material passes a given point as a function of time is called the residence time distribution (RTD) [8]. This distribution shows how long material is inside a given volume of a process. Experimentally it is found by measuring the quantity of tracer passing by a region of the process [9]. Modeling of these distributions has been pursued because characterizing processes can be costly.

Puaux et al. [10] compare various different models to fit collected RTD data. The best fitting of the RTD curves was obtained with the axial dispersion and the back flow cell models. The general from of the RTD density function is:

$$E(t) = U\left(t - t_D\right) E_M\left(t - t_D\right) \tag{2.1}$$

The models for E_M are based on stirred tank reactors and model recirculation. The mixing zone RTD density when using the axial dispersion model with open boundary conditions is:

$$E_M(\tau) = \frac{1}{2}\sqrt{\frac{Pe}{\pi\tau}}\left[-\frac{(1-\tau)^2}{4\tau}Pe\right] \tag{2.2}$$

The back flow cell model is:

$$\begin{aligned} E_M(\tau) &= \sum_{i=1}^{N} \exp\left(s_i \tau\right) \\ A_i &= -2N\gamma^{-N/2} \frac{\sin^2 \theta_i}{D'\left(\theta_i\right)} \end{aligned} \tag{2.3}$$

The authors conclude that the most reasonable model is the back flow cell model because it fits better, and has analytical expressions for the RTD density function $E_m(t)$. The models presented, though, are not presented in a form easily relatable to classical control models.

Others have developed models that provide insight with little computational cost. Continuing work by Gasner et al. [11], Gao et al. [12] present a model for the mean residence time, t_m. Their model (Equation 2.4) predicts within 10% when the percent drag flow is not large.

$$t_m = \frac{A}{Q} + \frac{B}{N} \tag{2.4}$$

Q is the throughput. N is the screw speed. A and B are calculable from parameters of the geometry, and respectively have to do with the filled and partially filled regions of the extruder. Elkouss et al. [13], Gao et al. [14] have used this model to show that different geometries lead to different A and B constants, and the agreement with experimental data was good.

Gao et al. [15] present Equation 2.5, a predictive RTD model. a is the shape factor, and t_d the delay time.

$$f(t) = \frac{a^3}{2}(t - t_d)^2 e^{-a(t-t_d)} \tag{2.5}$$

The shape of the RTD is dominated by throughput. Constant N and increasing Q moves the RTD to shorter times and make it sharper. constant Q and

increasing N move the RTD to shorter times, but without changing the shape much. Where the RTD is in the domain of time, the residence volume distribution (RVD) and the residence rotation distribution (RRD) are respectively in the domain of volume and rotations (the article also has analogous models for the RVD and RRD). The RVD and RRD are made using the transforms Equations 2.6 and 2.7. c and b are the volume and revolution shape factors and v_d and n_d are the volume and revolution delays. The authors also show that two conditions with the same Q/N and same material viscosity, should have the same RVD and RRD curves, although "this result needs to be interpreted against the fact that the rheology changes with screw speed." Different operating conditions on the same screw geometry have the same RVD after subtraction of the volume delay. This shows that the axial distribution of tracer is not dependent on the operating conditions for a screw geometry. This leads to the conclusion that changing the axial distribution of tracer depends on changing the screw geometry. Larger Q/N leads to a larger delay volume (Q_d), and smaller screw-revolution delay (N_d).

$$\begin{aligned} c &= {}^{a}/_{Q} \\ v_d &= t_d Q \end{aligned} \tag{2.6}$$

$$\begin{aligned} b &= {}^{a}/_{N} \\ n_d &= t_d N \end{aligned} \tag{2.7}$$

2.2 Extruder Modeling

Elkouss et al. [13], Gao et al. [14] predict t_m with an estimate for the filled length within the extruder. Elkouss [16] presents an equilibrium model, Equation 2.8, for the fill length in a starve-fed co-rotating twin screw extruder. This simple

model, which is derived for Newtonian fluids, shows that the filled lengths within the extruder are functions of screw geometry through geometric terms K_N and K_P, the drag and pressure flow constants. This model can be used to better predict A and B of Equation 2.4.

$$FL_F = \frac{\sin(\theta_F)K_{P_F}}{\sin(\theta_R)K_{P_R}}\left[\frac{K_{N_R} + Q/N}{K_{N_F} - Q/N}\right]FL_R \tag{2.8}$$

In addition, the difference present in the denominator causes the model to indicate that as the specific throughput, Q/N, approaches the one hundred percent drag flow value, K_{N_F}, the denominator will approach zero, and the FL_F infinity. A physical interpretation is that the forward feed zone can be filled all the way back to the end of the previous zone. In that case, the assumptions of the model are no longer valid. An interesting observation for this simple model is that viscosity is not a factor, it cancels out. Another model is also presented that accounts for leakage flows. Both models provide calculations for the filled length which is useful for Equation 2.4.

2.3 Vis-Breaking of Polypropylene

Tzoganakis et al. [6] propose a kinetic model for the peroxide promoted degradation of polypropylene. The model is based on using the evolution of molecular weight moments to simulate the reaction for the whole molecular weight distribution. A comprehensive model is given as well as a simplified model.

Strutt et al. [17] use a finite element method to investigate the effect of N, peroxide concentration, Q/N and channel geometry on the "mixing characteristics of steady non-isothermal reactive flows." The specific throughput, Q/N, and channel geometry were both found to have significant influence on the mixing.

Using the model of polypropylene degradation from Tzoganakis et al., Berzin et al. [18] build a model to predict the evolution of the average molecular weight along the length of the screw for a polypropylene degradation reaction. They study the effects of operating parameters such as the feed peroxide concentration, Q, and N upon the reaction. Their model has good agreement with size exclusion chromatography (SEC) measurements.

Pabedinskas et al. [7] use SEC to determine the MWD's of three different polypropylene's degraded for various initiator concentrations. A kinetic model [6] and a new kinetic-melting model are compared to the MWD results. The latter model provides significantly improved results because it also models the melting mechanism within the extruder. The model is related to an easily measurable quantity with a new relation of viscosity to molecular weight distribution that is useful for the viscosity at non-zero shears. With the kinetic-melting model and the viscosity to molecular weight distribution relation, the gain of the process can be expressed as a function of the initiator concentration. This is useful for predicting experimentally the DC gain of a plant model for the process.

2.4 Controls Modeling

Walsh et al. [1] present a simple physically motivated model based on plant operating conditions, a characterization of the sensors employed, and the results of the experiments showing the disturbance rejection are shown. Equation 2.9 is the third order model identified by RTD tests.

$$G(s) = \frac{a^3 e^{-t_d a}}{(s+a)^3} \tag{2.9}$$

The parameters for this equation are the same as for Equation 2.5. This model uses a third order form as opposed to the first order forms typically employed in other controls articles. The authors use a third order model with delay because it is applicable for three uncoupled stirred tank reactors in series with delays in between them. The authors studied an extruder whose screw geometry created three zones of partially and fully filled channels. This bulk flow behavior is responsible for the analogy to the stirred tank reactors.

There is significant structured uncertainty, so adaptive control is applied. There are three regions of disturbances (Figure 2.1). They are grouped by their volume scales or frequencies. The highest frequencies, of volume scale much smaller than the plant's filled volume are attenuated by the extrusion process. For the $30mm$ extruder, these are typically greater then $1hz$ and due to screw rotation as well as periodic error in the raw feed rate. The intermediate range has a volume scale on the order of the size of the filled volume of the machine. It is caused by "pressure surges due to periodic breaking up of the solid bed in the melting process" and feeder errors due to refills. The range is from 1 to 15 cycles per minute. The lowest frequency range are primarily caused by variations in the raw material properties. These are not attenuated by the extruder and are the main cause of poor quality product.

2.5 Warped Time Models

Although, not specifically for extruders, the lamellar model, Ottino [19, chap. 9], is a one dimensional model of material transfer useful for studying laminar mixing and reaction. The motion within a process can be modeled with parameters to describe fluid stretching within a process. This model can be transformed for

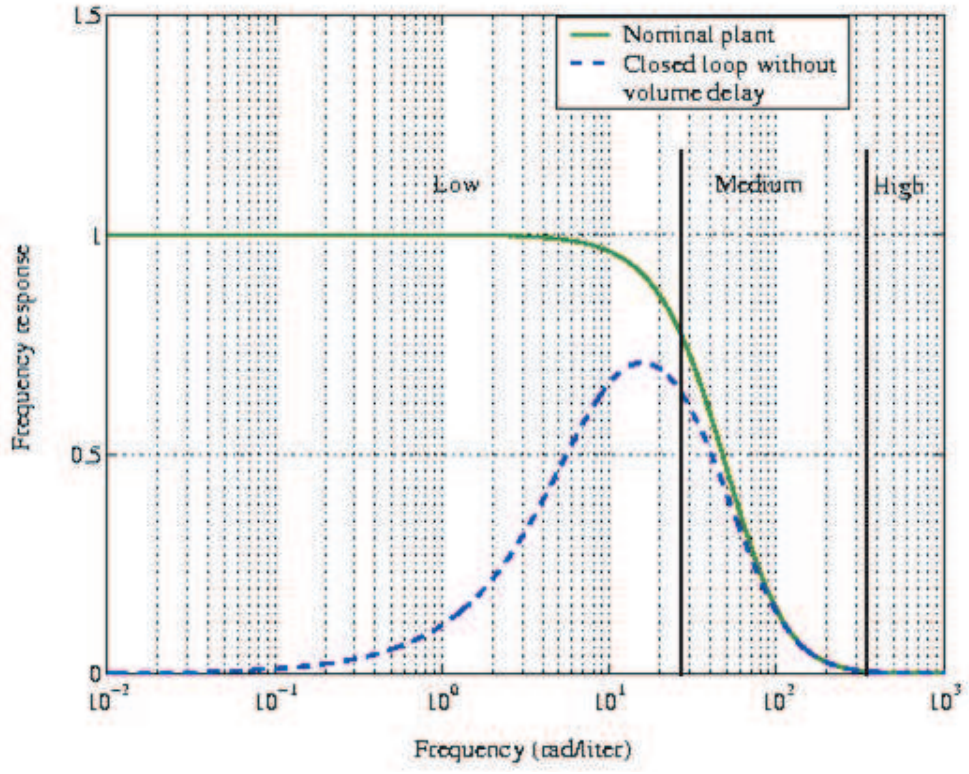

Figure 2.1: Frequency response of nominal and closed loop plants [1].

the time to allow for accounting of the reaction and the fluid motion, while simplifying the system to a tractable diffusion problem by changing variables and warping time. This is used with the kinetic reaction model by Tzoganakis et al. in Chapter 10.

2.6 Closed Loop Control

Most models have been statistically created from empirical data. The models relate an operating condition to a material property that can be sensed. Among other things, sensors have measured changes in pressure drop, and viscosity using inline rotating drum and inline wedge rheometer. Apart from classical control techniques using *PID* controllers, other controllers have been tried. Some of these are gain schedule, smith predictor, and minimum variance (MV) controllers. Adaptive control has also been used Gao [20]. Most closed loop control schemes have the model developed from empirical data. Walsh et al. started to connect physical phenomena to the plant model for control purposes, correlating residence distribution to the plant model.

Costin et al. [2] use a transfer function model for the extruder. They concentrate on the regulation of the extruder pressure with regards to surging. Step tests and such were performed to characterize the system. *PI* and self-tuning regulator (STR) controllers were used. They found a first order model relating pressure to screw speed and also had a noise model for both the pressure surging and flight noise. The best controller was a digital *PI* with a 2 pole/2 zero band-pass filter. Also, the STR has poor results when used with filters that have dynamics on the order of the sampling frequency. The STR identifies the dynamics of the filter, and inverts them in the controller, thereby removing the benefit

of the filter.

Pabedinskas et al. [3] use die pressure drop is the measured variable, with peroxide as the controlling input. Die pressure drop decreased with increasing peroxide concentration. The effects of the peroxide initiator are the following:

- The weight average molecular weight (M_w) decreases with increasing initiator concentration.
- The molecular weight distribution (MWD) becomes narrower and shifts toward lower molecular weights as the peroxide concentration increases.

The modeling experiments indicate that a first order plus dead time model is sufficient. The process gain is negative and nonlinear, and the process time constant was smaller for increases in initiator than decreases. A standard PI controller performs sluggishly. Adding gain scheduling yields a faster response to the higher allowable gains. PI and Smith predictor and gain scheduling increased the response speed in an amount equal to the delay time.

Pabedinskas and Cluett [4] use an inline wedge rheometer with an empirical model. Minimum variance (MV), constrained minimum variance (CMV), and pole placement (PP) controllers were evaluated and compared in simulation. A simulation technique with input and noise signals is discussed. The PP controller is used for the implementation (note, the sampling interval is $10s$). This controller is preferable due to acceptable control signal variation and he controller being more robust to dead time variation. It also did not have the large initial control signals of MV and CMV nor the CMV's oscillatory behavior. The selected pole location determined the speed and amplitude of the response. "variations in the process gain due to changes in the operating region (desired output

viscosity) or the feed material had a large effect on the performance of the controller." The performance of the control deteriorated as the model and process gains diverged, although, Pabedinskas et al. [7] provide a model for the gain.

Broadhead et al. [5] present control of ethylene methacrylic acid ionomer neutralization using an in-line melt rheometer (*ILR*). The *ILR* allows for minimization of the time delay with independent control of the shear rate. In spite of this minimum time delay, there was still appreciable time delay. *PI* and *MV* controllers were used with generally good results, but the non-linearity of the process indicated that adaptive control techniques could improve controller performance.

2.7 Summary

Although, a great amount of research has been performed to characterize and control extruders, there exists a great possibility for more research. Extruders have been studied kinematically using RTD's, and the extruder RTD's have been modeled with simple [11, 12, 15] and relatively complex methods [10]. Other models describe the bulk flow within the extruder [16].

Reactive extrusion has been of interest, and to better understand it, different models have been made to explain the mechanisms involved. The reaction kinetics have been modeled for peroxide initiated degradation of polypropylene [6], and *FEM* has been used to investigate the mixing characteristics of steady non-isothermal reactive flows [17]. The kinetic model has also been used to model polypropylene degradation along the extruder [18]. Kinetics models have also been combined with a model for the melting behavior of the extruder to provide more accurate predictions of extrudate molecular weight [7]. Walsh et al. [1] present a simple, physically motivated, plant model for the reactive extru-

sion process based on plant operating conditions that is applicable to automatic control schemes.

In general, most control of reactive extrusion processes starts with characterization of the plant. Statistical system identification methods have been used to relate the input and output using a fitted models of arbitrary order and delay [2–5], even though physically motivated models have been published [1]. Different sensors have been used to determine the extrudate quality for these control systems, and different control techniques have been applied [2–5, 20]; one of the most important issues has been sensor delay and how this affects the stability of the control scheme.

Modeling of the reactive extrusion process has relied on computationally intensive models to predict the output of an extrusion process. It is not known yet if the simple lamellar model can reflect what happens within the extruder.

Although Walsh et al. [1], Gao [20] begin to develop a physically motivated model suitable for control purposes, the model has not yet been related to all the necessary parameters. For example, Equation 2.9, is of the third order and was used to describe the whole screw within the extruder. A model of the extruder as a single entity improperly accounts for the feed of the initiator additive being in the middle of the screw and not at the beginning. Additionally the control scheme used a gain function that was a function initiator concentration, without the effect of other operating conditions.

This work (Chapter 8)shows how such a model would change if the peroxide does not see three distinct zones within the extruder. This work also accounts for the individual contribution of the viscometer to the dynamics. A superior non-linear gain function is also described (Chapter 6) that adds the influence

of operating conditions and the associated volume mixing effects. Although an adaptive controller is not used, the new model is shown to be suitable for a broader range of set point changes and disturbance rejection (Chapter 11).

Chapter 3

Proposed Research

In the realm of reactive extrusion, modeling is central to understanding and controlling the process. To better understand the kinematics of the extruder it is necessary to characterize the process by acquiring residence distributions from the extruder. The time response of the peroxide reaction was studied with step changes in peroxide feed percentage to the extruder. This information was used as input to creating the control algorithms to control the reactive extrusion process.

3.1 Proposed Research

As shown in Figure 3.1, the following are the major steps of this research:

- Perform experiments to acquire the residence time distribution (RxD).
- Perform experiments to record the dynamics of the peroxide induced degradation of polypropylene (Degradation).
- Characterize the kinematics of the extruder (Dynamic Response).
- Apply system identification techniques to the data.

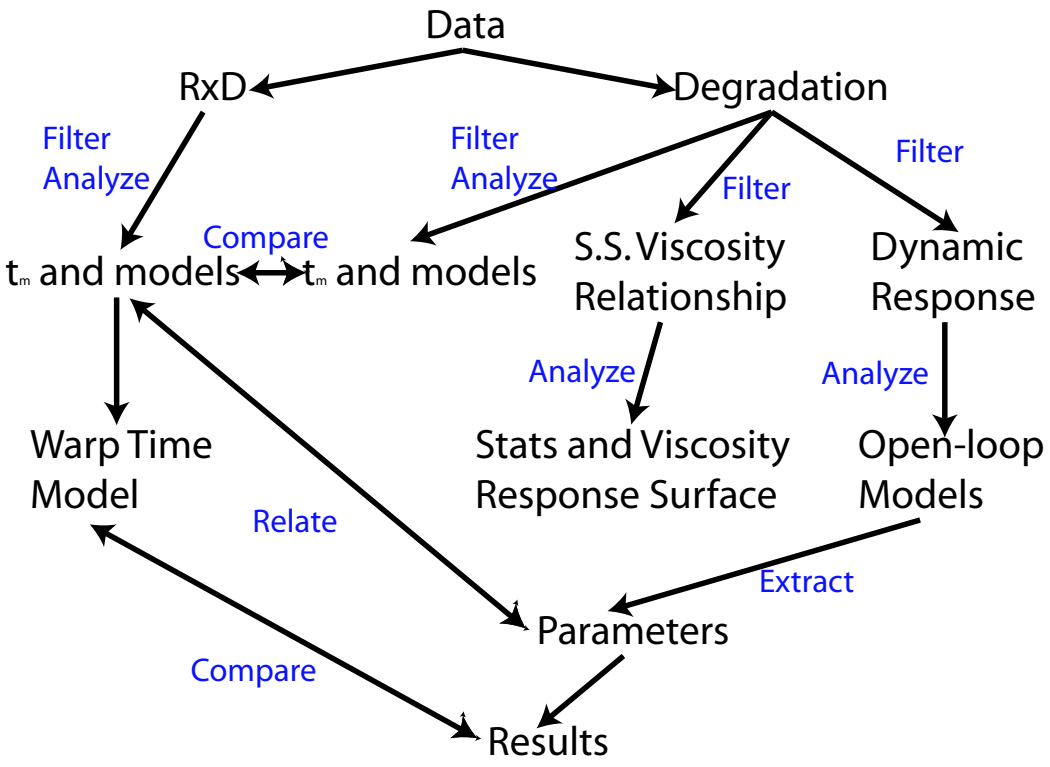

Figure 3.1: Diagram of Research Plan

- Relate the residence distribution to the plant model.
- Simulate the plant model
- Create a closed loop control scheme

The residence time distribution will be used to find the mean residence times for a multitude of operating conditions. It will also be used to find the parameters for the third-order residence distribution model - Equation 2.5. These parameters provide the delay time and the shape factor, a. The response curves for the three reflectance probes, which are placed at the end of the melting, mixing and die sections will be used to provide deconvolved signals representing the mixing and metering zones. Thus, each zone will have its own residence time distribution.

The experiments for the peroxide induced degradation of polypropylene will provide various pieces of information. Step changes in input peroxide levels and polymer viscosity have a transient response of extrudate viscosity as well as the steady state value of viscosity after the plant has stabilized. The steady state response will be correlated with the operating conditions influencing the process using regression analysis. This steady-state data will provide insight into the control effect that peroxide has upon the extrudate viscosity and is used to experimentally determine the gain of the open loop plant. The dynamic response is used to develop open loop models for the purposes of automatic closed loop control.

The open loop model will be comprised of the residence time distribution as well as the operating conditions so that it is more general. Additionally, the characteristic times determined from the residence time distribution, as well as the operating parameters of the extruder, will be used as parameters for a

lamellar model. The kinematic plant model combined with the dynamic response information is used to create a feedback control loop for the melt viscosity. When this model is combined with the warped time lamellar reaction model, a predictive model is created that can expand the envelope for which the controller is suitable.

3.2 Investigative Work

Experiments were performed on a 30mm co-rotating twin-screw extruder with an on-line viscometer at the Dupont Experimental Station. Following the steps proscribed above for performing this research, material residence time distributions were first recorded and then the viscosity was measured for step changes in the peroxide initiator feed (Chapter 4). The residence distribution data was quite good and behaved as expected (Chapter 5). The residence time distributions were also deconvolved and RTD's have been obtained for each zone within the extruder. Additionally a new model of the residence distribution was developed using convolutions of first order models with delay (Chapter 8). This new model allows for individual description of regions.

In the process of performing this work, additional research was done to analyze which aspects of the complex polymer rheology affected the characteristics of the residence distribution curves. Chapter 9 illustrates that knowledge of the complex rheology of the material is important when comparing residence distributions for different materials.

The peroxide step change experiments were used for statistical analysis of the steady state data (Chapter 6), as well as system identification analysis (Chapter 7). This data was also used for system identification with the convoluted first order model (Chapter 8). The statistical analysis indicates dependence on the

volume mixing and on the residence time from the specific throughput of the extruder, and of course, the peroxide has a great effect on the extrudate viscosity. The system analysis showed that a plant model with three poles and a time delay could capture the system dynamics. Closed Loop control was achieved using a Smith predictor with proportional integral control (Chapter 11).

Chapter 4

Experimental Facilities and Data Acquisition

4.1 Introduction

Experiments have been carried out in order to model the extruder and peroxide initiated polymer degradation reaction, and to control the reactive extrusion process. The residence time distributions where used to find the mean residence times for a multitude of operating conditions. It was also be used to find the parameters for the third order plant model (Equations 2.5) and the transfer functions for the individual zones (Equation 8.2). These experiments provide the delay time as well as the shape factor, a.

The experiments for the peroxide induced degradation of polypropylene provide a great deal of information. Each step change has a transient response of extrudate viscosity as well as the steady state value of viscosity after the plant has stabilized. The steady state response was correlated using regression analysis with the operating conditions influencing the process. This data will also provide insight into the control effect that peroxide has upon the extrudate viscosity. The dynamic response will be used to develop open loop models for the purposes of automatic closed loop control.

4.2 Experimental Facilities

All experiments were performed at the Dupont Experimental Station in Wilmington, Delaware, with operators present. Montell KF6100 Polypropylene, Basell PDC1277 Polypropylene, and Network Polymers PP NPP 30-0300 were used as the feed-stocks into a Werner and Pfleiderer 30mm co-rotating twin-screw extruder (CoTSE). Three different polypropylenes were used due to terminations of product lines. The peroxide initiator was Atofina Luperox 101. The extruder used a screw configuration as seen in Figure 4.1 and comprehensive instrumentation and data acquisition equipment. In addition to thermocouple temperature sensors for each barrel section, this extruder was instrumented with three sets of pressure probes and light reflectance probes located in filled regions of the extruder, the melt zone, the mixing zone, and the die region. Additionally, the die was instrumented with an in-line rheometer fed by material diverted from the die and then reintegrated into the output stream.

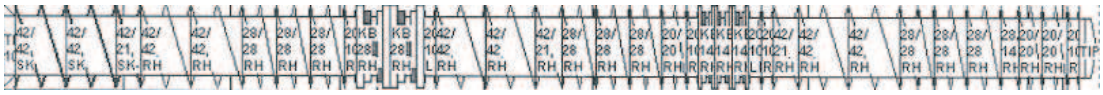

Figure 4.1: Experimental screw design.

4.3 Operating Conditions and Techniques

The first set of experiments studied the kinematics of the extrusion process using reflectance tracers. The extrudate was processed with the barrels set at 210 C, and the parameters studied were material flow rate and extruder screw speed. A fractional design of experiment (DOE) of twelve conditions (Table 4.1), with

three replicates each, were selected to study the effects of varying screw speed with constant flow rate, the effects of varying flow rate with constant screw speed, and also to allow for numerous conditions to have nearly similar specific throughputs, the ratio of flow rate to screw speed. For each condition, three replicates of the same experiment, residence time distribution, were performed. This experiment consisted of depositing ten 20% TiO_2 pre-blended pellets into the entry of the extruder. The time of deposit is recorded as well as the response of the three reflectance probes.

The second set of experiments recording the behavior of a polypropylene degradation reaction was conducted using system identification techniques as well as other statistical tools. After the RTD experiments, the viscometer was attached to the machine to instrument the open-loop response to step changes in initiator concentration for various operating conditions (Table 4.2). Following the experiments, data was processed to extract the information necessary for analysis. The RTD information was extracted as well as the signal from the viscometer. The RTD analysis was performed as before for the previous RTD analysis of the extruder.

Experiments were also performed to characterize the behavior of the PDC1277 within the extruder. Using the same techniques as for the KF6100, RTD's were determined at the conditions listed in Table 4.3. Likewise, with the change of material, a new set of peroxide step changes were performed. The conditions are contained within Table 4.4.

Q	N	Q/N
$[mL/s]$	$[rps]$	$[mL/r]$
1.49	1.75	0.85
1.49	3.50	0.43
2.98	2.33	1.28
2.98	3.50	0.85
2.98	3.50	0.85
2.98	4.42	0.67
2.98	5.83	0.51
4.47	2.67	1.68
4.47	3.50	1.28
4.47	3.50	1.28
4.47	5.33	0.84
5.96	2.33	2.55
5.96	3.50	1.70
5.96	4.67	1.28

Table 4.1: Operating Conditions of RxD Analysis of KF6100. These are the conditions used to explore the residence distributions of material within the extruder. Three replicates were performed at each condition.

Q $[mL/s]$	N $[rps]$	Q/N $[mL/r]$
2.98	2.33	1.28
2.98	3.50	0.85
2.98	4.42	0.67
2.98	5.83	0.51
5.96	3.50	1.71

Table 4.2: Operating Conditions of Viscosity Analysis of KF6100. These are the conditions used to explore the relationships between extrudate viscosity and operating conditions.

Q $[mL/s]$	N $[rps]$	Q/N $[mL/r]$
1.49	1.75	0.85
1.49	3.50	0.43
2.98	2.33	1.28
2.98	3.50	0.85
2.98	4.42	0.67
2.98	5.83	0.51
4.47	2.67	1.68
4.47	3.50	1.28
4.47	5.33	0.84
5.96	2.67	2.24
5.96	3.50	1.70
5.96	4.67	1.28

Table 4.3: Operating Conditions of RxD Analysis of PDC1277. These are the conditions used to explore the residence distributions of material within the extruder. Three replicates were performed at each condition.

Q $[mL/s]$	N $[rps]$	Q/N $[mL/r]$
2.98	2.33	1.28
2.98	3.50	0.85
4.47	2.67	1.68
4.47	3.50	1.28
4.47	5.33	0.84

Table 4.4: Operating Conditions of Viscosity Analysis of PDC1277. These are the conditions used to explore the relationships between extrudate viscosity and operating conditions.

Chapter 5

Residence Distribution Analysis

5.1 Introduction

The residence time distribution will be used to model the process and can be used to find the mean residence times for a multitude of operating conditions. It will also be used to find the parameters for the third order RTD Model (Equation 2.5). These parameters provide the delay time, t_d, and also the shape factor, a. The open loop model will use the residence time distribution as its kinematic base, While the operating conditions will factor into the non-linear gain function.

The experiments measuring the material residence distribution in the extruder were performed at twelve different combinations of operating conditions. These conditions are displayed in Table 4.1. These were selected to replicate specific throughputs within the set, as well as for comparison with historic data sets [20].

5.2 Data Processing

For each operating condition, three replicates of data were recorded. For each replicate, ninety seconds of baseline data were recorded and then the entirety of the residence time distribution was recorded. Following the experiments, the

data was processed using MatLAB software. The reflectance data included a matrix containing time, pressure readings (2), reflectance readings (3), temperature readings (2), a pulse signal, indicated feed rates, and extrudate viscosity; although, not all of these signals were used for this set. The first step of analysis was to determine the time of the tracer input, and this is contained within the pulse signal. This was used to determine the starting point of the experiment. Following this, averages of the reflectance signals were found from the means of the three reflectance signals at times before the TiO_2 input. Then the replicate signals were summed for each reflectance probe. The three signals were then filtered using a low-pass Butterworth filter to remove the noise from high frequency interference. Afterwards, each signal was normalized to give a unit integral. In addition to this, parameters for a third order impulse response model were fitted for each signal. This model from is [15]:

$$E(t) = {a^3}/{2}\,(t - t_d)^2\, e^{-a\cdot(t-t_d)} \tag{5.1}$$

Where a is the shape factor, and t_d is the time delay. Equation 5.1 is the same as Equation 2.5. For all the conditions and reflectance probes, the output of this model was compared to the processed data. This model was fit to the signal using a non-linear least squares optimization. The model fit the data quite well, although it did not capture the fine nuances of the tail of the RTD that the physical data expresses, which could impact signal deconvolution.

As mentioned earlier, the three reflectance probes take readings at the end of each filled region. This implies that for these experiments, each probe provides the residence history of the TiO2 as it travels from the entrance past the probe. Therefore the first probe records the history through the melting zone. The

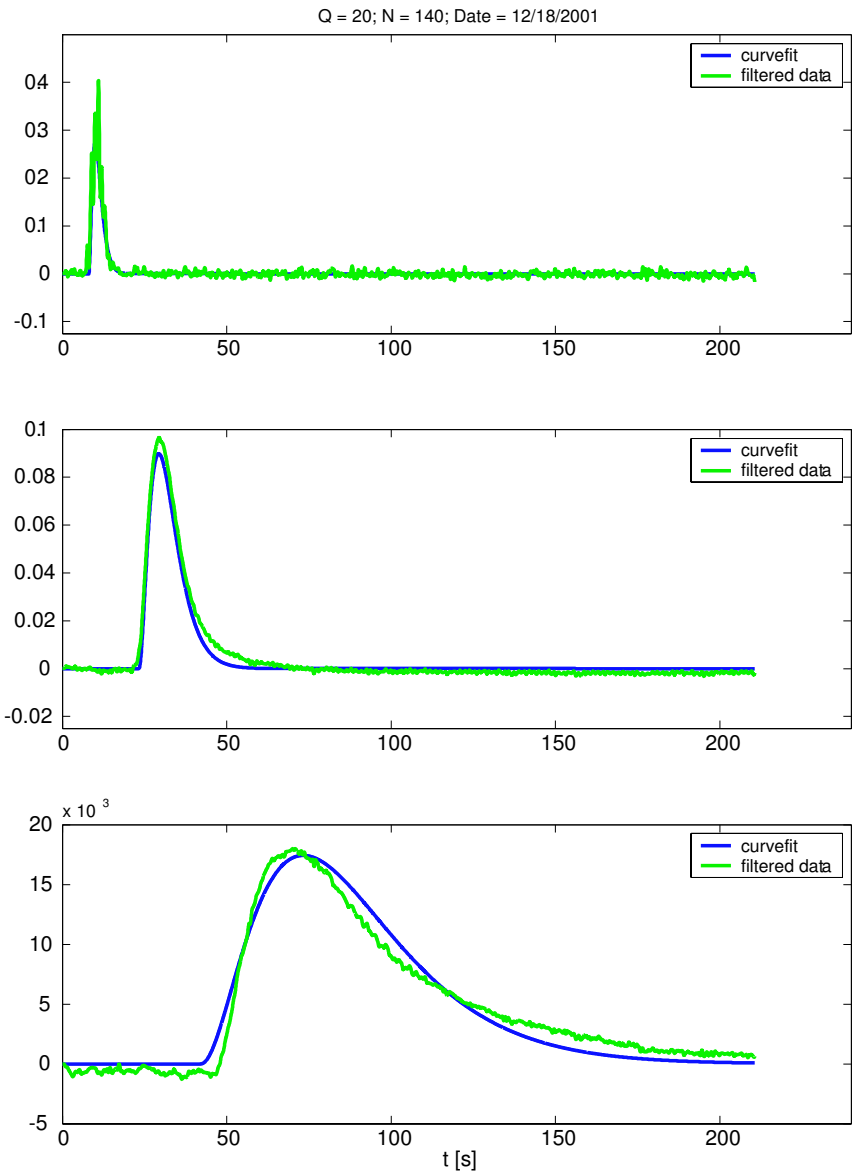

Figure 5.1: *RTD* data plotted with the fit using Equation 5.1. Normalized intensity is plotted against time. The graphs are for the first, second, and third optical probes.

second records the history through the melting and mixing zones, and the third records the history through the melting and mixing zones as well as the metering (die) zone. To determine the histories for the mixing and metering zones, it is necessary to deconvolve the model fits to the signals.

The deconvolution calculates signals for the different zones of the extruder that cannot be directly measured. Although the data was filtered, it, specifically the melting zone, is still too noisy for use with the deconvolution techniques; the model fits were used instead. The first reflectance probe corresponds to the melting zone, but the other two probes do not correspond to sections of the extruder. They correspond to combinations of extruder sections. A deconvolution of the models for the second and first probes provides the mixing zone. A deconvolution of the models for the third and second probes provides the metering region, and that of the models for the third and first probes provides the mixing and die zones together. This deconvolution is performed by convolving a guess of the model for a section with the model of a previous section to approximate the model fit of a reflectance probe. To illustrate, the model output of the first reflectance probe is convolved with a model output using a "guess" of the mixing zone parameters to approximate the reflectance probe's output. To arrive at the optimal guess, the command "`lsqcurvefit`" is used to solve the non-linear least squares problem for the best "guess" of the model parameters. The analogue is done to deduce the die region, and also to deduce the combination of the mixing and die regions. When this combination of the mixing and die regions is compared to the convolution of the mixing and die zones, the two agree well for all conditions.

5.3 Interpretation of Data

Mean residence times were computed for the reflectance signals as well as the deconvoluted signals. This was performed using the model fits as well as the reflectance data. Table 1 shows the mean residence times computed for the model fits of the optical probes as well as the deconvolutions; it also shows the mean residence times from the reflectance probes. The table shows that agreement is good for the third reflectance probe, the one with the cleanest signal, and the model fit. There is less agreement at the second probe, and less so at the first. In fact, the data of the first probe gives negative mean residence times. The disagreement is most likely due to the noise that survived the filtration. The deconvolutions can be inspected by adding the mean residence times of the first reflectance probe with the deconvolutions for second and third zones. Their sum is quite close to the mean residence time for the third probe location. For all the conditions, the deconvolutions seem to be consistent. The figures for the residence distributions are located within the appendix.

Using Equation 2.4, it is possible to solve for the parameters A and B which correspond to the filled and partially filled regions of interest (Table 5.2). With these parameters available, it is possible to predict t_m.

5.3.1 RTD Data

The data from the RTD's of reflectance probe 1 show no discernible trend with regards to Q or N, this is as expected (Section A.1). No model seems to explain the melting zones behavior yet. The data from reflectance probes 2 and 3 follows accepted trends. For equal throughput, a higher screw speed causes the peak to occur earlier. Also, for equal screw speed, a higher throughput causes the

Cndtn	DP 1	MP 1	DP 2	MP 2	DP 3	MP 3	DCZ 2	DCZ 3	DCZ 2+3
1	-20.11	11.01	9.54	32.36	96.66	88.66	21.07	55.92	77.67
2	-16.39	8.95	5.68	27.38	88.06	82.81	18.13	55.12	73.88
3	21.48	8.83	32.86	26.00	88.86	76.85	16.80	50.25	67.99
4	15.40	9.01	30.10	24.15	82.25	73.84	14.57	48.96	64.65
5	33.89	8.11	48.65	20.74	57.34	50.56	12.34	29.13	42.34
6	63.01	7.13	29.19	17.32	57.71	45.78	9.73	27.91	38.43
7	-6.80	16.01	53.35	55.48	165.92	156.47	38.88	101.16	141.09
8	25.83	14.77	65.26	48.51	146.66	139.30	32.80	89.73	124.65
9	-16.09	9.48	18.35	25.57	76.07	66.12	15.89	40.13	56.59
10	20.01	8.08	38.92	23.49	71.02	60.97	15.19	36.85	52.82
11	18.46	6.62	20.81	19.07	55.45	53.17	12.24	33.54	46.48
12	-45.93	8.93	-29.86	22.25	69.26	57.59	13.19	35.04	48.63

Table 5.1: Mean Residence Times. These are computed using the measured data and using the fitted model, Equation 5.1, as indicated. Model, Data, $De C$onvolution, Probe, and Zone are the abbreviations. The unit of all the values is seconds.

	A $[cc]$	B $[rev]$
Probe 1	15.9	14.1
Probe 2	34.2	55.5
Probe 3	70.9	177.6
Zone 2	18.6	40.0
Zone 3	36.5	121.0
Zones 2,3	54.8	163.9

Table 5.2: Parameters for mean residence time.

peak to occur earlier. When comparing results of these two probes, the figure for reflectance probe 3 has curves with similar heights for the same throughput, whereas the figure for reflectance probe shows more variability. This is possibly due to effects of the differences between the model and the actual data.

All the deconvolutions show the correct trends. As is the case for reflectance probe 2, the peaks are not consistently the same height for the same feed rate. This is due to the deconvolution process and the normalization of the curves. Visually the curves can be compared by examining where the peaks of the curves are. The curves have different spreads and when normalized the area is made a unit in size, which affects the peak height. This normalization does not change the where in time the peak exists.

5.3.2 RVD Data

The reflectance data was plotted into a residence volume distribution figure (Section A.2). This figure has the reflectance plotted against the volume passing the probe. In this domain all of the curves have the same shape, which is a function of the screw configuration. It can be described by the volume shape factor, a_v, which is equivalent to the experimentally determined constant C. As before there is difficulty explaining the results for reflectance probe 1, but both reflectance probes 2 and 3 provided data whose peaks were consistent, with probe 3 giving a response later in the volume domain then probe 2.

The deconvolution for the mixing zone and die zone combined shows the same specific throughput dependency. The deconvolution of just the die zone also shows the same behavior. The mixing zone, though, does not show this behavior. This is most likely due to the data from the first reflectance probe. This data did not

have the same trend as others, and the deconvolution of that data and the second optical probe is quite effected by the firsts' results.

All of the RVD data was also plotted with the delay removed. In this situation, it is expected that for the same geometry, the curves will approximately superimpose. This is the case for the reflectance probe 3 and the deconvolutions for the die zone and for the die and mixing zones combined. The others do not follow this well, most likely due to effects from the melting zone. Table 5.3 shows C as well as its sample standard deviation. The results in the table support the assertion that the metering zone (die zone), provides consistency to the RVD.

	Probe 1	Probe 2	Probe 3	Zone 2	Zone 3	Zones 2,3
C $[s/cc]$	0.2596	0.0899	0.0200	0.1018	0.0209	0.0201
Std. Dev.	0.0697	0.0164	0.0013	0.0187	0.0015	0.0013
Pct. Dev.	25.7	17.5	6.2	17.6	7.0	6.0

Table 5.3: Experimental screw constants, C, and their standard deviations expressed as a percent. C is equivalent to the shape factor of the *RVD* curve.

5.3.3 RRD Data

The residence rotation distribution has the normalized reflectance plotted against the number of screw rotations passing the probe, $t \cdot N$ (Section A.3). When the data is plotted in this manner the accepted trend is for the number of revolutions to peak response to increase with decreasing specific throughput, Q/N . As expected, in this domain, the data from the melting zone does not follow this trend. The data for the other two probes do follow this trend nicely; in fact data with the same Q/N have peak times in the same location. Unlike plotting in the

other domains, the deconvolution for the mixing zone follows the trends nicely. The other two deconvolutions also follow suit. The data was also plotted with the delay removed; this accentuated the similarity between conditions with the same Q/N. Otherwise the observations are as before.

5.4 Summary

This data set provided results that behave in a manner which allow the date to be used in the subsequent analyses steps. The results follow the observations of Gao et al. [15] that provide a separate verifying experiment to the concept. This data can reliably be used to provide mean residence times for different regions of the extruder allowing the determination of how long peroxide stays in particular regions of the extruder. However it is still based upon a third order model designed for a screw with three filled regions.

Chapter 6

Steady State Analysis

6.1 Introduction

The experiments for the peroxide induced degradation of polypropylene also provide steady state viscosity information which is used for the model prediction in combination with the process dynamics. Each step change has a transient response of extrudate viscosity as well as the steady state value of viscosity after the plant has stabilized. In this section, the steady state response has been correlated using regression analysis with the operating conditions influencing the process. This data will also provide insight into the control effect that peroxide has upon the extrudate viscosity, it also can be used to calculate the DC gain of the process.

6.2 Data Processing

The data from the peroxide degradation experiments was processed using the Minitab software package to determine the statistical information.

The viscometer data was retrieved for each condition. Initial analysis used a low pass filter to clean the data. This was unsatisfactory, though. Due to hard-

ware handshaking issues with the prototype viscometer and the data acquisition system, periodically, a data point would be dropped. This was a reported as a zero response for that point. The data acquisition system applied a low pass filter that transformed this dip in the data into a "surge" in the signal. Further low pass filtration only amplified this. Due to this, a median filter was used to clean the data. This filter uses a moving median with a window set to 119 data points. For the statistical analysis of the steady state data, the final 15 seconds of the viscosity signal were averaged to indicate a steady state value at a combination of operating conditions and peroxide concentration. The transient data will be used for system identification.

The data sets, for each run, possess approximately $30,000$ data points. This quantity of data is quite large for the desired model determination. In order to change the size of the data signal, while maintaining the shape of the data signal, the data was resampled to make it more tractable. Resampling changes the frequency at which data is recorded by regularly sampling the data at the desired frequency. The new frequency $20hz/100$ or $0.2hz$. The resampled data has approximately 300 data points.

6.3 Initial Analysis

Initial analysis was performed upon the data to explore some of the relationships exhibited. A response surface was created to see how the polymer viscosity depends on different operating conditions such as the percentage of peroxide feed, Q, N, and Q/N. A subset regression analysis was performed to determine which combination of variables would provide the best indication of steady state viscosity, while reducing the number of variables (Section B.1). The indications from

this analysis were used to perform a regression to relate polymer viscosity to the percentage of peroxide fed, N_m, v_m, and peroxide feed wt% $*Q/N$ (Section B.2). In spite of the subset regression analysis, not all the terms of the regression were significant, so more analysis was performed to get a better correlation (Sections 6.4 and 6.5).

6.3.1 Exploratory Regressions

Initially, the data was analysed to determine the best subset of data that would capture as much of the response as possible. This was done for the data with an outlier removed. The analysis indicates that an $R^2 = 93.8\%$ can be achieved with the initiator, $[I]$ $[wt\%]$, revolution delay, N_m $[r]$, volume delay, v_m $[mL]$, and the intiator pecentage multiplied by the specific throughput, $[I] \cdot Q/N$, as the factors for the regression. This can be seen in Section B.1 of this document. Knowing this, a regression was performed for viscosity with $[I]$, N_m, v_m, and $[I] \cdot Q/N$ as the factors. The coefficients for v_m, and $[I] \cdot Q/N$ were both statistically significant, although the other two were not. Since the interaction, $[I] \cdot Q/N$, has such a high significance, another set of subset regressions was performed. This can be seen in Section B.2.

6.4 Best Subset Regression

A best subsets regression was performed using Minitab to find the optimal variable choice to model the viscosity response, η $[Pa \cdot s]$, of the extrudate to operating conditions and peroxide feed. The results are shown in Table 6.1. "R^2 describes the proportion of variation in the response data explained by the predictors in

the model. Adjusted R^2 is a modified version of R^2 that has been adjusted for the number of predictors in the model. C_p is another statistic for assessing how well the model fits the data. s is the error standard deviation. ... A good model should have high R^2 and adjusted R^2, small s, and C_p close to the number of predictors contained in the model." [21]. Using these criteria, Section 6.5 shows the results of a regression relating only two interaction terms, v_m and $[I] \cdot Q/N$, to the viscosity.

Var's	R^2	R^2_{adj}	C_p	S	N_m rev	v_m mL	t_m s	Q/N mL/r	$[I] \cdot N_m$ $wt\% \cdot r$	$[I] \cdot v_m$ $wt\% \cdot mL$	$[I] \cdot t_m$ $wt\% \cdot s$
1	92.2	91.2	1.8	127.83		X					
1	91.4	90.3	3.1	133.98				X			
2	93.1	91.6	2.2	124.40					X		X
2	93.1	91.6	2.2	124.41						X	X
3	93.8	91.9	2.9	122.29		X				X	X
3	93.8	91.9	2.9	122.43		X			X		X
4	94.0	91.5	4.6	125.18	X	X	X		X		
4	94.0	91.4	4.7	125.95	X	X			X		X
5	94.6	91.7	5.5	123.79	X	X	X		X		X
5	94.4	91.4	5.9	126.50		X	X	X		X	X
6	94.9	91.3	7.0	126.62	X	X	X	X		X	X
6	94.8	91.2	7.1	127.42	X	X	X	X	X		X
7	94.9	90.4	9.0	133.47	X	X	X	X	X	X	X

Table 6.1: The table shows the results from a best subsets regression for viscosity $[Pa \cdot s]$ versus $[I] \cdot Q/N$ and other variables as noted above. Eighteen cases were used for the regression.

6.5 Regression Analysis for Predictive Viscosity

This regression is composed entirely of only two interaction terms (Section 6.4), v_m and $[I] \cdot Q/N$. The regression yields the following equation.

$$\eta = 438 + 7.11 v_m - 33230 [I] \cdot Q/N \tag{6.1}$$

v_m is the interaction of $t_m 23$, the mean residence time for the mixing and metering regions, and Q. This term is related to the volume mixing effects. The other term, $[I] \cdot Q/N$, is the interaction of the peroxide concentration with Q/N, which influences the degree to which the extruder is filled. Table 6.2 shows that the two terms are quite significant. The largest P value is 0.002. The regression constant does not seem to be significant, although it is more so then the previous regression discussed in Section 6.3.1. The analysis of variance (Table 6.3) shows that the regression is quite significant. In fact, the F value is 88.80.

Predictor	Coefficient	s Coeff	t-value	P
Constant	437.7	426.4	1.03	0.321
v_m $[mL]$	7.106	1.839	3.86	0.002
$[I] \cdot Q/N$ $[wt\% \cdot Q/N]$	-33230	2520	-13.18	0.000

Table 6.2: Regression Analysis Coefficient Significance for Equation 6.1. The following values were also determined: $s = 127.8$, $R^2 = 92.2\%$, Adj.$R^2 = 91.2\%$.

More information from this regression can be gleaned from Figures 6.1 and 6.2. Figure 6.1 indicates that the error for the data is distributed normally because the points roughly indicate a straight line. Figure 6.2 shows that the residuals

Source	DF	SS	MS	F	P
Regression	2	2902074	1451037	88.80	0.000
Residual Error	15	245120	16341		
Total	17	3147194			

Table 6.3: Analysis of Variance

indicate that there may be an outlier in the data.

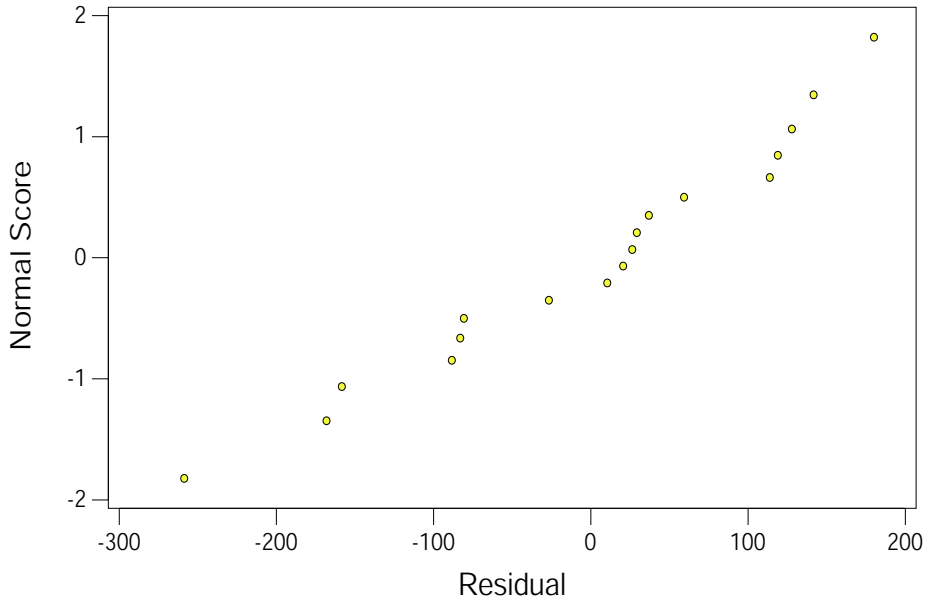

Figure 6.1: Normal probability plot of the residuals for KF6100. The response studied is the melt viscosity. This data has a trend that looks nearly normal. This indicates that the error for the data is distributed nearly normally. It is not clear why the residual do not behave completely normally.

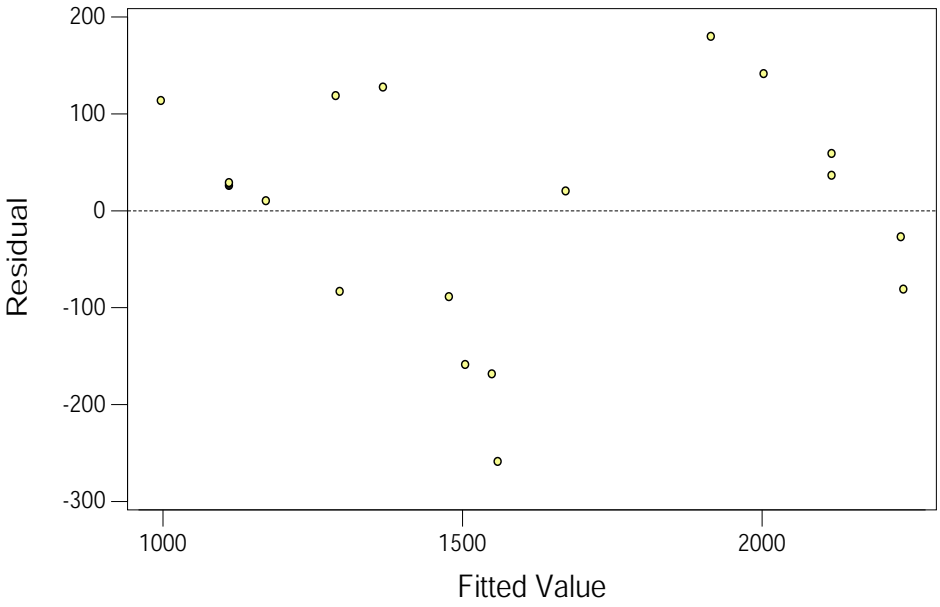

Figure 6.2: Residuals versus the fitted values for KF6100. The response studied is the melt viscosity. These residuals show no trend and support that the regression is a good fit.

6.5.1 Second Polypropylene used in experiment

Due to material shortages, the original analysis which were performed on Montell KF6100 needed to be repeated with the new Basell PDC1277. Using the same type of regression as in Equation 6.1, Equation 6.2 is the regression for PDC1277.

$$\eta = 428 + 5.21 v_m - 17632[I] \cdot Q/N \tag{6.2}$$

Table 6.4 shows that the two terms in the regression are quite significant. The largest P value is 0.001. The analysis of variance (Table 6.5) shows that the regression is quite significant. In fact, the F value is 181.86 and greater then that for the KF6100 regression.

Predictor	Coefficient	s Coeff	t-value	P
Constant	427.6	114.1	3.75	0.001
v_m $[mL]$	5.2078	0.5832	8.93	0.000
$[I] \cdot Q/N$ $[wt\% \cdot Q/N]$	-17632.4	978.4	-18.02	0.000

Table 6.4: Regression Analysis Coefficient Significance for Equation 6.2. The following values were also determined: $s = 58.8$, $R^2 = 93.6\%$, Adj.$R^2 = 93.1\%$. This is for PDC 1277.

Source	DF	SS	MS	F	P
Regression	2	1265256	632628	181.86	0.000
Residual Error	25	86968	3479		
Total	27	1352225			

Table 6.5: Analysis of Variance for PDC1277

More information from this regression can be gleaned from Figures 6.3 and 6.4. Figure 6.3 indicates that the error for the data is distributed normally because the points roughly indicate a straight line. Figure 6.4 shows that the residuals indicate that there may be two outliers in the data.

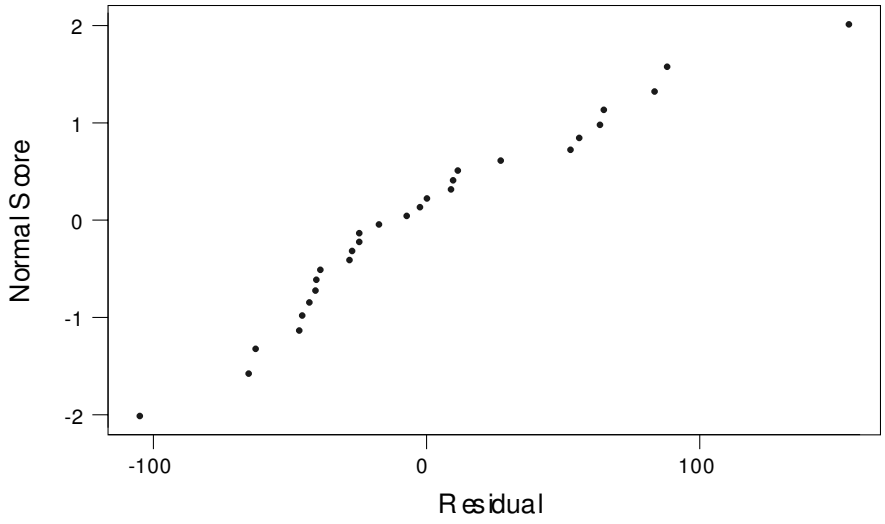

Figure 6.3: Normal probability plot of the residuals for PDC1277. The response studied is the melt viscosity. This data has a trend that looks normal. This indicates that the error for the data is distributed normally.

The parameters of Equations 6.1 and 6.2 are not the same. This difference is due to the polypropylene's different interactions with the peroxide initiator. These two polymers are not the same. The Basell PDC1277 was made to replace the Montell KF6100 and the manufaturer indicates it has different material properties. One of these is the molecular weight distribution, and because thaction of

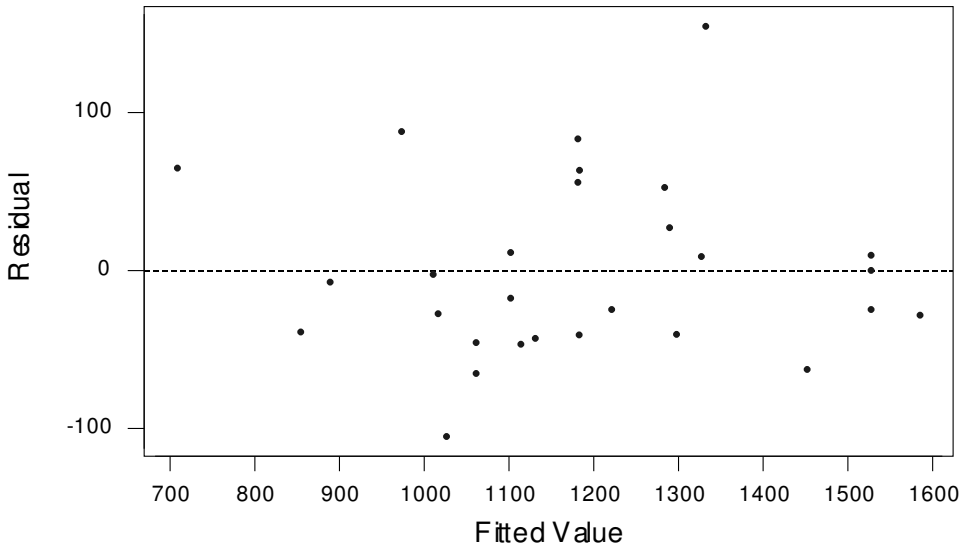

Figure 6.4: Residuals versus the fitted values for PDC1277. The response studied is the melt viscosity. These residuals show no trend and support that the regression is a good fit.

the initiator affects the molecular weights of the polymers, the parameters of the equations are different.

6.6 Conclusion

A response surface for viscosity as a function of operating parameters (Equation 6.1) is developed using analysis of variance techniques. The response surface indicates that the peroxide has a very large effect on the polypropylene viscosity. Additionally, it can be seen that the flow rate and screw speed contribute to the degradation of the polypropylene. Their interaction in the form of the specific throughput also affects this property. Higher order interactions are quite significant in the dynamics of the process, and capture a great deal of the response in a regression. the response surface is composed entirely of two interaction terms, v_m and $[I] \cdot Q/N$. The significance of these two terms indicates a dependence on the volume mixing, v_m, and on the residence time scaled with the specific throughput. The regression for PDC1277has an $R^2 = 92.2\%$ and the ANOVA of the regression shows that it also is quite significant. These regressions can be used to predict viscosity with terms that come from known quantities such as Q, N, and peroxide concenration. The mean residence time is necessary for the mean residence volume, v_m, and that can be obtained from calculations and/or experimentation.

Chapter 7

System Identification

7.1 Introduction

System Identification is the process of determining the transfer function of a plant. One goal of this research is to develop methods to do this analytically. In the interim though, statistical techniques were used to inspect the system (Section 7.2), and a physical model was developed (Chapter 8). Each peroxide step change has a transient response of extrudate viscosity as well as the steady state value of viscosity after the plant has stabilized. The dynamic response will be used to develop open loop models for the purposes of automatic closed loop control. The open loop model will be related back to the residence time distribution as well as the operating conditions so that it is more general. Section 7.2 describes statistical techniques for statistically determining the open loop transfer function. Section 8.2.1, in contrast, describes a physically motivated model.

System identification can be done by modelling a system taking advantage of physical insights, or the system can be treated as an unknown system and statistical techniques can identify it. Techniques for system identification depend wholly or with modifications on least squares optimizations techniques. Essen-

tially parameters are selected to minimize the residuals for a function relating an input or collection of inputs to an output or collection of outputs. Although effective statistical techniques have little generality and offer less insight then physically motivated models.

7.2 MatLAB System Identification

7.2.1 MatLAB Code

Statistical determination of the system is done using data from experiments. This data relates step changes in peroxide initiator concentration to extrudate melt viscosity. This is the same data is used as in Chapter 6. Data was prepared as in Section 6.2. The code used for the system identification is located within the appendix in Section C. This code uses statistical techniques from MatLAB to determine plant models from sets of empirical data.

7.2.2 Results

Experiments were performed at five different operating conditions as described in Table 4.2. Transfer functions for the data were created in both discrete and continuous time for different operating conditions. The discrete system was found using ARX techniques, and MatLAB was used to transform the discrete model to a continuous one as shown in Section C. Tables 7.1, 7.2, 7.3, 7.4, and 7.5 show the parameters obtained from the analysis. Equations 7.1, 7.3, 7.5, 7.7, and 7.9 are the discrete time transfer functions with out the delay for the respective combinations of Q and N. Equations 7.2, 7.4, 7.6, 7.8, and 7.10 are likewise the respective continuous time transfer functions. The transfer functions are shown

without the time delay, because it is more facile to program the MatLAB to determine the transfer function in separate steps from the time delay. Figures 7.1, 7.2, 7.3, 7.4, and 7.5 show the Bode plots for the discrete and continuous transfer functions. Discussion of these results is in Section 7.2.3.

Condition: Q 30 N 210

These are the results of the system identification for a throughput of 30 pounds per hour, and 210 *rpm*.

Parameter	Value
N_a (poles)	3
N_b (num coeff)	2
N_{delay}	15
time delay $[s]$	75
sampling time	5
system DC gain	-21.8564

Table 7.1: System Identification Results for $Q = 30pph$ and $N = 210rpm$.

The discrete transfer function with out time delay is:

$$H(s) = \frac{-0.1018}{z^3 - 1.261z^2 - 0.2816z + 0.5475} \tag{7.1}$$

Transforming the previous equation, the continuous transfer function with out time delay is:

$$G(s) = \frac{0.01325s^3 - 0.01016s^2 + 0.005581s - 0.00108}{s^4 + 0.2162s^3 + 0.4088s^2 + 0.01001s + 4.943e - 005} \tag{7.2}$$

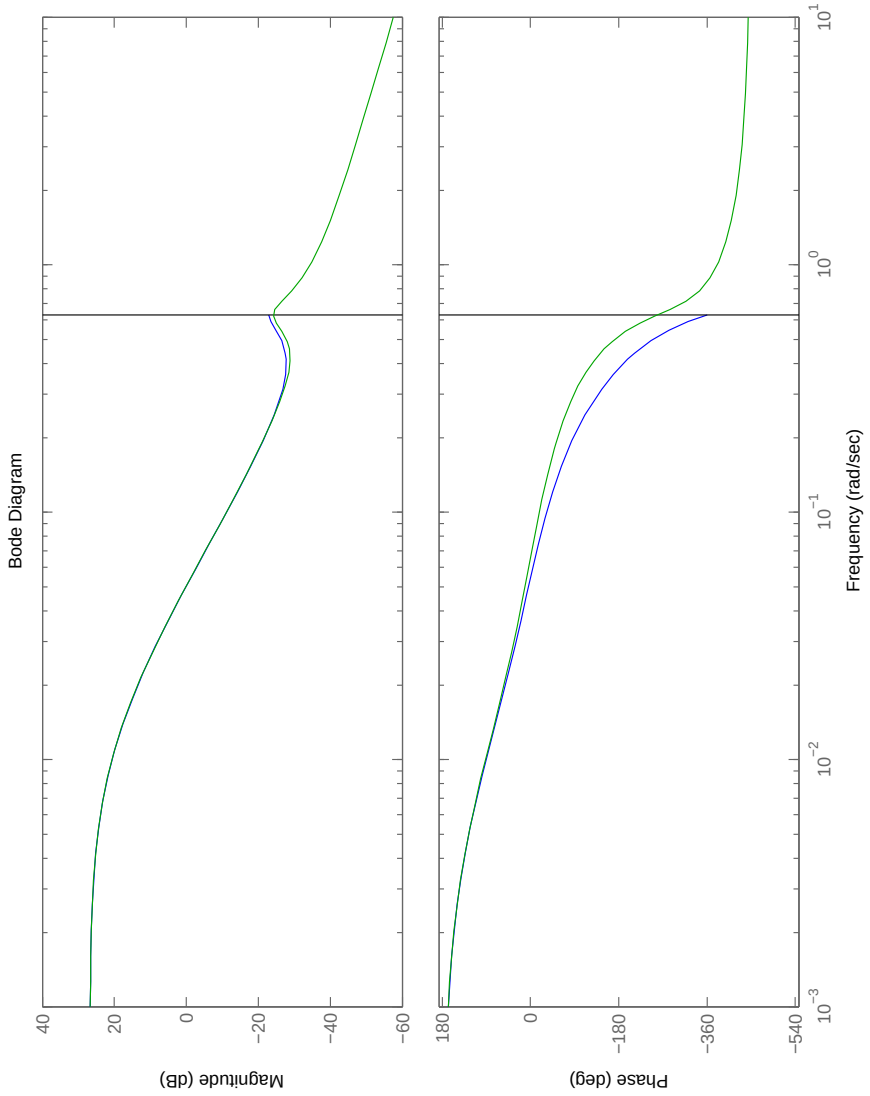

Figure 7.1: A Bode plot of the discrete and continuous system models for $Q = 30pph$ and $N = 210rpm$. The green curve is the continuous model, the blue is the discrete model.

Condition: Q 30 N 160

These are the results of the system identification for a throughput of 30 pounds per hour, and 160 *rpm*.

Parameter	Value
N_a (poles)	3
N_b (num coeff)	2
N_{delay}	17
time delay $[s]$	85
sampling time	5
system DC gain	-23.9028

Table 7.2: System Identification Results for $Q = 30pph$ and $N = 160rpm$.

The discrete transfer function with out time delay is:

$$H(s) = \frac{-0.1398}{z^3 - 1.186z^2 - 0.4129z + 0.6051} \tag{7.3}$$

Transforming the previous equation, the continuous transfer function with out time delay is:

$$G(s) = \frac{0.01796s^3 - 0.0131s^2 + 0.007273s - 0.001414}{s^4 + 0.175s^3 + 0.4044s^2 + 0.01039s + 5.916e - 005} \tag{7.4}$$

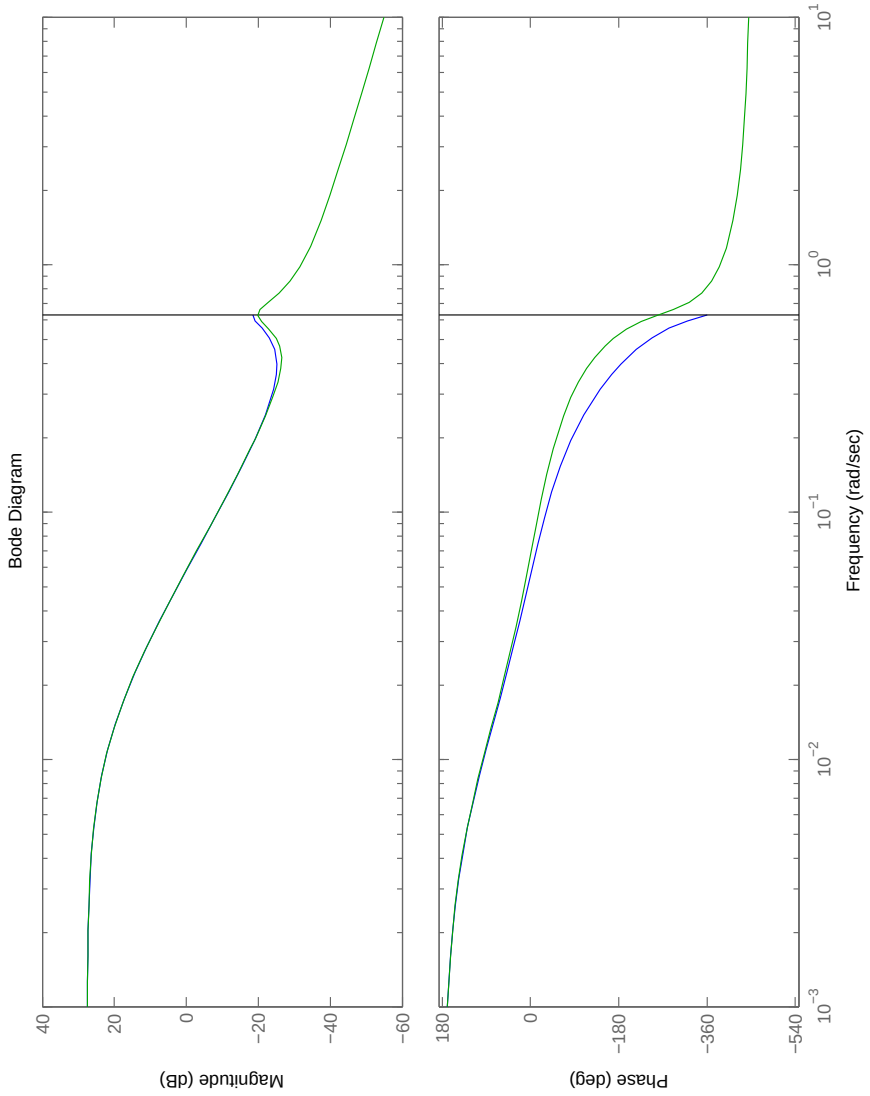

Figure 7.2: A Bode plot of the discrete and continuous system models for $Q = 30pph$ and $N = 160rpm$. The green curve is the continuous model, the blue is the discrete model.

Condition: Q 30 N 320

These are the results of the system identification for a throughput of 30 pounds per hour, and 320 *rpm*.

Parameter	Value
N_a (poles)	3
N_b (num coeff)	2
N_{delay}	16
time delay $[s]$	80
sampling time	5
system DC gain	-24.0417

Table 7.3: System Identification Results for $Q = 30pph$ and $N = 320rpm$.

The discrete transfer function with out time delay is:

$$H(s) = \frac{-0.1064}{z^3 - 1.193z^2 - 0.4081z + 0.6052} \tag{7.5}$$

Transforming the previous equation, the continuous transfer function with out time delay is:

$$G(s) = \frac{0.01363s^3 - 0.009969s^2 + 0.005533s - 0.001076}{s^4 + 0.1757s^3 + 0.4044s^2 + 0.0101s + 4.475e - 005} \tag{7.6}$$

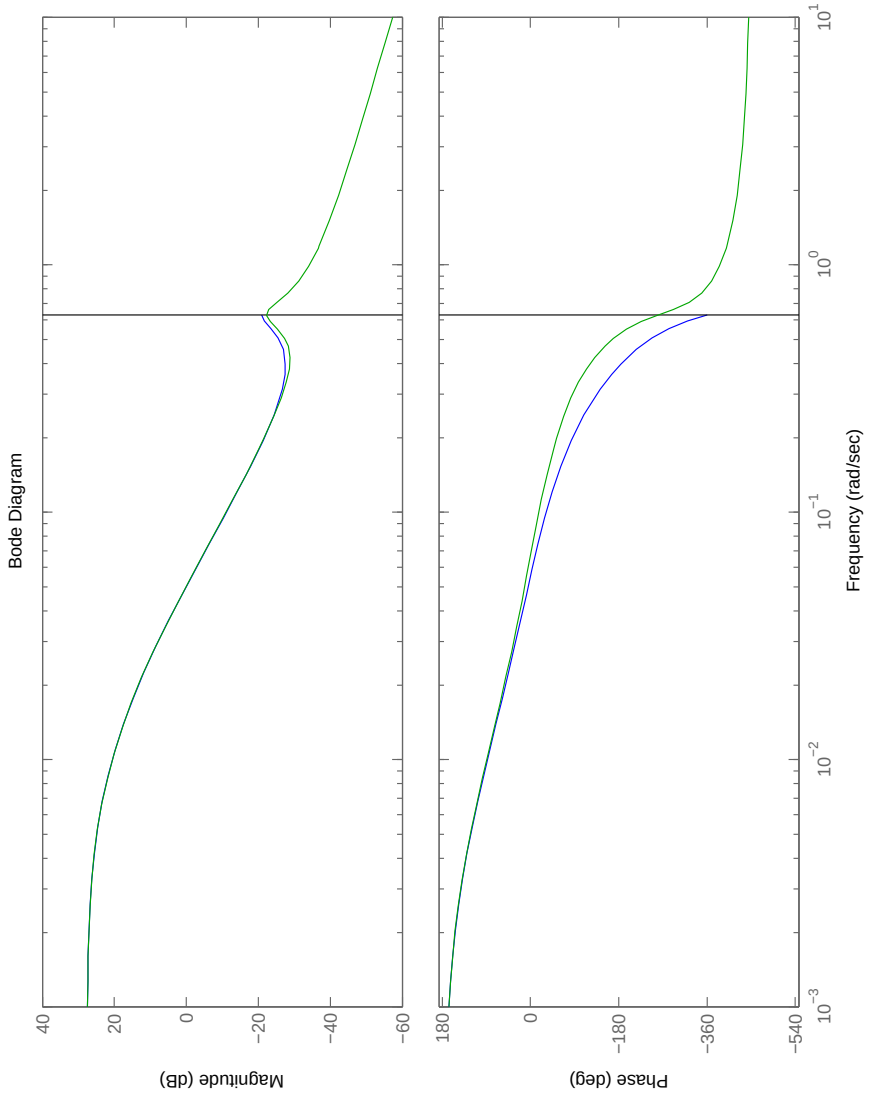

Figure 7.3: A Bode plot of the discrete and continuous system models for $Q = 30pph$ and $N = 320rpm$. The green curve is the continuous model, the blue is the discrete model.

Condition: Q 40 N 210

These are the results of the system identification for a throughput of 40 pounds per hour, and 210 *rpm*.

Parameter	Value
N_a (poles)	3
N_b (num coeff)	2
N_{delay}	16
time delay $[s]$	80
sampling time	5
system DC gain	-22.0116

Table 7.4: System Identification Results for $Q = 40pph$ and $N = 210rpm$.

The discrete transfer function with out time delay is:

$$H(s) = \frac{-0.4893}{z^3 - 1.091z^2 - 0.09166z + 0.2045} \tag{7.7}$$

Transforming the previous equation, the continuous transfer function with out time delay is:

$$G(s) = \frac{0.1092s^3 - 0.08527s^2 + 0.04529s - 0.008233}{s^4 + 0.4996s^3 + 0.4781s^2 + 0.05818s + 0.000374} \tag{7.8}$$

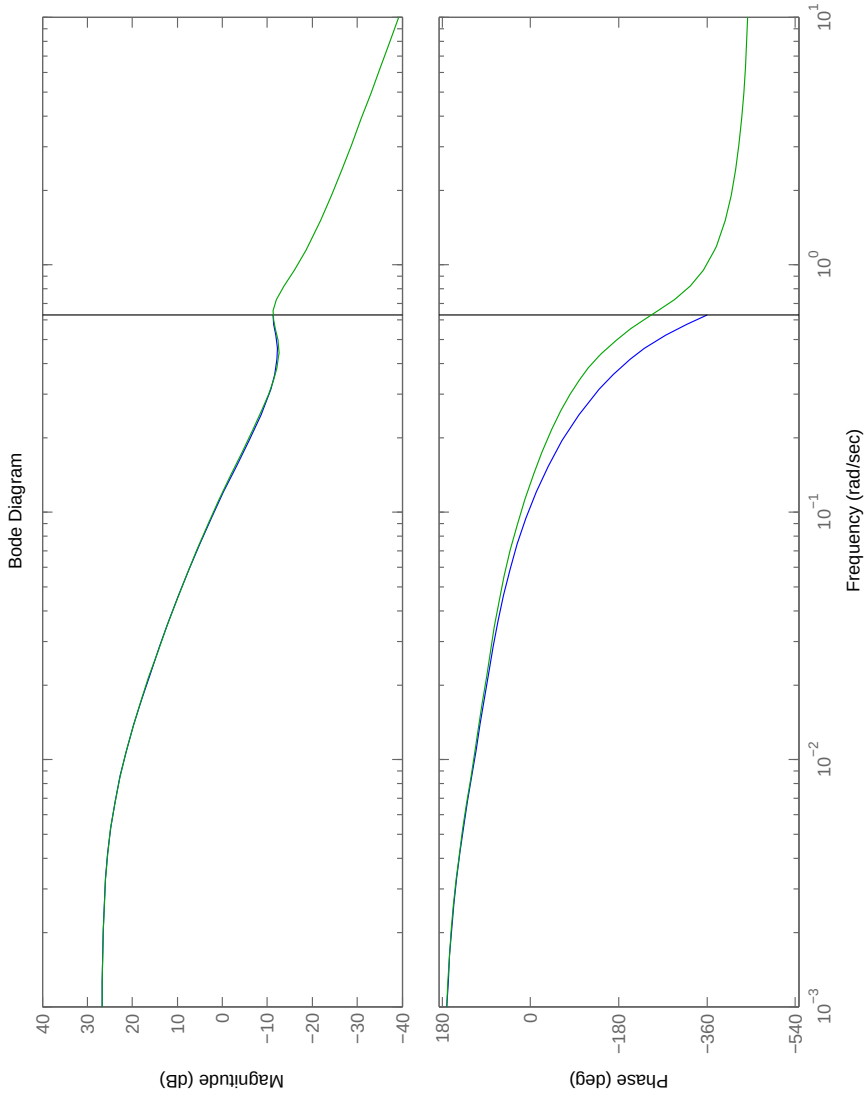

Figure 7.4: A Bode plot of the discrete and continuous system models for $Q = 40pph$ and $N = 210rpm$. The green curve is the continuous model, the blue is the discrete model.

Condition: Q 20 N 210

These are the results of the system identification for a throughput of 20 pounds per hour, and 210 *rpm*.

Parameter	Value
N_a (poles)	3
N_b (num coeff)	2
N_{delay}	18
time delay $[s]$	90
sampling time	5
system DC gain	-15.7582

Table 7.5: System Identification Results for $Q = 20pph$ and $N = 210rpm$.

The discrete transfer function with out time delay is:

$$H(s) = \frac{-0.09803}{z^3 - 1.17z^2 - 0.3405z + 0.5163} \tag{7.9}$$

Transforming the previous equation, the continuous transfer function with out time delay is:

$$G(s) = \frac{0.01377s^3 - 0.01004s^2 + 0.005562s - 0.00107}{s^4 + 0.2224s^3 + 0.4107s^2 + 0.01697s + 6.793e - 005} \tag{7.10}$$

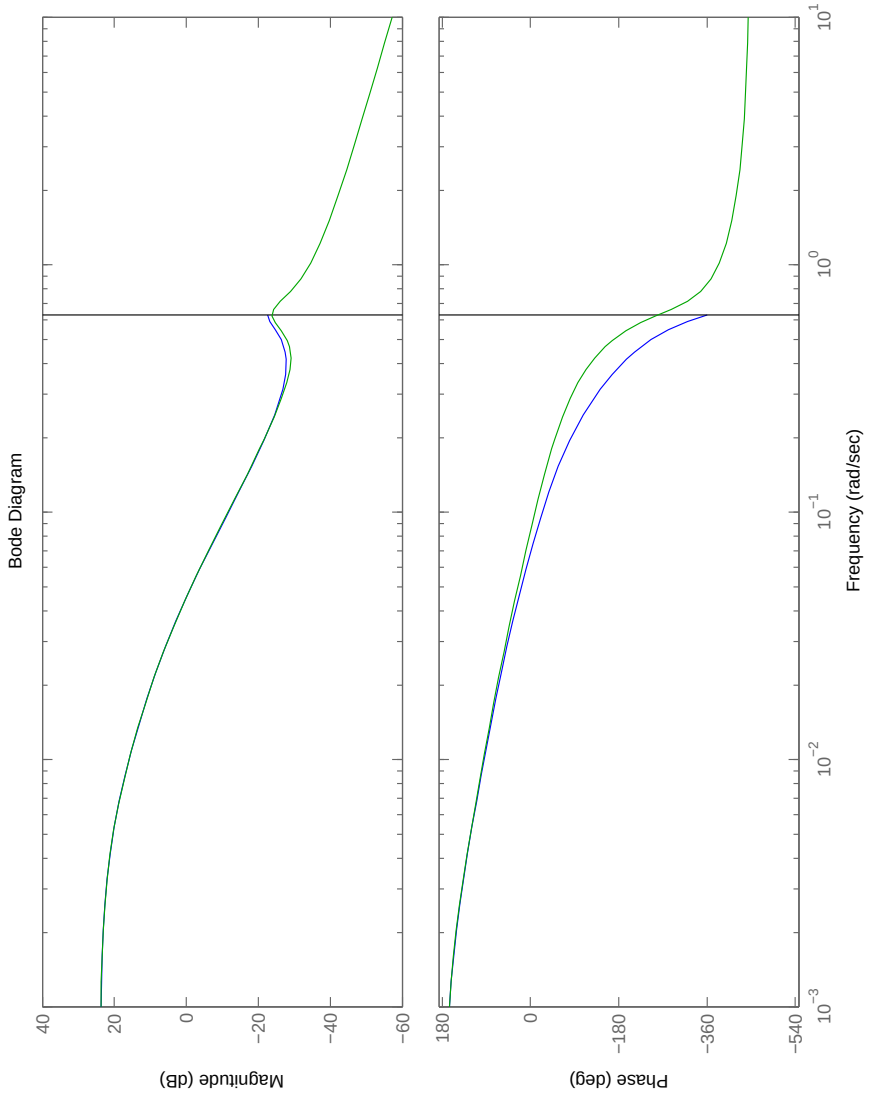

Figure 7.5: A Bode plot of the discrete and continuous system models for $Q = 20pph$ and $N = 210rpm$. The green curve is the continuous model, the blue is the discrete model.

Q	N	Q/N	t_m Z23	t_d	$t_d - t_m$	G_p
pph	rpm	mL/rev	s	s	s	
30	210	1.27	52.8	75	22.2	-21.9
30	160	1.68	56.6	85	28.4	-23.9
30	320	0.84	46.5	80	33.5	-24.0
40	210	1.70	42.3	80	37.7	-22.0
20	210	0.85	73.9	90	16.1	-15.8

Table 7.6: Some System Identification Results. t_m is the mean residence time. t_d is the delay time. G_p is the process gain.

7.2.3 Analysis of Results and Summary

Some results from the system identification are displayed in Table 7.6. The system analysis shows that the time delay for the system is from 75 to 90 seconds. Additionally, the delay from the viscometer, $t_d - t_m$, is from 16 to 37 seconds. The DC gain is mostly around -22. The Bode plots for the five transfer functions look similar as well. This agrees with work by Walsh et al. [1] which illustrates that the extruder can be looked at like a series of stirred tanks with time delays which would have three poles as well as time delays. Additionally, Figures 7.1, 7.2, 7.3, 7.4, and 7.5 show that the Bode plots for the discrete and continuous transfer functions for all the conditions are very similar, and they diverge close to $\frac{1}{2}\frac{rad}{s}$. In agreement with previous studies, the Bode plots show that low frequency disturbances do not get attenuated [1] as can be seen in Figure 2.1.

7.3 Conclusion

A method is described for finding a model of the dynamic reactive system. However, this system is based only on the statistics of the system and has no direct physical input. Due to this a model that also accounted for geometric effects was also studied (Chapter 8).

Chapter 8

A New Residence Distribution Model for Extruders

8.1 Derivation

With a more advanced experimental setup then previously available [15], it became possible to examine the RTD of each zone of the extruder. Continuing with the same screw design (Figure 4.1) as the previous work [14, 15], it is known that three fully-filled regions exist within the extruder.

For each individual partially filled and fully filled combination of the screw, Equation 8.1, a first order model, can describe the RTD curve. Again, a is the shape factor, and t_d the delay time.

$$G(s) = \frac{a_i e^{-s\left(t_{d_i}\right)}}{(s + a_i)} \tag{8.1}$$

Due to the uncoupled nature of the filled zones, n of Equation 8.1 can be convoluted n times to make Equation 8.2, an n^{th} order model, which describes a screw with n fully filled regions.

$$G(s) = \prod_{i=1}^{n} \frac{a_i e^{-s\left(t_{d_i}\right)}}{(s + a_i)} \tag{8.2}$$

In the time domain, for $n = 3$, Equation 8.2 becomes:

$$G(t) = a_1 a_2 a_3 \left[\begin{array}{l} \frac{e^{-a_1(t-t_d)}}{(a_3-a_1)(a_2-a_1)} \\ -\frac{e^{-a_2(t-t_d)}}{(a_3-a_2)(a_2-a_1)} \\ +\frac{e^{-a_3(t-t_d)}}{a_3^2+a_1 a_2-a_1 a_3-a_2 a_3} \end{array} \right] \tag{8.3}$$

Equation 8.3 applies for $t > t_d$, where $t_d = t_{d_1} + t_{d_2} + t_{d_3}$. When $t < t_d$, $G(t) = 0$. When Equations 2.5, 8.1, and 8.2 are expressed in the volume domain, they maintain a very similar form. Equation 8.2 becomes:

$$G(\hat{s}) = \prod_{i=1}^{n} \frac{c_i e^{-\hat{s}\left(v_{d_i}\right)}}{(\hat{s} + c_i)} \tag{8.4}$$

Similarly to Equation 2.6 the following transforms can be made:

$$\begin{aligned} c_i &= {}^{a_i}\!/_{Q} \\ v_{d_i} &= Q \cdot t_{d_i} \end{aligned} \tag{8.5}$$

Where v_{d_i} is the volume delay for each section i, and c_i is the volume domain shape factor for each section i. As mentioned earlier, when the RVD is used, the volume domain equivalent of Equation 2.5 provides a new shape factor, c, that is very similar over a range of conditions.

The model can also be shown in the revolution domain with the use of Equations 8.6.

$$\begin{aligned} b_i &= {}^{a_i}\!/_{N} \\ n_{d_i} &= N \cdot t_{d_i} \end{aligned} \tag{8.6}$$

Where n_{d_i} is the revolution delay for each section i, and b_i is the volume domain shape factor for each section i.

8.2 RTD Deconvolution Technique

For the experimental screw design, the extruder screw is analogous to a series of continuous stirred tank reactors (CSTR) with transport delay in between them. Where the partially filled regions are like the transport delays, and the fully filled regions are like the CSTR's. The partially filled regions uncouple the flow in one filled section from another.

The three reflectance probes provide us with RTD's for the melting portion, the melting and mixing portion, and the entire screw. To determine the response for any section other then the melting portion, we must deconvolve the signal from the probe located before it from the probe located within it. For example, the mixing sections signal is given by the deconvolution of the signal from the probe measuring the melting zone from the probe measuring the melting and mixing zones.

A nonlinear solver (Appendix C)was used to determine the parameters for Equation 8.1 that best fit the signal from probe 1. These parameters describe the melting zone. The parameters from this equation were used in Equation 8.2, $n = 2$, and the remaining parameters, for the mixing zone, were found by using the nonlinear solver to most closely match the signal from probe 2. The two sets of parameters for the melting and mixing zones were used in Equation 8.2, with $n = 3$, and the remaining parameters, for the metering zone, were found by using the nonlinear solver to most closely match the signal from probe 3.

8.2.1 Coupled Regions

An assumption of Equation 8.2 is that the different regions are uncoupled. This is necessary for the convolution of Equation 8.1 with itself to represent the CSTR's

in series. However, for the experimental plant, a viscometer is to be attached to the die. The filled regions within the extruder, which are connected by partially filled portions of the screw, are uncoupled. From the melt seal before the die to the exit of the viscometer, the system is fully filled. It cannot be assumed that the viscometer is uncoupled from the other regions of the extruder.

However, in spite of this, tests were performed to test the kinematics of the viscometer. An impulse response is not ideally suited for testing the viscometer, so step changes were used to find the parameters. The experimental setup had the peroxide additive introduced after the melting zone. The only regions to see the addition of the peroxide are the mixing, die and viscometer regions. So with and a step input, the inverse Laplace transform of Equation 8.2 can be made.

$$G(t) = a_1 a_2 a_3 \begin{bmatrix} \frac{1}{a_1 a_2 a_3} - \frac{e^{-a_1(t-t_d)}}{a_1(a_2-a_1)(a_3-a_1)} \\ \frac{e^{-a_2(t-t_d)}}{a_2(a_3-a_2)(a_2-a_1)} \\ -\frac{e^{-a_3(t-t_d)}}{a_3\left(a_1 a_2 - a_2 a_3 - a_1 a_3 + a_3^2\right)} \end{bmatrix} \tag{8.7}$$

The subscripts of Equation 9 are general, but in this case correspond to the mixing, die and viscometer regions. The parameters for the viscometer can be found by using the already found parameters for the mixing and die regions, and then solving for those of the viscometer region.

8.3 RTD Characterization Results

The results of the deconvolution can be seen in Table 8.1. Additionally, an example of the data and the curve fits can be seen in Figure 8.1. A calculation was performed to get the c_i from this set of experiments using Equations 8.5, and they are displayed in Table 8.2. A calculation was also performed to get the b_i

from this set of experiments using Equations 8.6, and they are displayed in Table 8.3. In the time domain, a smaller shape factor indicates more time spent in the associated region, while in the volume domain, a smaller shape factor indicates more volume spent in the associated region.

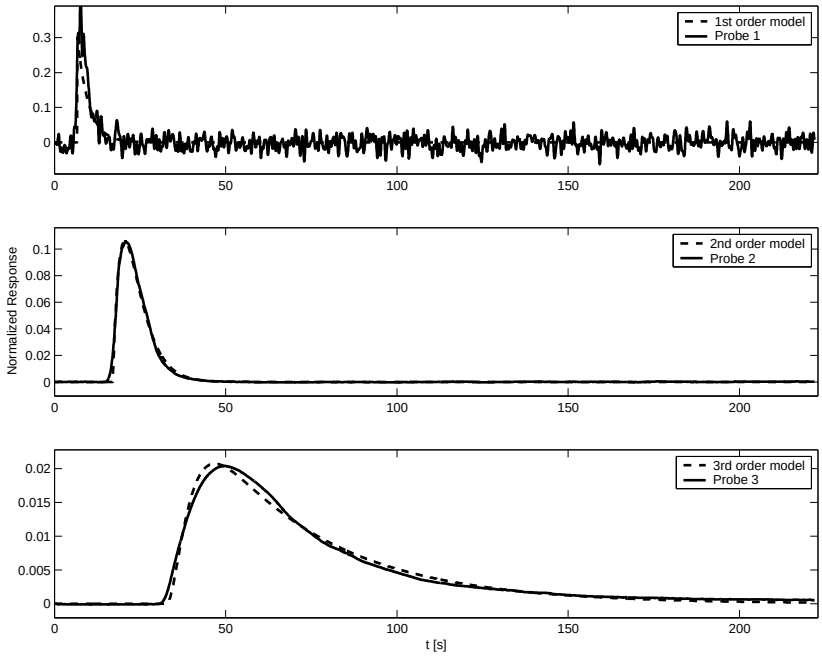

Figure 8.1: Example of model fits with Equation 8.2. The condition is 2.98 mL/s and 3.50 rps.

Equation 8.2 fits the RTD better then Equation 2.5. This can be seen in Figure 8.2 where the new rtd model better captures the shape of the data. When the sum of square errors are computed for each model compared to the filtered data, Equation 2.5 has a value of 5.6848×10^{-3} and Equation 8.2 has a value of 1.1024×10^{-3}. This is approximately 5.2 times larger and supports the conclusions drawn from the figure. The figure also illustrates how the extruder damps out the noise evident in Figure 8.1 from the melting region.

			Time Delays				Time Domain Shape Factor			
Q	N	Q/N	t_{d_1}	t_{d_2}	t_{d_3}	t_{d_4}	a_1	a_2	a_3	a_4
$[mL/s]$	$[rps]$	$[mL/rev]$	$[s]$	$[s]$	$[s]$	$[s]$	$[s^{-1}]$	$[s^{-1}]$	$[s^{-1}]$	$[s^{-1}]$
2.98	2.33	1.28	8.1	13.2	21.7	59.6	0.2571	0.2646	0.02505	0.005830
2.98	3.50	0.85	6.7	10.4	15.8	77.2	0.3012	0.2741	0.02868	0.006852
4.47	2.67	1.68	6.9	11.5	14.3	47.6	0.2653	0.5300	0.03624	0.005242
4.47	3.50	1.28	6.2	8.0	14.7	91.7	0.4475	0.3250	0.04539	0.007755
4.47	5.33	0.84	4.5	7.2	9.9	97.1	0.3308	0.3696	0.04414	0.010444
2.98	2.33	1.28	8.2	13.8	19.5		0.3163	0.2635	0.02685	
4.47	3.50	1.28	5.7	8.8	12.3		0.4218	0.3432	0.03462	
5.96	4.67	1.28	4.5	6.3	10.5		0.4338	0.5298	0.05464	

Table 8.1: Time delays and first order time shape factors for the experimental extruder. Zones 1, 2, 3, and 4 are respectively the melting, mixing, die, and viscometer zones. The experimental material is PDC1277.

			Volume Delays				Volume Domain Shape Factor			
Q	N	Q/N	v_{d_1}	v_{d_2}	v_{d_3}	v_{d_4}	c_1	c_2	c_3	c_4
$[mL/s]$	$[rps]$	$[mL/rev]$	$[mL]$	$[mL]$	$[mL]$	$[mL]$	$[mL^{-1}]$	$[mL^{-1}]$	$[mL^{-1}]$	$[mL^{-1}]$
2.98	2.33	1.28	24.1	39.4	64.8	177.5	0.08627	0.08878	0.008406	0.001956
2.98	3.50	0.85	20.0	30.9	47.0	230.2	0.10105	0.09196	0.009623	0.002299
4.47	2.67	1.68	30.8	51.4	64.0	212.7	0.05933	0.11856	0.008105	0.001172
4.47	3.50	1.28	27.5	35.7	65.9	409.8	0.10011	0.07270	0.010152	0.001735
4.47	5.33	0.84	19.9	32.4	44.2	434.0	0.07399	0.08266	0.009873	0.002336
2.98	2.33	1.28	24.4	41.3	58.1		0.10611	0.08841	0.009009	
4.47	3.50	1.28	25.7	39.2	54.9		0.09434	0.07676	0.007743	
5.96	4.67	1.28	26.8	37.7	62.8		0.07277	0.08889	0.009166	

Table 8.2: Volume delays and first order volume shape factors for the experimental extruder. Zones 1, 2, 3, and 4 are respectively the melting, mixing, die, and viscometer zones. The experimental material is PDC1277.

			Revolution Delays				Revolution Domain Shape Factor			
Q	N	Q/N	n_{d_1}	n_{d_2}	n_{d_3}	n_{d_4}	b_1	b_2	b_3	b_4
$[mL/s]$	$[rps]$	$[mL/rev]$	$[rev]$	$[rev]$	$[rev]$	$[rev]$	$[rev^{-1}]$	$[rev^{-1}]$	$[rev^{-1}]$	$[rev^{-1}]$
2.98	2.33	1.28	18.9	30.9	50.7	139.0	0.11020	0.11340	0.010738	0.002499
2.98	3.50	0.85	23.5	36.2	55.2	270.3	0.08605	0.07831	0.008194	0.001958
4.47	2.67	1.68	18.4	30.7	38.2	126.9	0.09947	0.19877	0.013588	0.001966
4.47	3.50	1.28	21.5	28.0	51.6	320.8	0.12787	0.09286	0.012967	0.002216
4.47	5.33	0.84	23.7	38.6	52.7	517.7	0.06202	0.06929	0.008276	0.001958
2.98	2.33	1.28	19.1	32.3	45.5		0.13554	0.11292	0.011507	
4.47	3.50	1.28	20.1	30.7	43.0		0.12051	0.09805	0.009891	
5.96	4.67	1.28	21.0	29.5	49.2		0.09295	0.11353	0.011708	

Table 8.3: Revolution delays and first order revolution shape factors for the experimental extruder. Zones 1, 2, 3, and 4 are respectively the melting, mixing, die, and viscometer zones. The experimental material is PDC1277.

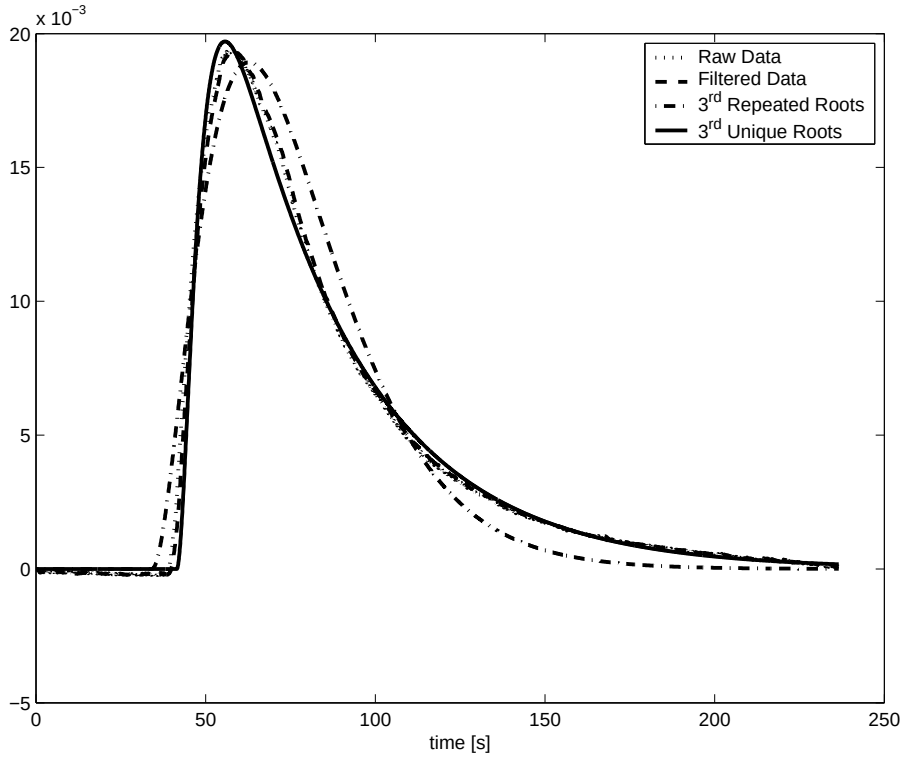

Figure 8.2: Comparison of RTD data and model fits. The operating condition is 2.98 mL/s and 2.33 rps. The figure shows a curve, "Raw Data", from a single experiment and a curve, "Filtered Data", that is made by averaging and filtering three replicates of RTD's at the given operating condition. The "3^{rd} Repeated Roots" curve shows results using Equation 2.5. The "3^{rd} Unique Roots" curve shows results using Equation 8.2.

Table 8.4 displays the means and the standard deviations of the various shape factors. The time domain shape factors have standard deviations of on the order of 30%, while those of the volume domain shape factors are 19.1%, 15.6%, and 9.6% for the melting, mixing and die zones respectively. This difference indicates two things. First, the volume domain is another valid domain with which to use this model. These shape factors are much more consistent then those of the time domain. Second, the melting and the mixing zone are not as consistent as the metering zone. This variability does not necessarily preclude this model from being used in the volume domain for other operating conditions.

The root of this higher consistency has to do with the nature of the solution method. The first zone to be solved for is the melting zone. This zone is not nearly as well behaved as the other two regions. It is noisy and not as consistently shaped. This behavior is probably due to the variability of the physical process. This adds variability to the shape factor determination. Additionally, this variability impacts the determination for the melting zone, as that solution is dependent on the previous one.

This solution technique does have a great advantage over using a single probe and Equation 2.5. When using Equations 8.1 and 8.2, constants that represent the behavior of the different regions are developed. This allows for description of a portion of the whole screw without new experimentation. For example, to describe the response of the screw described by the mixing and metering sections, one could use Equation 8.2 with the corresponding variables. This type of situation could occur when side-stuffing material after the melt zone. The ability to determine individual responses of each zone is an advantage where that zone is critical to the ultimate product quality, such as in reactive processing.

	Time Domain Shape Factor				Volume Domain Shape Factor				Revolution Domain Shape Factor			
	a_1 $[s^{-1}]$	a_2 $[s^{-1}]$	a_3 $[s^{-1}]$	a_4 $[s^{-1}]$	c_1 $[mL^{-1}]$	c_2 $[mL^{-1}]$	c_3 $[mL^{-1}]$	c_4 $[mL^{-1}]$	b_1 $[rev^{-1}]$	b_2 $[rev^{-1}]$	b_3 $[rev^{-1}]$	b_4 $[rev^{-1}]$
Mean	0.3467	0.3625	0.03695	0.007224	0.08675	0.08859	0.009010	0.001900	0.10433	0.10964	0.010859	0.002119
Std. Devn.	0.0768	0.1103	0.01038	0.002041	0.01659	0.01382	0.000865	0.000477	0.02421	0.03966	0.001991	0.000239
% Std. Devn.	22.2%	30.4%	28.1%	28.2%	19.1%	15.6%	9.6%	25.1%	23.2%	36.2%	18.3%	11.3%

Table 8.4: Means of different shape factors. c_2 and c_3 which represent zones of interest for the reactive extrusion show a great deal of uniformity. The fourth region, representing the viscometer, seems to be consistent with respect to the revolution domain.

For automatic control purposes, Equation 8.4 has many advantages. Only one control scheme would need to be determined, because one set of parameters can describe a family of curves. This allows for more general use of the extruder, and simplifies its control.

The viscometer was also characterized to find a shape factor and delay (Tables 8.1, 8.2 & 8.3). The delay introduced by the viscometer is much greater then that of the different screw regions. Table 8.4 also shows statistical information for the viscometer parameters, and it can be seen that in the revolution domain, the most consistency of the shape factor is seen.

8.4 Conclusion

A new kinematic RTD model is described (Equations 8.1 and 8.2). This model allows for the individual description of the zones of the extruder through a shape factor and a delay time. Determination of the parameters is performed by deconvolution of the reflectance probe signals. The deconvolution process allows for the determination of individual zones from probes describing composite regions of the screw.

When this model is used in the volume domain, the corresponding RVD description, Equation 8.4 is made. It possesses parameters that are consistent over a broad range of conditions, and allow for description of the family of curves with one set of parameters. This simplification of the extruder description can make other tasks simpler to analyze.

Chapter 9

Residence Distribution and Rheology for Different Materials in Extrusion

9.1 Introduction

Residence time distributions are often used to characterize and compare process devices and process materials. Danckwerts [8] explains how a distribution function such as the RTD can be defined and measured, additionally various calculations are provided for understanding the information supplied by the distribution functions. The RTD is the distribution of how long material takes to pass a given point. The RTD is utile for describing an extruder as the mixing quality and the average time that a polymer stays inside an extruder directly affect the quality of the extrudate. The axial mixing (fluid flow patterns) taking place in a CoTSE is influenced by and related to the processed material, the operating conditions and the screw geometry, and these factors can also affect the RTD. Modeling of these distributions has been pursued because characterizing processes can be costly. The dynamic description of the process available from the RTD is also useful for automatic control applications.

Previous work has been performed that investigates geometric effects as well

as operating conditions upon the RTD in extrusion systems. RTD's have also been used as kinematic basis for automatic control systems [1]. However, the ramifications on the change of material are not yet obvious with regards to the similarity of RTD's, or if one group of RTD's can be substituted for another.

Data have shown that, for the same extruder at the same conditions, two different materials could give very similar RTD's. In order to investigate this, data from experiments to characterize the Residence Time Distribution from various experiments on the same machine, but with different materials: Two viscosities of polypropylene (PP): Montell KF6100, and Basell PDC1277 were used; and two viscosities of polyethylene (PE): Alathon HDPE 6018, and Alathon HDPE 6060 were used. Tables and figures show the results of experiments to characterize residence distributions as well as the complex viscosity of the materials. The complex viscosities were studied to help explain the results of the residence distribution studies.

9.2 Experiment Setup

Experiments were performed on a Werner & Pfleiderer 30mm CoTSE. The screw design can be seen in Figure 4.1. This is the same screw as screw number 2 from Gao et al. [14]. The extruder screw is designed such that there existed three regions of complete melt fill. These were the melting, mixing, and die zones. These are listed in the order that freshly added polymer would be exposed to them. Each is created by a pressure obstruction being placed on the screw. In the case of the first two, a reverse thread screw element is used. In the case of the third, the die hole pressure causes the fluid build up. Montell KF6100 and Basell PDC1277 polypropylenes were used as well as Alathon HDPE 6018 and Alathon

HDPE 6060. Processing was performed at 210C and 180C for the polypropylenes and polyethylenes respectively.

In addition to typical instrumentation like melt pressure transducers and thermocouples, it was desired to measure the RTD. The RTD can be measured by taking samples periodically and performing tests off-line, or through on-line measurement. Gendron et al. [22] have shown how an in-line ultrasonic sensor can be used to measure the RTD. However, for these experiments, the extruder had a reflectance probe to measure the reflectance of the molten polymer for measuring RTD's, as described by Wetzel et al. [9]. It was located at the center of the extruder in the die zone. The RTD's were measured by adding premixed pellets containing TiO_2. This addition can be considered an impulse response because the additional material is negligible in comparison to the main feed, and it should not change the flow properties. The data acquisition system samples the data at $60hz$. It is then down sampled to $20hz$ and stored on a personal computer. Three replicates were taken. The data was averaged and normalized such that the area under the curve was the unit area. RTD's were performed for numerous conditions.

The analysis of the RTD data involved capturing the RTD using light reflectance probes place at the die and mixing zones, and then fitting the data to a model (Equation 5.1) to get a shape factor, a, and a delay time, t_d. This equation can also be expressed in the volume and revolution domains, which yields the shape factors c and b respectively.

The four polymers were also examined using a Rheometrics RDA-III. For each material, two tests were performed at the corresponding processing temperature. The rheometry measurement used a frequency sweep experiment with 5% strain

amplitude that is held constant. The averages of the two tests are reported.

9.3 Results

Inspecting RTD curves (Figures 9.1, 9.2, 9.3, & 9.4) reveals that the residence time increases with decreasing screw speed, and decreasing material flow rate. The RVD curves (Figures 9.5, 9.6, 9.7, & 9.8) generally collapse to one curve when the delay is removed, although the KF6100 material seems to have more variation. The RRD curves (Figures 9.9, 9.10, 9.11, & 9.12) behave typically, and have the peaks of the curves lining up for the same specific throughput, Q/N, and they show more rotations necessary for lower specific throughputs.

The shape factors were computed for each material (Tables 9.1, 9.2, 9.3, & 9.4). The shape factor is a convenient tool for quantitatively comparing different curves. Similar shape factors indicate similar curves. The standard deviation of the volume shape factor for KF6100 was an order of magnitude higher then the others (Table 9.5). When outliers are removed, Table 9.5 also shows that the standard deviation is still at least double any other standard deviation at approximately 17%. The two PE's share similar mean shape factors, whereas the PDC1277 has the smallest, and the KF6100 has the largest.

To help explain the variability in c for KF6100, the volume domain shape factor can be compared against the operating conditions. The one with the most effect is the screw speed, N. Figure 9.13 shows that c is partially dependent on N. The $R^2 = 0.44$ for the linear regression indicates that N explains some of the variability. This dependence on N indicates that the elastic behavior of the KF6100 plays an important role. The shear rate in the fluid channel is directly proportional to the screw speed (Equation 9.4. The partial correlation

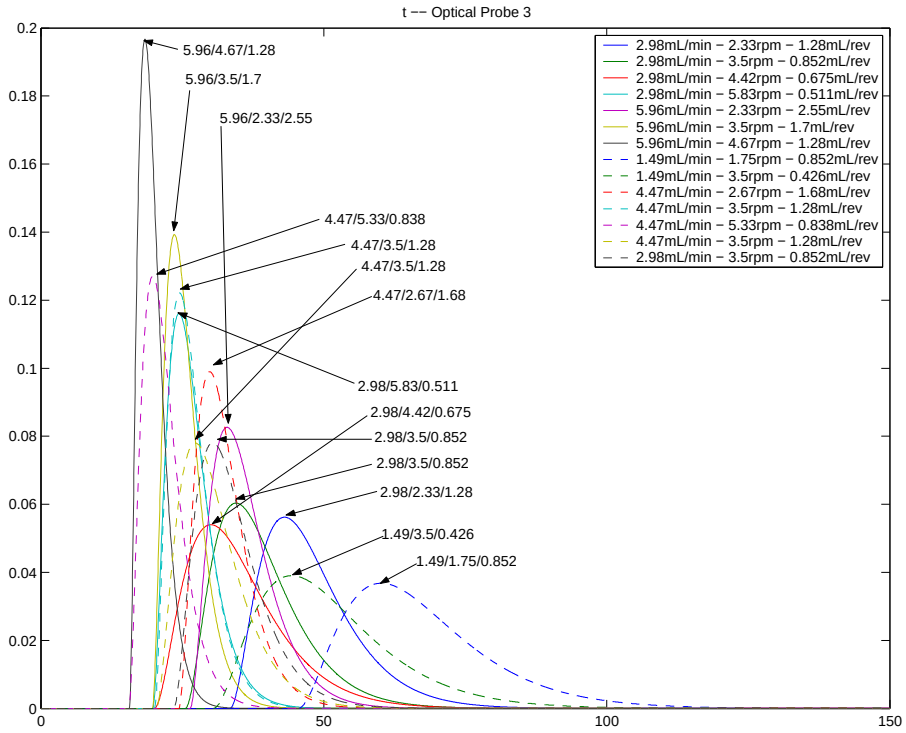

Figure 9.1: Residence time distributions for KF6100 at various operating conditions.

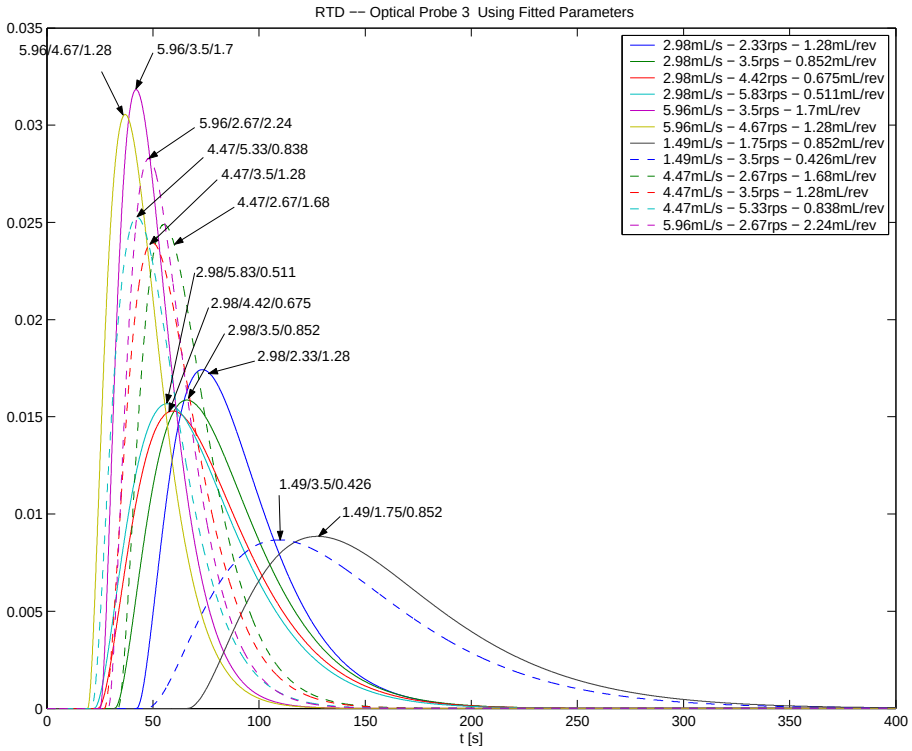

Figure 9.2: Residence time distributions for PDC1277 at various operating conditions.

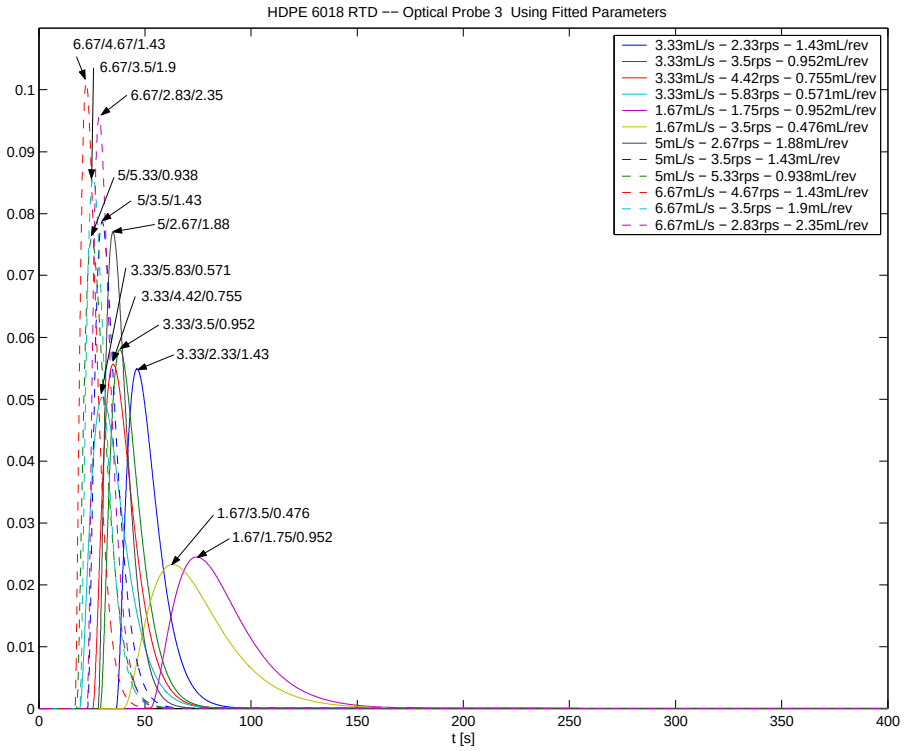

Figure 9.3: Residence time distributions for HDPE6018 at various operating conditions.

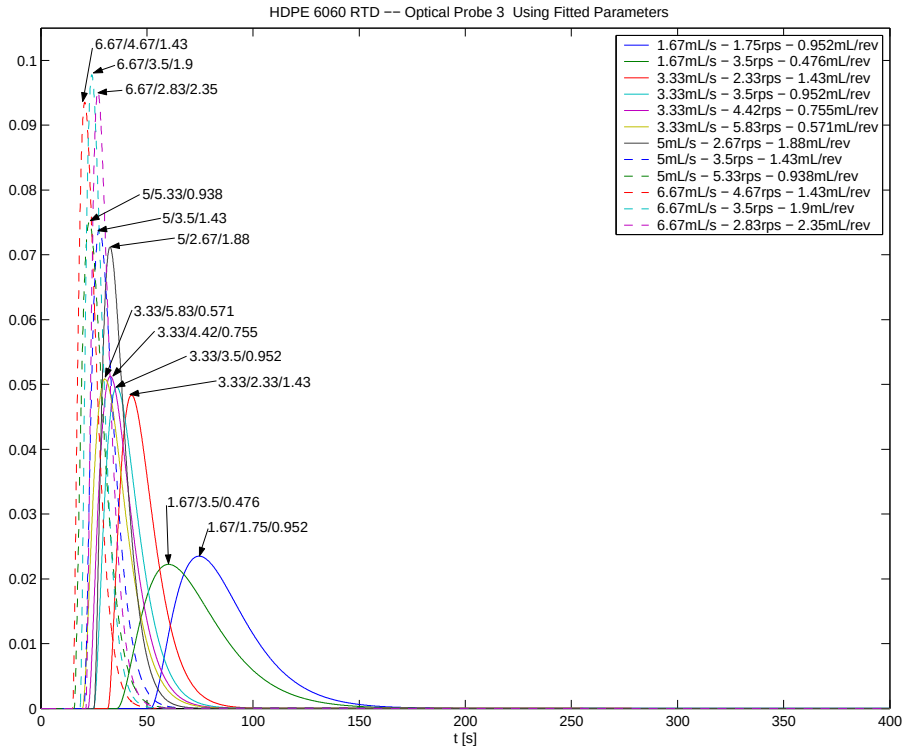

Figure 9.4: Residence time distributions for HDPE6060 at various operating conditions.

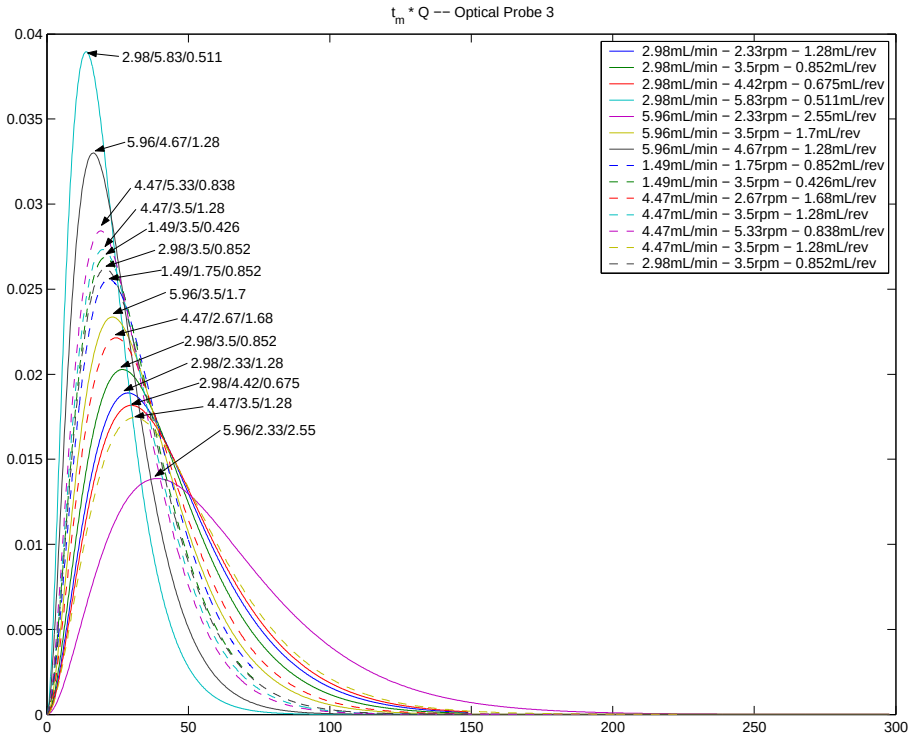

Figure 9.5: Residence volume distributions for KF6100 at various operating conditions.

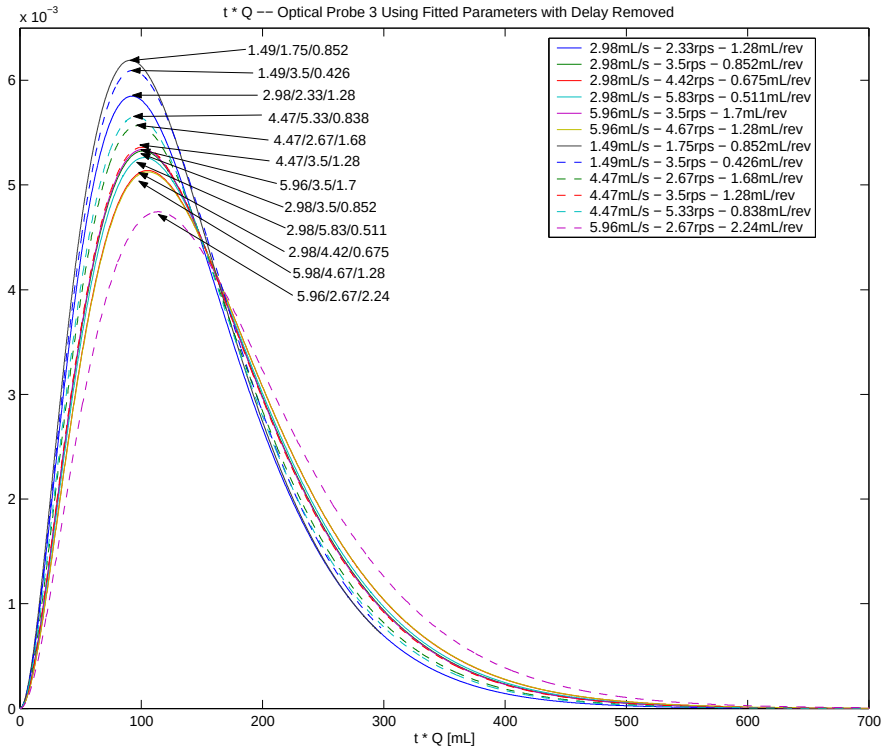

Figure 9.6: Residence volume distributions for PDC1277 at various operating conditions.

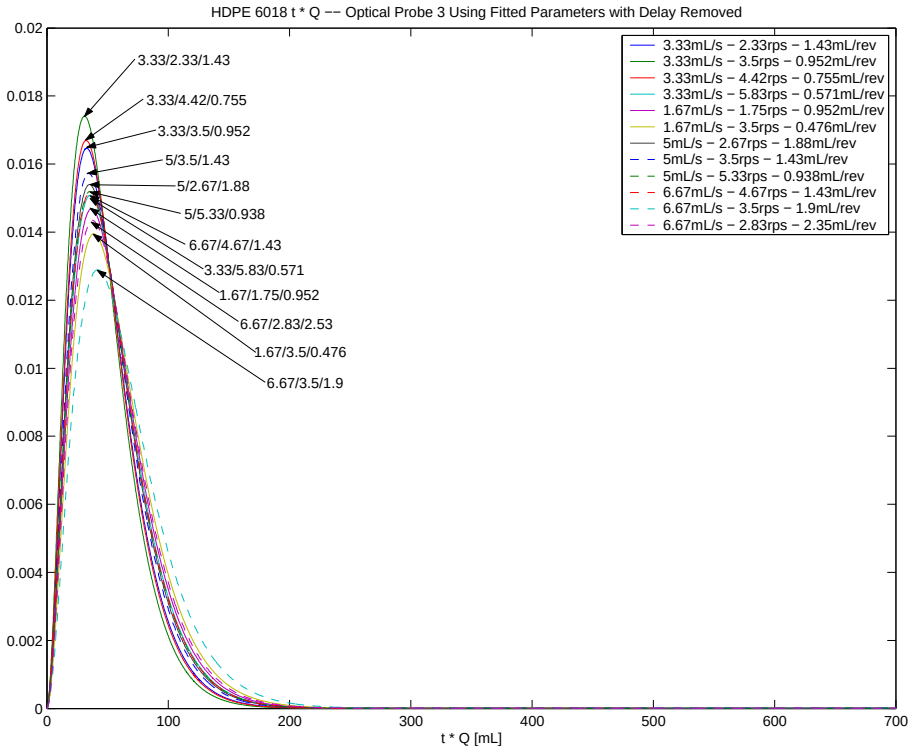

Figure 9.7: Residence volume distributions for HDPE6018 at various operating conditions.

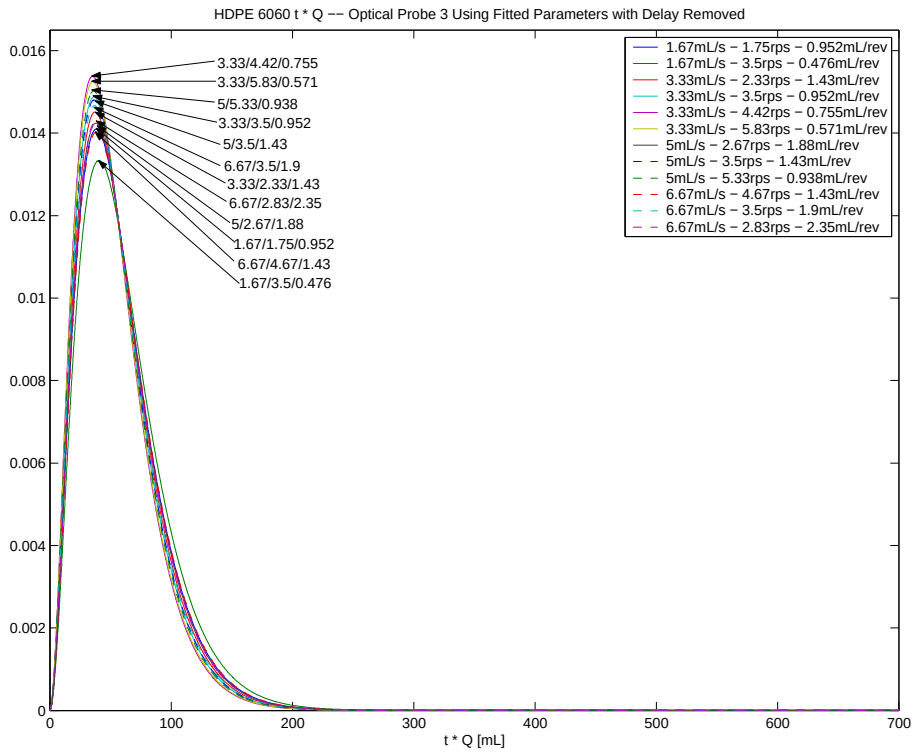

Figure 9.8: Residence volume distributions for HDPE6060 at various operating conditions.

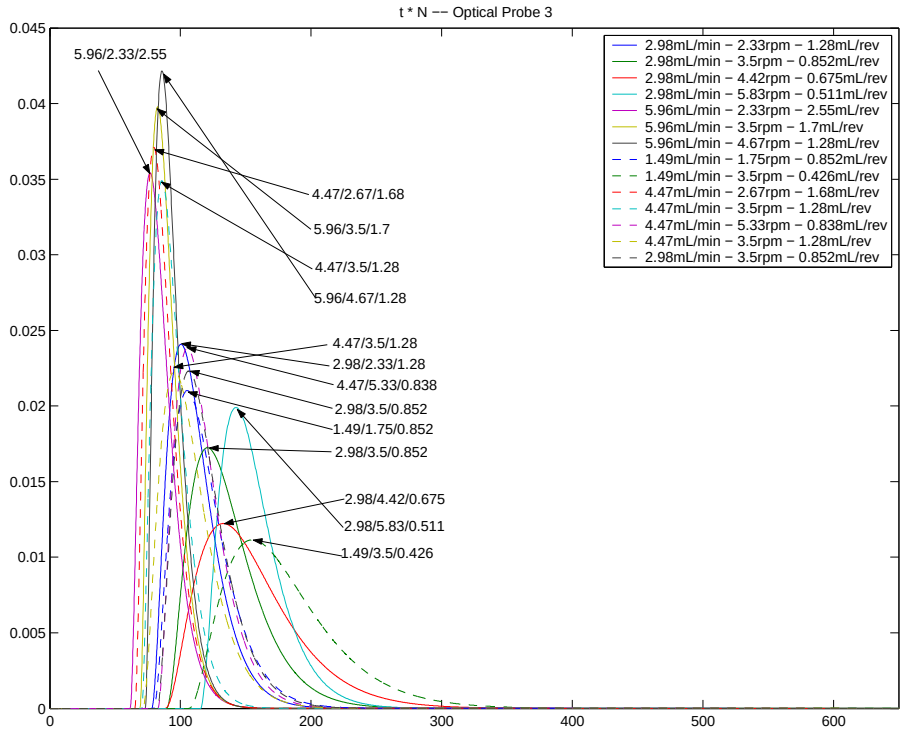

Figure 9.9: Residence rotation distributions for KF6100 at various operating conditions.

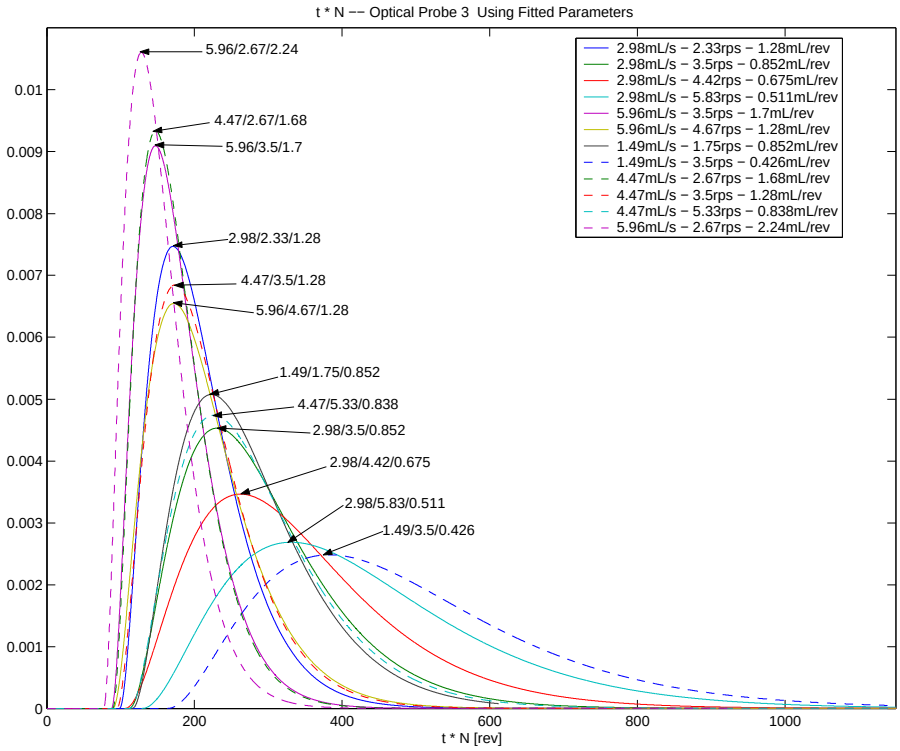

Figure 9.10: Residence rotation distributions for PDC1277 at various operating conditions.

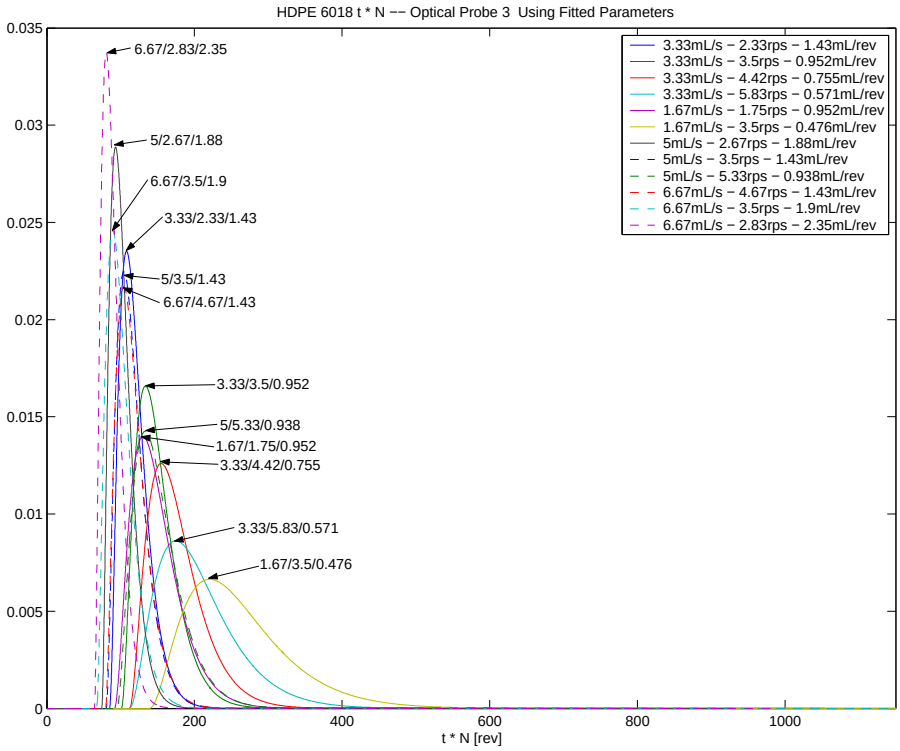

Figure 9.11: Residence rotation distributions for HDPE6018 at various operating conditions.

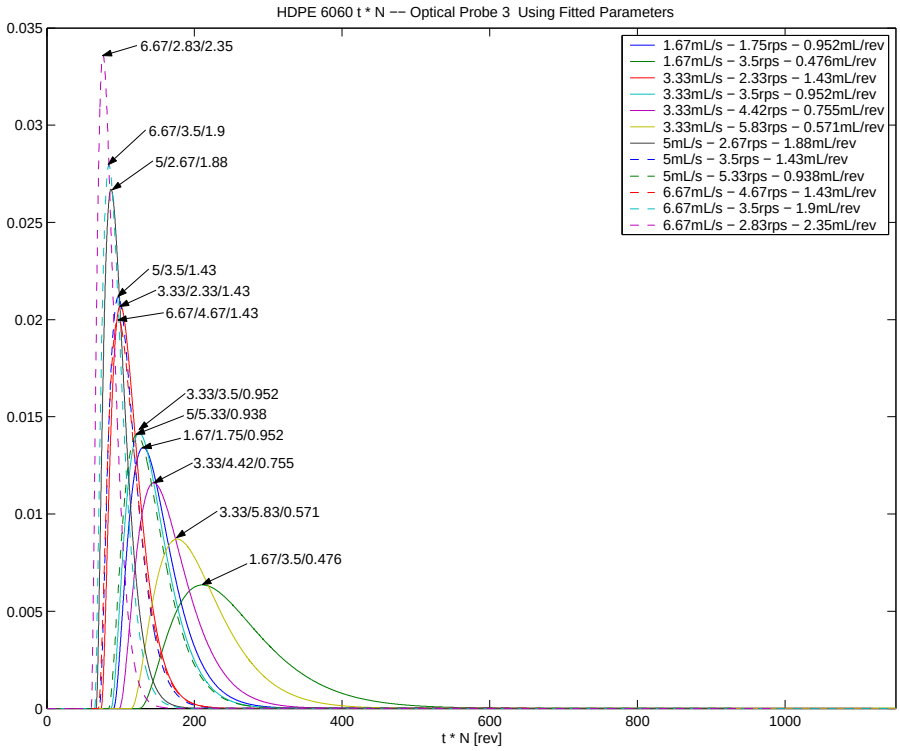

Figure 9.12: Residence rotation distributions for HDPE6060 at various operating conditions.

Q $[mL/s]$	N $[rps]$	Q/N $[mL/rev]$	a $[s^{-1}]$	c $[mL^{-1}]$	t_d $[s]$	t_m $[s]$
1.49	1.75	0.85	0.1359	0.0912	45.4	67.5
1.49	3.50	0.43	0.1442	0.0968	30.4	51.3
2.98	2.33	1.28	0.2077	0.0697	33.4	47.9
2.98	3.50	0.85	0.2230	0.0748	25.5	39.0
2.98	3.50	0.85	0.2885	0.0968	23.5	33.9
2.98	4.42	0.67	0.1995	0.0669	20.0	35.1
2.98	5.83	0.51	0.4289	0.1439	19.8	26.8
4.47	2.67	1.68	0.3657	0.0818	24.4	32.6
4.47	3.50	1.28	0.4513	0.1009	20.1	26.7
4.47	3.50	1.28	0.2883	0.0645	20.3	30.8
4.47	5.33	0.84	0.4694	0.1050	15.5	21.9
5.96	2.33	2.55	0.3053	0.0512	26.4	36.2
5.96	3.50	1.70	0.5145	0.0863	19.7	25.5
5.96	4.67	1.28	0.7268	0.1219	15.6	19.8

Table 9.1: KF6100 fits to Equation 2.9.

Q $[mL/s]$	N $[rps]$	Q/N $[mL/rev]$	a $[s^{-1}]$	c $[mL^{-1}]$	t_d $[s]$	t_m $[s]$
1.49	1.75	0.85	0.0327	0.0219	66.4	156.5
1.49	3.50	0.43	0.0320	0.0215	46.9	139.3
2.98	2.33	1.28	0.0644	0.0216	42.3	88.7
2.98	3.50	0.85	0.0586	0.0197	31.9	82.8
2.98	4.42	0.67	0.0565	0.0190	24.1	76.9
2.98	5.83	0.51	0.0579	0.0194	22.2	73.8
4.47	2.67	1.68	0.0920	0.0206	33.5	66.1
4.47	3.50	1.28	0.0885	0.0198	27.1	61.0
4.47	5.33	0.84	0.0934	0.0209	21.0	53.2
5.96	2.67	2.24	0.1045	0.0175	28.9	57.6
5.96	3.50	1.70	0.1176	0.0197	25.1	50.6
5.96	4.67	1.28	0.1129	0.0189	19.2	45.8

Table 9.2: PDC1277 fits to Equation 2.9.

Q	N	Q/N	a	c	t_d	t_m
$[mL/s]$	$[rps]$	$[mL/rev]$	$[s^{-1}]$	$[mL^{-1}]$	$[s]$	$[s]$
1.67	1.75	0.95	0.0904	0.0542	52.3	85.4
1.67	3.50	0.48	0.0859	0.0515	39.8	74.7
3.33	2.33	1.43	0.2028	0.0608	36.4	51.2
3.33	3.50	0.95	0.2144	0.0643	28.9	42.9
3.33	4.42	0.75	0.2056	0.0617	25.3	39.9
3.33	5.83	0.57	0.1858	0.0557	19.2	35.3
5.00	2.67	1.87	0.2844	0.0569	27.9	38.4
5.00	3.50	1.43	0.2906	0.0581	22.9	33.3
5.00	5.33	0.94	0.2808	0.0562	17.8	28.5
6.67	2.83	2.35	0.3532	0.0530	22.7	31.2
6.67	3.50	1.90	0.3175	0.0476	19.3	28.7
6.67	4.67	1.43	0.3737	0.0561	17.0	25.0

Table 9.3: HDPE6018 fits to Equation 2.9.

Q $[mL/s]$	N $[rps]$	Q/N $[mL/rev]$	a $[s^{-1}]$	c $[mL^{-1}]$	t_d $[s]$	t_m $[s]$
1.67	1.75	0.95	0.0868	0.0521	51.6	86.1
1.67	3.50	0.48	0.0821	0.0493	35.9	72.4
3.33	2.33	1.43	0.1787	0.0536	31.5	48.3
3.33	3.50	0.95	0.1832	0.0550	24.8	41.2
3.33	4.42	0.75	0.1894	0.0568	22.2	38.1
3.33	5.83	0.57	0.1878	0.0563	19.6	35.6
5.00	2.67	1.87	0.2631	0.0526	25.0	36.4
5.00	3.50	1.43	0.2735	0.0547	20.3	31.3
5.00	5.33	0.94	0.2775	0.0555	15.7	26.5
6.67	2.83	2.35	0.3517	0.0528	21.2	29.7
6.67	3.50	1.90	0.3612	0.0542	18.5	26.8
6.67	4.67	1.43	0.3456	0.0518	14.9	23.6

Table 9.4: HDPE6060 fits to Equation 2.9.

Material	Mean mL^{-1}	Standard Deviation	% Std. Deviation
KF6100	0.0894	0.0244	27.30%
KF6100*	0.0850	0.0144	16.91%
PDC1277	0.0200	0.0013	6.50%
HDPE6018	0.0564	0.0046	8.14%
HDPE6060	0.0538	0.0022	4.14%

Table 9.5: Mean volume shape factors, c, for various materials. KF6100* is without outliers greater than $0.12mL^{-1}$ and less than $0.06mL^{-1}$.

with screw speed indicates that viscoelastic effects are important to the behavior of the KF6100 melt.

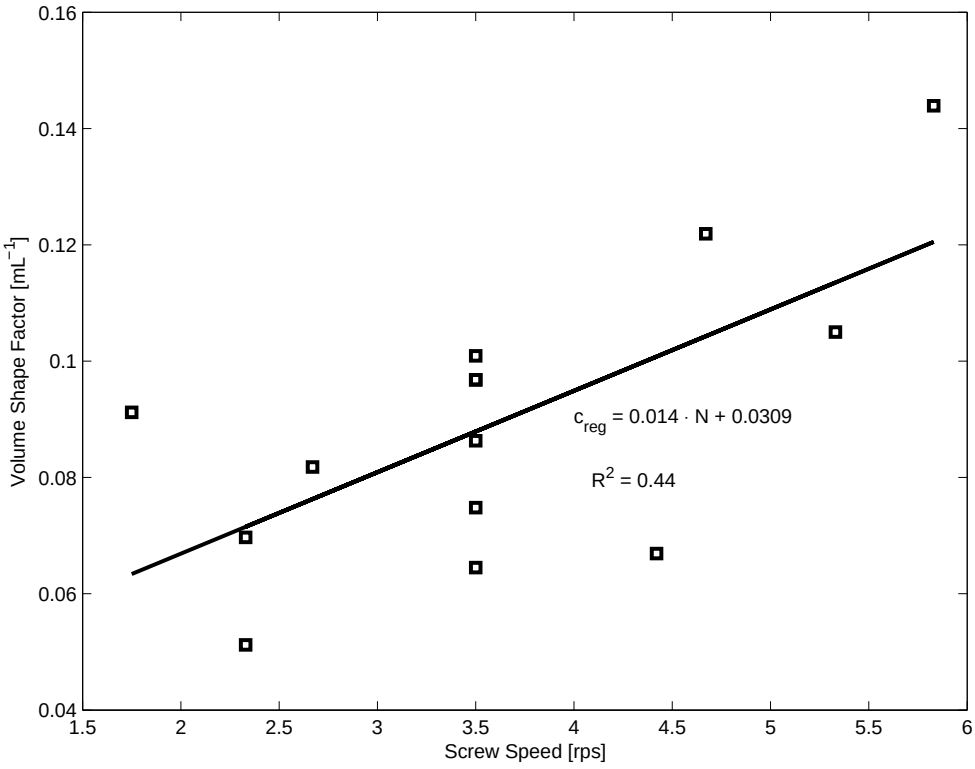

Figure 9.13: c vs. N for KF6100.

The behavior of the PE's as indicated by their respective family of t_m's (Tables 9.3 and 9.4) and their curves (Figure 9.14) do not support the concept that decreasing material viscosities would yield longer residence times as indicated by the t_m's when this is done by using lower viscosity materials [23]; and would indicate that the concept is not absolute. The PP's, which had similar viscosity curves, did not share similar curves.

The data can also be plotted on the axes $t_m N$ vs. N/Q (Figure 9.14) [13, 14]. The curves for the polyethylenes are very similar. This illustrates again how similar their RTD's are, as well as indicating that those systems have similar

filled volumes. In contrast, the polypropylenes have very different curves.

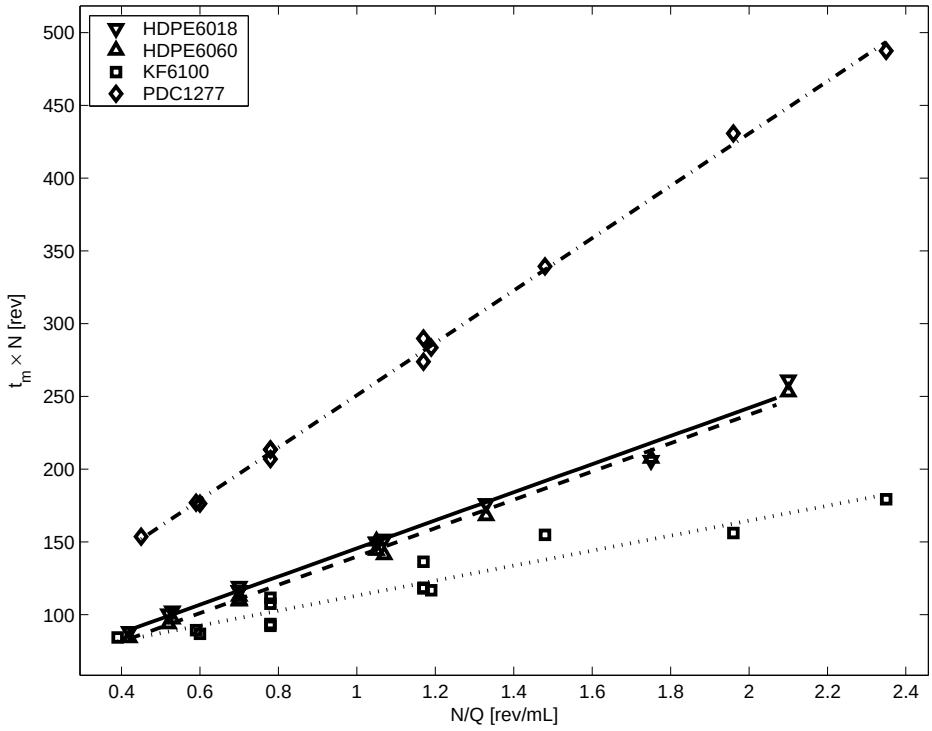

Figure 9.14: Mean number of rotations versus inverse of specific throughput for four studied polymers.

The viscosity testing (Figures 9.15, 9.16, & 9.18) showed that the PE's had very different viscosities, but with similar viscous behavior. Additionally, Figure 9.17, which plots the moduli against each other, shows a straight line in the $\log - \log$ domain indicating a power law relationship. The PP's showed more elastic behavior, and had very similar viscosities. Figure 9.19 illustrates this by taking the root square of the viscosity differences at each sampled frequency, for each type of material. It further emphasized the large viscosity difference of the PE's and the similarity of the PP's. This also does not explain the difference in

the volume domain residence, but could help explain the different lines exhibited in Figure 9.14.

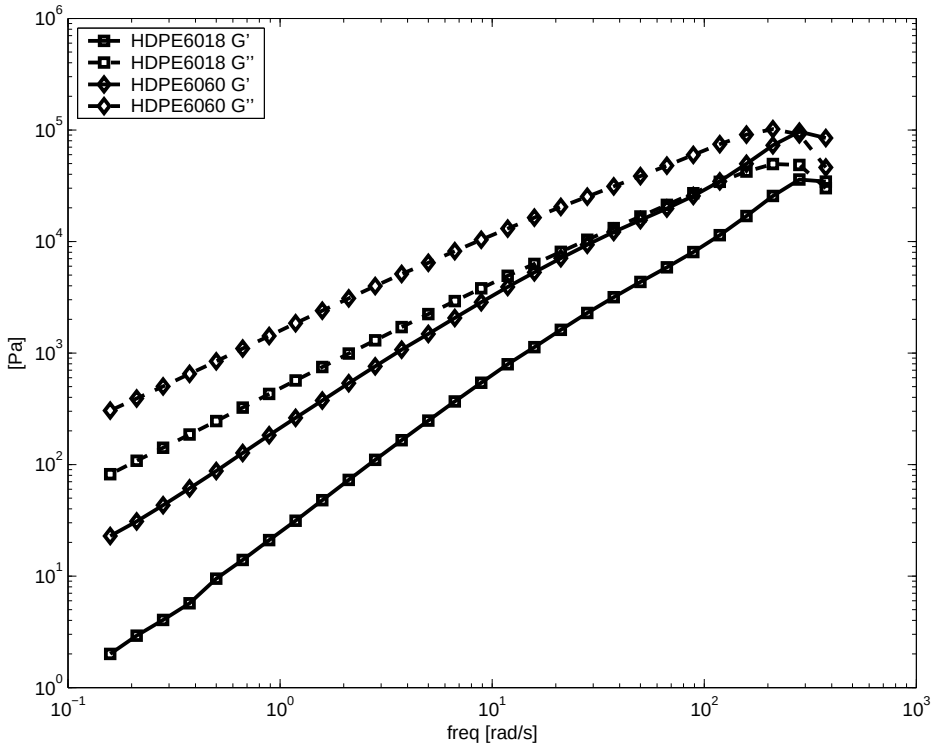

Figure 9.15: Storage and loss moduli for polyethylene samples.

9.4 Dimensionless Number Calculations

Two dimensionless numbers are very useful to gain understanding into viscoelastic flows. They are the Deborah number and the Weissenberg number. The Deborah number is a dimensionless number used to characterize how fluid a material is (Equation 9.1). It is computed as the quotient of the relaxation time of the material, λ, and a characteristic time of the flow, t_c. A Deborah number much

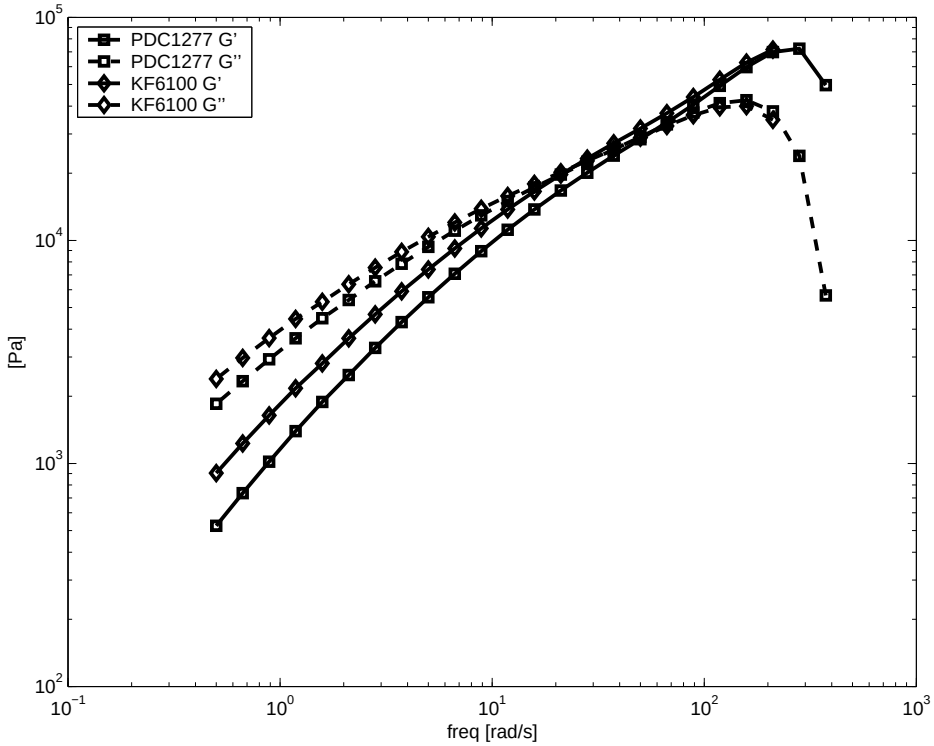

Figure 9.16: Storage and loss moduli for polypropylene samples.

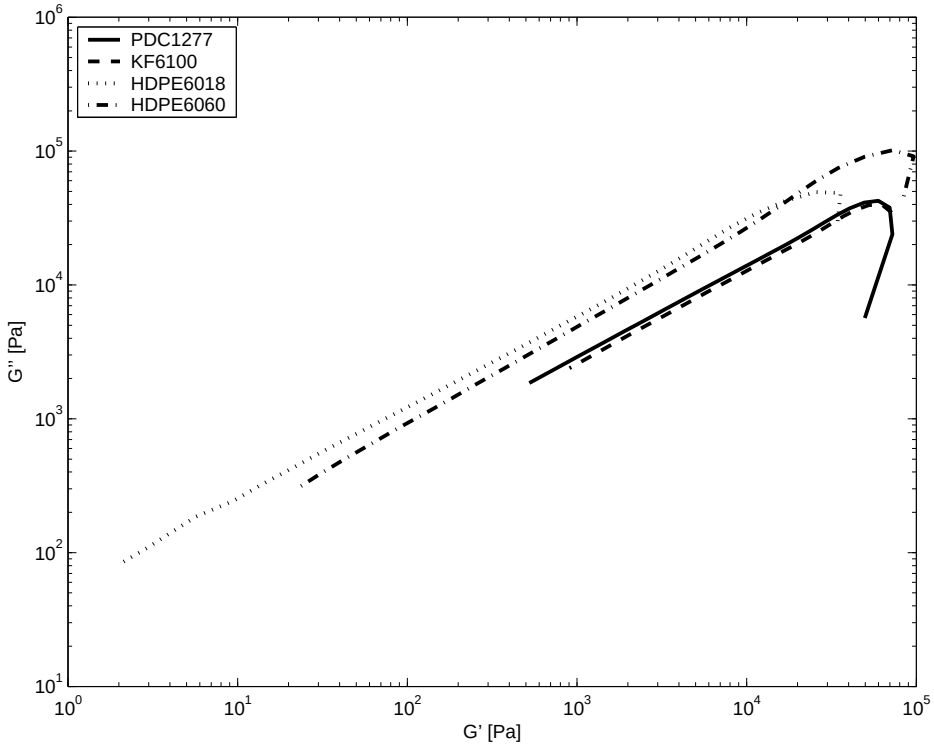

Figure 9.17: The Loss moduli plotted against the Storage moduli for the polyolefin samples. The four polymers exhibit similar responses.

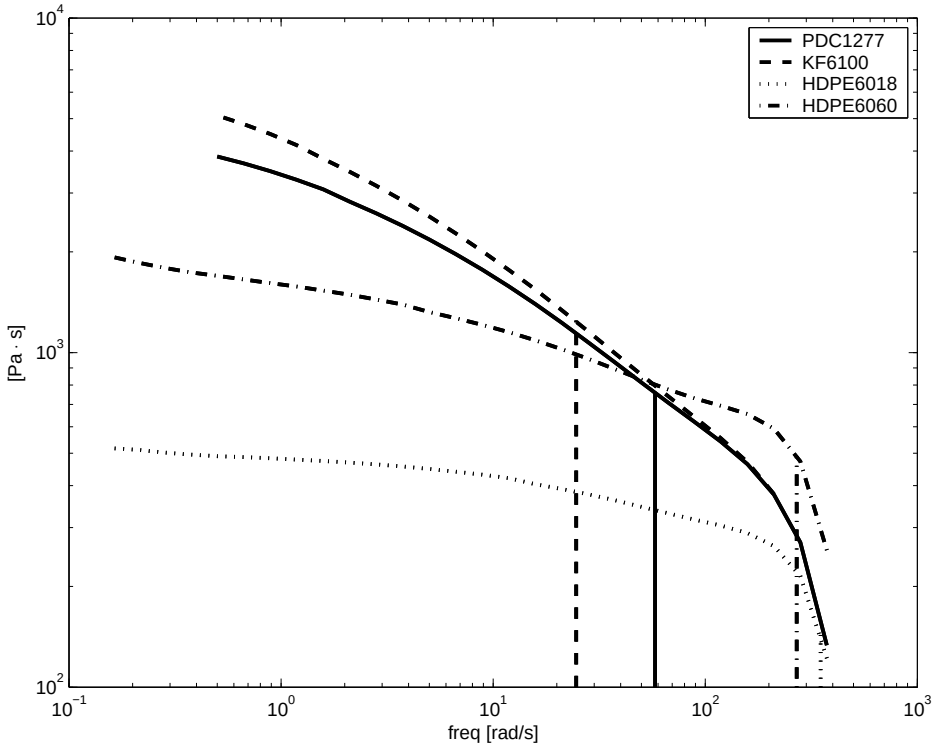

Figure 9.18: Viscosities of polypropylenes and polyethylenes. The polypropylenes have very similar viscosity curves. The vertical lines indicate the crossover frequencies.

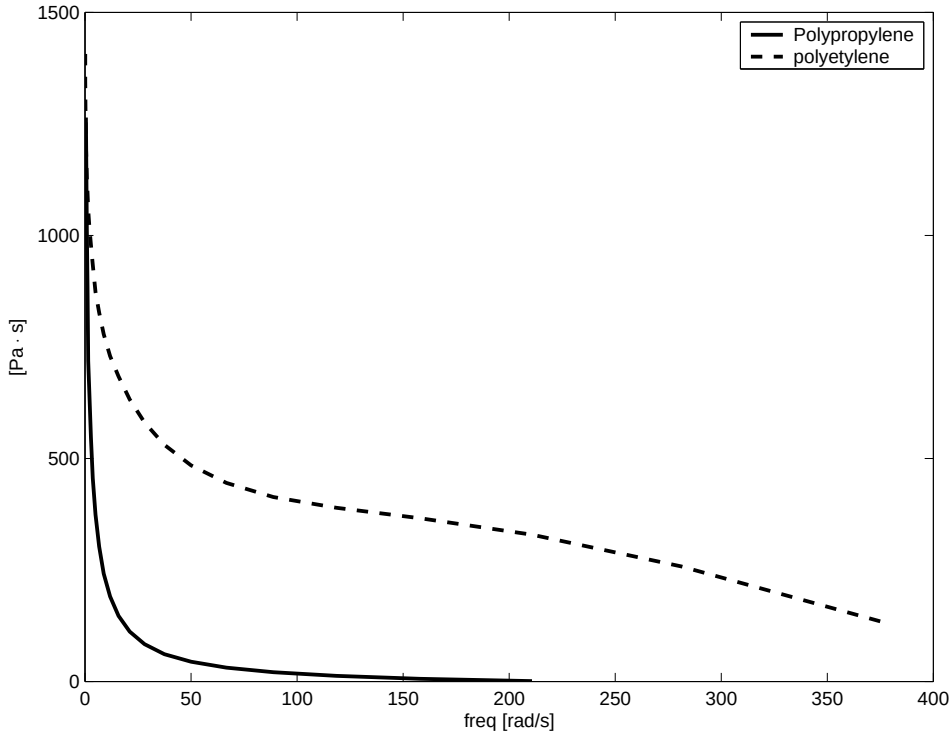

Figure 9.19: Comparison of viscosity curves. For each species, the root square of the viscosity difference was taken and plotted.

less then 1 implies that the material behaves like a viscous liquid, whereas a number much greater then 1 implies elastic or solid behavior.

$$N_{De} = \frac{\lambda}{t_c} \tag{9.1}$$

The Weissenberg number has a similar interpretation and can be formed using a different characteristic time of the experiment. The authors prefer a definition of the Weissenberg number which relates the stress caused by the flow to the first normal stress difference. It is the product of the polymer characteristic relaxation time and the shear rate, $\dot{\gamma}$ (Equation 9.2).

$$N_{We} = \lambda\dot{\gamma} \tag{9.2}$$

The relaxation times of the different polymers were found from the crossover points [24] of the modulus curves (Table 9.6).

Material	Crossover Frequency $[s^{-1}]$	Dominant Relaxation Time, λ $[s]$
PDC1277	58.10	1.72×10^{-2}
KF6100	24.63	4.06×10^{-2}
HDPE6018	350.67	2.85×10^{-3}
HDPE6060	270.50	3.70×10^{-3}

Table 9.6: Dominant relaxation times.

The number used to characterize the behavior of the system is the volume domain shape factor, c. The characteristic time of the process, t_c, can be computed from equation 9.3, where Q is chosen to be $3mL/s$. Generally, where c is

consistent, Equation 2.6 holds and t_c is the inverse of a. Choosing the inverse of a as the characteristic flow time makes sense from a controls and modeling perspective. a is the inverse of the characteristic time for the system, and exploring it with dimensionless numbers is also appropriate.

$$t_c = \frac{1}{Qc} \tag{9.3}$$

With a specific throughput, Q/N, of $1.3mL/rev$ chosen, the corresponding screw speed, N, is equal to $2.31rev/s$. With a $30mm$ co-rotating twin screw extruder, the shear rate, $\dot{\gamma}$, can be computed (Equation 9.4) from the screw speed and channel depth, $4.7mm$. The shear rate for the channel is chosen for the characteristic shear rate because the fluid is exposed to this shear for the most time.

$$\dot{\gamma} = \frac{\pi DN}{depth} \tag{9.4}$$

The Weissenberg number calculations, as shown in Table 9.7, imply that the polyethylenes exhibit more viscous behavior then elastic behavior. The polypropylenes have less viscous behavior in comparison. The Basell PDC1277 is more viscous in nature then the Montell KF6100, which has more elastic behavior. This also is a result of the KF6100 possessing a crossover frequency that is double that of the PDC1277. The two polyethylenes, in spite of their different viscosities do have similar Weissenberg numbers. Of course this is a result of their similar modulus cross-over frequencies. This could be an explanation for why their RVD's are so similar. The different Weissenberg numbers and crossover frequency for the polypropylenes could also explain the disparity in the RVD's.

Figure 9.20 shows that these four different materials, of two different poly-

Material	η $[Pa \cdot s]$	G $[Pa]$	λ $[s$ $\times 10^{-2}]$	c $[mL^{-1}$ $\times 10^{-2}]$	t_c $[s]$	$\dot{\gamma}$ $[s^{-1}]$	N_{De} $\times 10^{-3}$	N_{We}
PDC1277	3851.4	525.3	1.72	2.00	16.7	46.3	1.03	0.80
KF6100	5115.4	905.4	4.06	8.94	3.7	46.3	10.9	1.88
HDPE6018	517.7	2.0	0.285	5.64	5.9	46.3	0.482	0.13
HDPE6060	1936.0	22.9	0.370	5.38	6.2	46.3	0.597	0.17

Table 9.7: Deborah and Weissenberg numbers for the different polymers.

mer types, do not support a simple functional relationship between the volume domain shape factor and the Weissenberg number. One conclusion that could be made is that the shape factors for the PE's, which essentially are the same, are associated with a low Weissenberg number, whereas the shape factors for the PP's, which differ greatly, are associated with Weissenberg numbers, which are higher and closer to unity and expressing more elastic effects. More work with different types of materials and additional types of resins such as polyamides and amorphous resins. More examination of different viscosity materials within families of polymers would also help elucidate this issue. It is possible that when elastic effects are at a minimum as shown with the Weissenberg numbers, even large differences in viscosity have minimum effect on the residence distributions. On the other hand, when elastic effects are present, even polymers of the same viscosity will show varying distributions.

These dimensionless numbers can be compared over all the operating conditions. Calculating N_{De} using a, the Deborah number showed a dependence on the volume throughput (Figure 9.21). The KF6100 showed more effect although it is clear other factors may also influence this. The figure indicates that as the

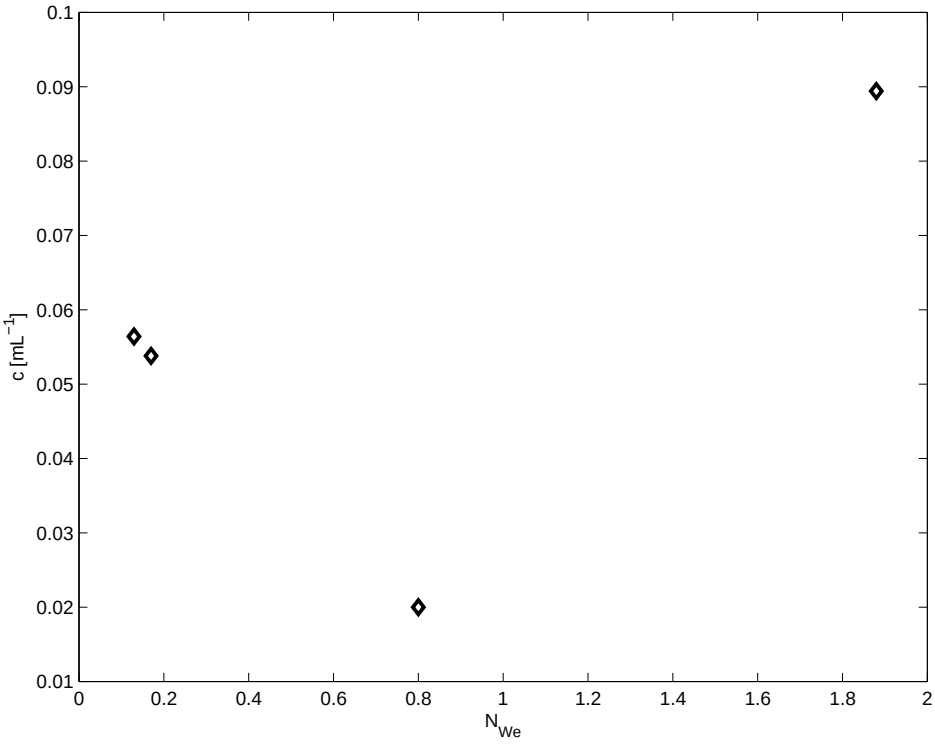

Figure 9.20: Comparison of volume domain shape factors to the N_{We}. This data does not support a functional relationship between these two quantities.

volume throughput increases, the fluid behaves more elasticly.

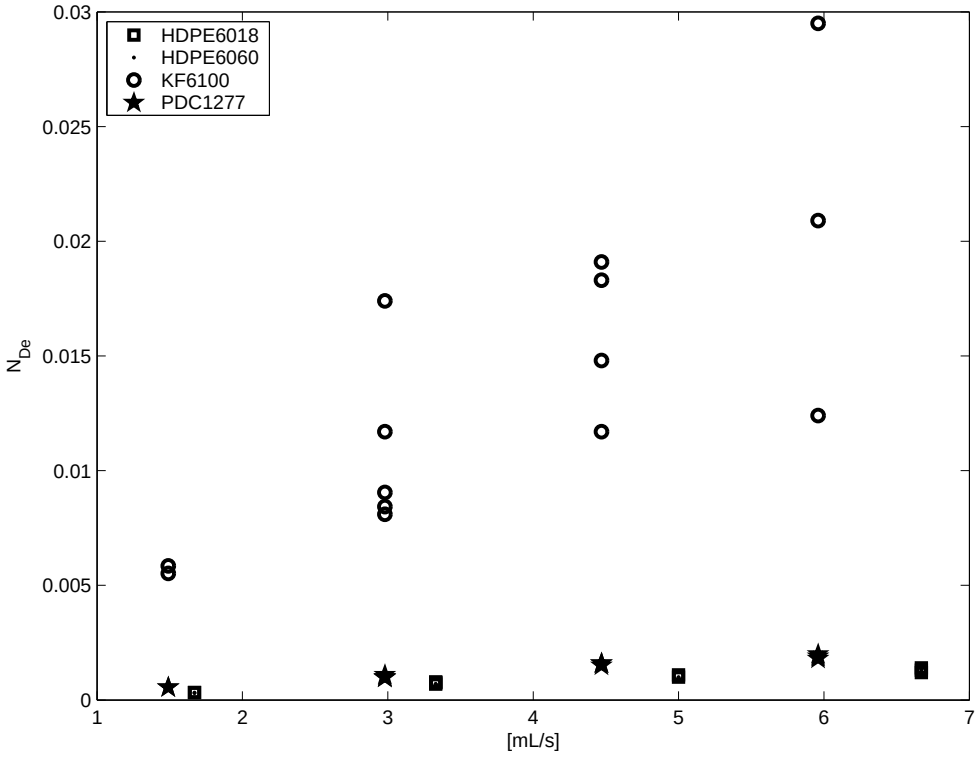

Figure 9.21: N_{De} vs. Q for the four polymers. The KF6100 has more variability than the other materials.

Over the range of experimental conditions, the Weissenberg number shows a dependence on N (Figure 9.22. This is consistent with the way the Weissenberg number has been defined (Equations 9.2 & 9.4). As the screw speed increases, the materials behave more elastically. The polyethylenes, show much less dependence on the screw speed. This is a result of their lower characteristic relaxation times; λ is like the slope for a straight line with $\dot{\gamma}$, which is a function of N, the ordinate.

The Deborah number proportionality to Q and the Weissenberg number proportionality to N are consistent with understanding of RTD curves for materials in extruders. The RTD's indicate that higher Q tightens the residence distribu-

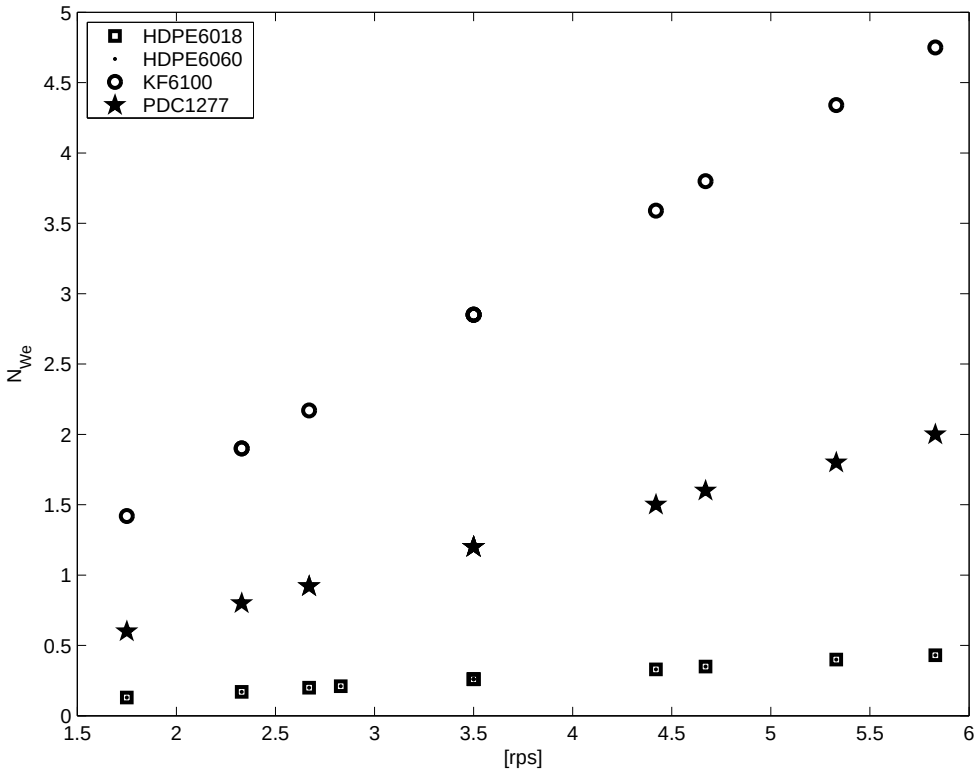

Figure 9.22: N_{We} vs. N for the four polymers.

tion and decreases the axial mixing. The higher Deborah number, due to higher Q, would lead to more elastic behavior, while the RTD indicates less mixing.

The Weissenberg number figure shows the KF6100 having a great deal of dependence on N and the other polypropylene less so, and the polyethylenes, even less. N_{We} can also be used as a ratio describing chain disentanglement, with N_{We} being the ratio of the first normal stress difference to the fluid stress. Low N_{We} corresponds to high chain disentanglement. High N_{We} is the converse. The dependence of the Weissenberg number upon the shear rate and thus N also corresponds to the similar relationship of c to N (Figure 9.13). Recall that low c means more axial mixing. The two relationships together indicate that low Weissenberg number indicates more disentanglement of the polymer chains, and more mixing. This explains the variability in the volume domain shape factor for KF6100.

Dealy and F.Wissbrun [25] discusses an inverse relationship between polydispersity and crossover modulus. For cracking reactions such as the vis-breaking of polypropylene [6], the average molecular weight is decreased, as well as the breadth of the distribution; this reduces the polydispersity. The crossover modulus would likely change and it would be necessary to test the complex rheology to make sure the Weissenberg number would not be too different post cracking, and change the RTD.

9.5 Conclusions

Experimental data have shown that the residence distributions can be very similar for two different materials. This is the case for the two polyethylenes, which in spite of having different viscosities have very similar residence distributions, as

indicated by their volume domain shape factors. The two polypropylenes did not show this same behavior.

The rheometric analysis of these phenomena have allowed for computation of the Weissenberg number for each polymer studied. The two polymers with similar RVD's, the polyethylenes, also have very similar Weissenberg numbers as a extension of having similar modulus crossover frequencies. Both Weissenberg numbers indicate viscous behavior. However, the Weissenberg numbers calculated for the polypropylenes, which had dissimilar modulus crossover frequencies, indicated more viscous behavior for one, while the other had more elastic behavior.

It is possible that when elastic effects are at a minimum as shown with the Weissenberg numbers, even large differences in viscosity have minimum effect on the residence distributions. On the other hand, when elastic effects are present, even polymers of the same viscosity will show varying distributions. This work does reinforce the assertion that the residence time distribution is independent of certain material properties for specific cases. However, inspecting the simple viscosity alone will not help explain why different materials have similar residence distributions, while others have different ones. Analysis of the complex viscosity and computation of the Weissenberg number may be a better tool for this comparison. A consequence of this is that visco-elastic properties are very important to the residence distributions.

Chapter 10

Warp Time Analysis

10.1 Introduction

The lamellar model using warped time will be used to predict changes in molecular weight for a polymer melt within the extruder. The goal of this is to use this to predict the gain of a physically based plant model. The lamellar model, Ottino [19], is a one dimensional model useful for studying laminar mixing. Transforming the time allows for accounting of the reaction and the fluid motion, while simplifying the system to a tractable diffusion problem. The following is the derivation of a diffusion-like equation for the cases of *constant*, *exponential*, and *logarithmic* stretching. The case of constant stretching is from Ottino also. Three types of stretching can be studied, constant, exponential and logarithmic. These three models are derived below as done by Muzzio et al. [26]. The best model for stretching must still be determined for this application.

10.2 Derivation

Three types of expressions for stretching are available: constant (Equation 10.2), exponential (Equation 10.3), and logaritmic (Equation 10.3).

$$\alpha(x,t) = \alpha \tag{10.1}$$

$$\alpha(x,t) = e^t \tag{10.2}$$

$$\alpha(x,t) = \ln t \tag{10.3}$$

10.2.1 General Equation Derivation

In general: The mass transfer equation.

$$\frac{\partial c_i}{\partial t} = -\overline{\nabla} \cdot \overline{N_i} + R_i \tag{10.4}$$

The flux equation.

$$\overline{N_i} = -D_i \overline{\nabla} c_i + c_i \overline{V} \tag{10.5}$$

Substituting:

$$\frac{\partial c_i}{\partial t} = -\overline{\nabla} \cdot \left(-D_i \overline{\nabla} c_i + c_i \overline{V}\right) + R_i \tag{10.6}$$

Assume D_i is constant.

$$\frac{\partial c_i}{\partial t} = D_i \nabla^2 \cdot c_i - \overline{\nabla}\left(c_i \cdot \overline{V}\right) + R_i \tag{10.7}$$

Expanding, (note incompressibility).

$$\frac{\partial c_i}{\partial t} = D_i \nabla^2 \cdot c_i - \overbrace{c_i \cdot \overline{\nabla V}}^{=0} - \overline{V} \cdot \overline{\nabla} c_i + R_i \tag{10.8}$$

Convective velocity:

$$\overline{V} = V_x(x,y)\,\overline{i} + V_y(x,y)\,\overline{j} = -\alpha x \overline{i} + \alpha y \overline{j} \tag{10.9}$$

One dimensional form:

$$\frac{\partial c_i}{\partial t} + V_x \frac{\partial c_i}{\partial x} = D_i \frac{\partial^2 c_i}{\partial x^2} + R_i \tag{10.10}$$

Convective Velocity:

$$V_x = -\alpha x \tag{10.11}$$

10.2.2 Transformation of Independent Variables

The new independent variables are:

$$\xi = \xi(x, t) \tag{10.12}$$

$$\theta = \theta(t) \tag{10.13}$$

Application of chain rule:

$$\begin{aligned} \frac{\partial c_i}{\partial t} &= \frac{\partial c_i}{\partial \theta}\frac{\partial \theta}{\partial t} + \frac{\partial c_i}{\partial \xi}\frac{\partial \xi}{\partial t} \\ \frac{\partial c_i}{\partial x} = \frac{\partial c_i}{\partial \theta}\frac{\partial \theta}{\partial x} &+ \frac{\partial c_i}{\partial \xi}\frac{\partial \xi}{\partial x} = \frac{\partial c_i}{\partial \xi}\frac{\partial \xi}{\partial x} \\ \frac{\partial^2 c_i}{\partial x^2} &= \frac{\partial c_i}{\partial \xi}\frac{\partial^2 \xi}{\partial x^2} + \frac{\partial \xi}{\partial x}\frac{\partial \xi}{\partial x}\frac{\partial^2 c_i}{\partial \xi^2} \end{aligned} \tag{10.14}$$

So plugging into mass transfer equation:

$$\frac{\partial c_i}{\partial \theta}\frac{\partial \theta}{\partial t} + \frac{\partial c_i}{\partial \xi}\left(\frac{\partial \xi}{\partial t} - \alpha x \frac{\partial \xi}{\partial x}\right) = D_i\left[\frac{\partial c_i}{\partial \xi}\frac{\partial^2 \xi}{\partial x^2} + \frac{\partial \xi}{\partial x}\frac{\partial \xi}{\partial x}\frac{\partial^2 c_i}{\partial \xi^2}\right] + R_i \tag{10.15}$$

Let

$$\frac{\partial \xi}{\partial t} - \alpha x \frac{\partial \xi}{\partial x} = 0 \tag{10.16}$$

10.2.3 Constant Stretching

Using the $\alpha(x, t) = \alpha$, a constant, and integrating by parts...

$$\xi = x e^{\alpha t} = \frac{x}{s(t)} \tag{10.17}$$

$$s(t) = s_0 e^{-\int_0^t \alpha \ \partial t'} = s_0 e^{-\alpha t} \tag{10.18}$$

where $s_0 = 0$. so the *position transform* is:

$$x = \xi s_0 e^{-\alpha t} \tag{10.19}$$

Also,

$$\begin{aligned} \frac{\partial \xi}{\partial x} &= \frac{1}{s} \\ \frac{\partial^2 \xi}{\partial x^2} &= 0 \end{aligned} \tag{10.20}$$

Which brings us to:

$$\frac{\partial c_i}{\partial \theta}\frac{\partial \theta}{\partial t} = \frac{D_i}{s^2}\frac{\partial^2 c_i}{\partial \xi^2} + R_i \tag{10.21}$$

Let:

$$\frac{\partial \theta}{\partial t} = \frac{\eta^2}{t_c} \tag{10.22}$$

where t_c is constant, and

$$\eta = \frac{s_0}{s} = \frac{s_0}{s_0 e^{-\alpha t}} = e^{\alpha t} \tag{10.23}$$

so...

$$\frac{\partial \theta}{\partial t} = \frac{e^{2\alpha t}}{t_c} \tag{10.24}$$

thus the *time transformation* is...

$$t = \frac{\ln\left[2\alpha t_c \theta + 1\right]}{2\alpha} \tag{10.25}$$

Substituting:

$$\frac{\partial c_i}{\partial \theta} = \frac{D_i t_c}{s_0^2}\frac{\partial^2 c_i}{\partial \xi^2} + \frac{t_c}{\eta} R_i \tag{10.26}$$

Dimensionless reaction term, characteristic reaction time and characteristic diffusion time, respectively:

$$\begin{aligned} R_i^* &= \frac{R_i}{|R_{j_0}|} \\ t_r &= \frac{c_{j_0}}{|R_{j_0}|} \\ t_d &= \frac{s_0^2}{D_i} \end{aligned} \tag{10.27}$$

So the *equation of mass transfer* becomes:

$$\frac{\partial c_i}{\partial \theta} = \frac{t_c}{t_d}\frac{\partial^2 c_i}{\partial \xi^2} + \frac{t_c}{t_r}R_i^* \tag{10.28}$$

Where t_c,t_d, and t_r are the characteristic, diffusive characteristic, and reactive characteristic times.

10.2.4 Exponential Stretching

Using the stretching function $\alpha(x,t) = e^t$, then integrating by parts and a similar derivation as used previously...

$$\xi = \frac{xe^{e^t}}{e} = \frac{x}{s(t)} \tag{10.29}$$

$$s(t) = s_0\frac{e}{e^{e^t}} \tag{10.30}$$

The constant $s_0 = 1$ so the *position transform* is:

$$x = \xi\frac{e}{e^{e^t}} \tag{10.31}$$

Which brings us to:

$$\frac{\partial c_i}{\partial \theta}\frac{\partial \theta}{\partial t} = \frac{D_i}{s^2}\frac{\partial^2 c_i}{\partial \xi^2} + R_i \tag{10.32}$$

Let:

$$\frac{\partial \theta}{\partial t} = \frac{\eta^2}{t_c} \tag{10.33}$$

and

$$\eta = \frac{s_0}{s} = \frac{s_0}{s_0 \frac{e}{e^{e^t}}} = \frac{e^{e^t}}{e} \tag{10.34}$$

so...

$$\frac{\partial \theta}{\partial t} = \frac{e^{2e^t}}{e^2 t_c} \tag{10.35}$$

thus the *time transformation* is...

$$\theta = \frac{\int_0^t e^{2e^{t'}} \, \partial t'}{t_c e^2} \tag{10.36}$$

Similarly the *equation of mass transfer* becomes:

$$\frac{\partial c_i}{\partial \theta} = \frac{t_c}{t_d} \frac{\partial^2 c_i}{\partial \xi^2} + \frac{t_c}{t_r} R_i^* \tag{10.37}$$

Where t_c,t_d, and t_r are the characteristic, diffusive characteristic, and reactive characteristic times.

10.2.5 Logarithmic Stretching

Using the stretching function $\alpha(x,t) = \ln t$,and integrating by parts and a similar derivation as used previously...

$$\xi = \frac{x t^t}{e^t} = \frac{x}{s(t)} \tag{10.38}$$

$$s(t) = s_0 \frac{e^t}{t^t} \tag{10.39}$$

The constant $s_0 = 1$ so the *position transform* is:

$$x = \xi \frac{e^t}{t^t} \tag{10.40}$$

Which brings us to:

$$\frac{\partial c_i}{\partial \theta} \frac{\partial \theta}{\partial t} = \frac{D_i}{s^2} \frac{\partial^2 c_i}{\partial \xi^2} + R_i \tag{10.41}$$

Let:

$$\frac{\partial\theta}{\partial t} = \frac{\eta^2}{t_c} \tag{10.42}$$

and

$$\eta = \frac{s_0}{s} = \frac{t^t}{e^t} \tag{10.43}$$

so...

$$\frac{\partial\theta}{\partial t} = \frac{t^{2t}}{e^{2t}t_c} \tag{10.44}$$

thus the *time transformation* is...

$$\theta = \frac{1}{t_c}\int_0^t \frac{t'^{2t'}}{e^{2t'}}\,\partial t' \tag{10.45}$$

Similarly the *equation of mass transfer* becomes:

$$\frac{\partial c_i}{\partial\theta} = \frac{t_c}{t_d}\frac{\partial^2 c_i}{\partial\xi^2} + \frac{t_c}{t_r}R_i^* \tag{10.46}$$

Where t_c,t_d, and t_r are the characteristic, diffusive characteristic, and reactive characteristic times.

10.3 Kinetic Model of Reaction

Work has been done to produce a kinetic model for the degradation of polypropylene by Tzoganakis et al. [6]. They propose a comprehensive model that accounts for the moments of the polymer distribution, and the moments of the polymer radical distribution. The i^{th} moments of the polymer distribution is:

$$Q_i = \sum_{r=2}^{\infty} r^i\,[P_r] \tag{10.47}$$

where r is the polymer chain length.

This model has many terms to keep track of, so after some simplification by the authors [6], only equations for the moments of the polymer distribution

are necessary. the simplifications were that the steady state hypothesis for the peroxide radicals was used, and that initiation and chain scission, Equations 10.48, govern the degradation process.

$$\begin{aligned} I &\xrightarrow{k_d} 2R^0 \\ P_n + R^0 &\xrightarrow{k_1} P_r + P^0_{n-r} + R \end{aligned} \tag{10.48}$$

where I is the initiator, R^0 is the peroxide radical, and P_i is the polymer of chain length i.

The following equations can be used to model the reaction kinetics within the warp time model. Q_i are the molecular moments derived from the molecular weight distribution (MWD).

$$\frac{d[I]}{dt} = -k_d[I] \tag{10.49}$$

$$\frac{d[Q_0]}{dt} = \theta\frac{Q_1 - 3Q_0}{Q_1 - Q_0} \tag{10.50}$$

$$\frac{d[Q_1]}{dt} = -\theta\frac{2Q_0}{Q_1 - Q_0} \tag{10.51}$$

$$\frac{d[Q_2]}{dt} = \theta\frac{-\frac{1}{3}Q_3 + \frac{1}{3}Q_1 - 2Q_0}{Q_1 - Q_0} \tag{10.52}$$

$$Q_3 = \frac{2Q_2}{Q_1Q_0}\left(2Q_2Q_0 - Q_1^2\right) \tag{10.53}$$

$$\theta = 2fk_d[I] \tag{10.54}$$

$$k_d = k_0\exp(-A'/T) \tag{10.55}$$

Using these equations, the molecular moments can be used to find the different weighted averages of the molecular weight. M_n, M_w, and M_z are respectively the number, weight, and z average molecular weights.

$$\bar{M}_n = m_0Q_1/Q_0 \tag{10.56}$$

$$\bar{M}_w = m_0 Q_2/Q_1 \tag{10.57}$$

$$\bar{M}_z = m_0 Q_3/Q_2 \tag{10.58}$$

These kinetic equations can be used for the reaction kinetics within the warp time model. Each species $[I]$, $[Q_0]$, $[Q_1]$, $[Q_2]$, and $[Q_3]$ will have a lamellar distribution. These different distributions can be simulated simultaneously.

10.4 Proposed Simulation Technique

This technique will be used to simulate the mixing and reaction within the extruder. In order to do this, the parameters of the model must be determined. The diffusive characteristic and reactive characteristic times can be determined from the materials and their reactions. The characteristic time depends on whether the system is diffusion or reaction limited. If it is diffusion limited, then the characteristic time is the diffusive characteristic time. It it is reaction limited, the converse will be the case. In the case of the peroxide initiated degradation of polypropylene, it is expected that diffusion will hamper the reaction. Another way to think of this is that different mixing regimes change the way the process performs, and this indicates that the reaction is much faster.

The mean residence times from the residence distribution analysis can be used as the times that the material undergoes mixing, or rather, how long the different stretching routines will be applied. Since the peroxide initiator enters the extruder in the partially filled region of the mixing zone, the residence times for the deconvolved mixing and metering zones will be important. The amount of time material spends within the melting zone should not affect the process. As an aside, the comparison of the residence times with the characteristic time

of reaction indicates how far the reaction travels within the extruder.

After the simulation technique has been shown successful, it will be used to determine the non-linear gain for the open-loop plant model. Unfortunately, implementation in software was not successful (Appendix F).

Chapter 11

Closed Loop Regulation of Polypropylene

11.1 Introduction

After a process is well characterized, it becomes possible to design a controller to regulate the process. However, the extrusion process has a long measurement delay as well as a significant material transport delay and these delays make simple classical control schemes impractical to implement.

One way to understand a process is to know how long it takes material to be processed. The distribution of how long material takes to pass a given point is called the residence time distribution RTD. Modeling of these distributions has been pursued because characterizing processes can be costly. These models are also useful because the form of the RTD is quite similar to an impulse response of the extruder. This is useful for designing control schemes of the extruder. Determining the RTD is useful for determining the dynamics of the process as well as the various delay times of the system.

11.2 experimental setup

The experimental setup used was the same as that used for the RTD characterizations of the plant. Additionally, the die was instrumented with an in-line rheometer fed by material diverted from the die and then reintegrated into the output stream. Two differences were necessary. The first is that due to material shortages, the intended polymer to be used, PDC, was changed to another polypropylene, Network Polymers PP NPP 30-0300 (NP). The NP was more viscous then PDC (Table 11.1). The second difference is that due to the higher viscosity of the NP, the settings on the viscometer were changed by increasing the temperature $5.\bar{5}$ Rankine. This served to lower the measured viscosity to make it similar to PDC.

Material	Melt Flow Index $[g/10min]$
Basell PDC1277	2.67
NPP 30-0300	1.67

Table 11.1: Melt flow indices of different polypropylenes. Each measurement was the average of three tests. The table shows that NP is more viscous then PDC.

The open loop tests and closed loop tests were performed and recorded with the use of LabVIEW software (Appendix E). This software was used to control the feed rates, and record the sensor properties. Additionally the controller was implemented as a "'virtual instrument"' within this software package. The controller used a PI design with a smith predictor. The gain was also determined as a function of the peroxide weight fraction.

11.3 Control Results

Experiments were performed to determine the ability of the control system to regulate the reactive extrusion process. One way to check the controller was with set point step changes to see how well the system tracked changes this value. Numerous set point step changes were performed, as well as changes to the operating conditions without changing the controller (smith predictor) parameters to see how disturbances were dealt with. Additionally, the controller was tested with a huge perturbation made to the raw material.

11.3.1 Open Loop Experiments

Due to the change in feed material from Basell PDC 1277 to Network Polymers PP NPP 30-0300, coupled with time constraints, the experiments had to begin without a thorough examination of the open loop behavior with the new material. With the purpose of finding a new gain function, because the one for PDC was much too different for the NP, four open loop runs were performed. Figure 11.1 shows an example of an open loop experiment.

Additionally, insufficient time was available to completely determine new material specific volume shape factors and delay times. Instead, the shape factors and delay times for the Basell PDC1277 were used (Table 8.1). Using these shape factors and delay times for the same conditions for PDC1277, various closed loop tracking tests were performed with the Network Polymers PP NPP 30-0300.

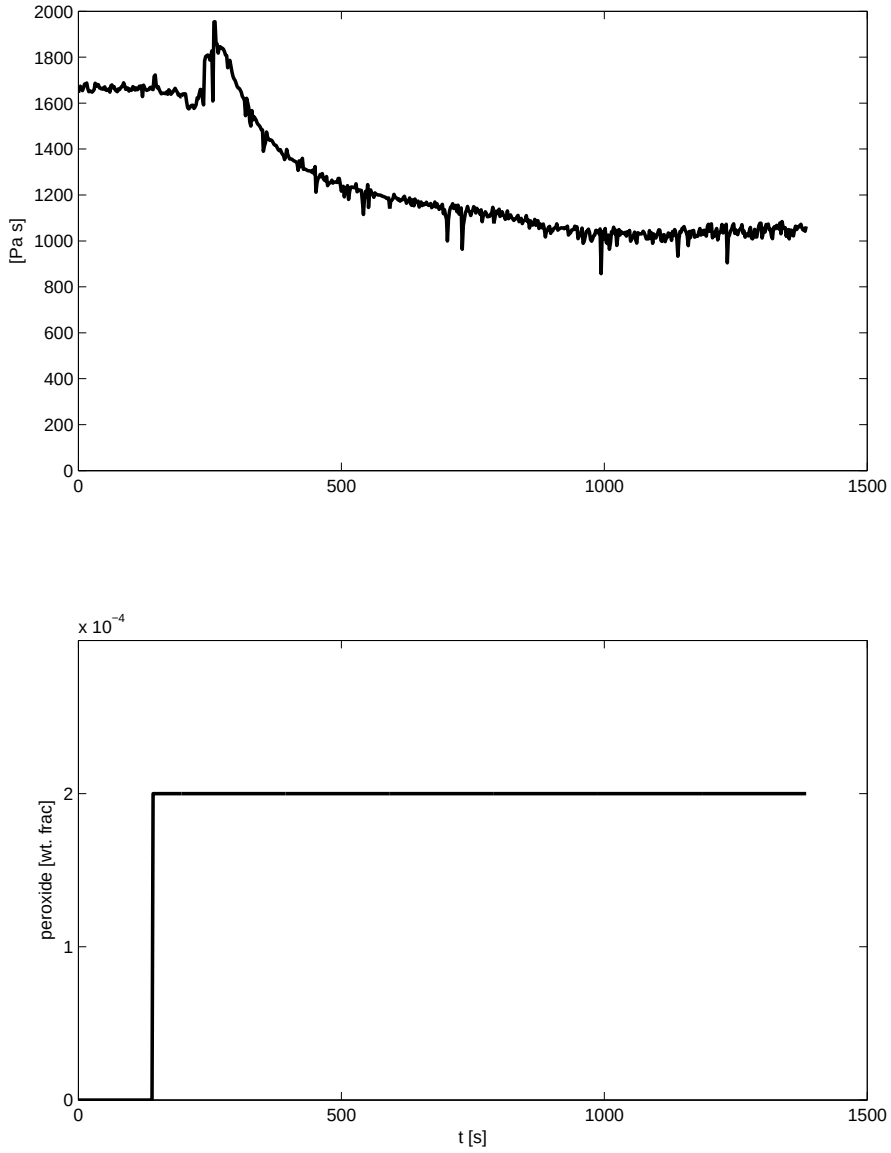

Figure 11.1: Open loop step change in feed peroxide concentration and the resulting change in viscosity. This was performed at $2.98mL/s$ and $2.33rps$.

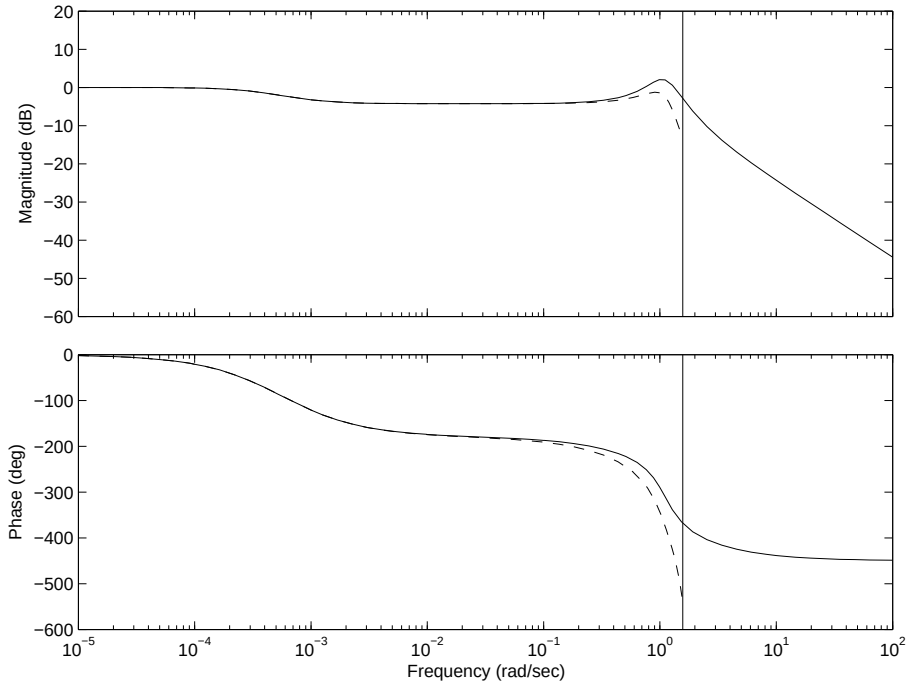

Figure 11.2: Bode plot for figure 11.1.

11.4 Gain Functions

The gain function is used to relate the control system to the extruder. The controller is designed in terms of melt viscosity because it is used to regulate the melt viscosity of the process. However, the extruder only knows feed rates, screw speeds and temperatures. The control system uses the gain function to relate the melt viscosity units to feed rates and peroxide concentration.

The gain functions used have been found experimentally. At the most basic level, open loop experiments are performed to determine steady state relationships between measured viscosity and peroxide percentage. In addition, other known parameters such as feed rate and screw speed can be used to help relate the peroxide concentration to steady state melt viscosity.

Extensive testing was done on two different polypropylenes, Montell KF6100 and Basell PDC1277, to determine their gain functions. However, due to material shortages neither was used for the closed loop experiments. The relationship for Montell KF6100 is shown in equation 11.1, and has an R^2 of 92%. This is the same as Equation 6.1 except the peroxide term, $wt.frac$, is used in place of $[I]$, a percentage.

$$\eta\,[Pa \cdot s] = 438 + 7.11 v_m\,[mL] - 3323000 c\,[wt.frac]\,{}^{Q}\!/_{N}\,[{}^{mL}\!/_{rev}] \qquad (11.1)$$

The relationship for Basell PDC1277 is shown in Equation 11.2, and has an R^2 of 93%. This is the same as Equation 6.2.

$$\eta\,[Pa \cdot s] = 428 + 5.21 v_m\,[mL] - 1763200 c\,[wt.frac]\,{}^{Q}\!/_{N}\,[{}^{mL}\!/_{rev}] \qquad (11.2)$$

In both these equations, melt viscosity is in terms of $Pa \cdot s$, v_m is the product of the mean residence time for a given operating condition as a function of the operating conditions and the federate in terms of mL. The ratio Q/N, the specific throughput, is in terms of mL/rev, and the peroxide weight fraction is c.

For the NP material, only four steady state experiments were performed. The corresponding gain function is in Equation 11.3, and has an R^2 of 99%.

$$\eta\,[Pa \cdot s] = 1605.4 - 2501928c\,[wt.frac] \tag{11.3}$$

Equation 11.3 shows a linear relationship between the melt viscosity and the peroxide concentration at a feed rate of $2.98mL/s$ and 2.33 revolutions per second (rps). It is not difficult to see that Equations 11.1 and 11.2 are also both linear with respect to the peroxide concentration for a given operating condition. For example, at $2.98mL/s$ and $2.33rps$, $v_m = 196.664mL$ for PDC, and Equation 11.2 becomes:

$$\eta\,[Pa \cdot s] = 1452.6 - 2256896c\,[wt.frac] \tag{11.4}$$

The same was not done for Equation 11.1 because data was not taken for the same operating condition, and the comparison would have the same meaning. Equations 11.3 and 11.4 are compared in figure 11.3

11.5 Closed Loop Experiments

The tracking was tested using parameters of $K_c = 0.11$ and $K_i = 0.18min$ (Figure 11.4). The response though overshot more then intended, so the gain of the controller was reduced to $Kc = 0.1$. The results of various tracking experi-

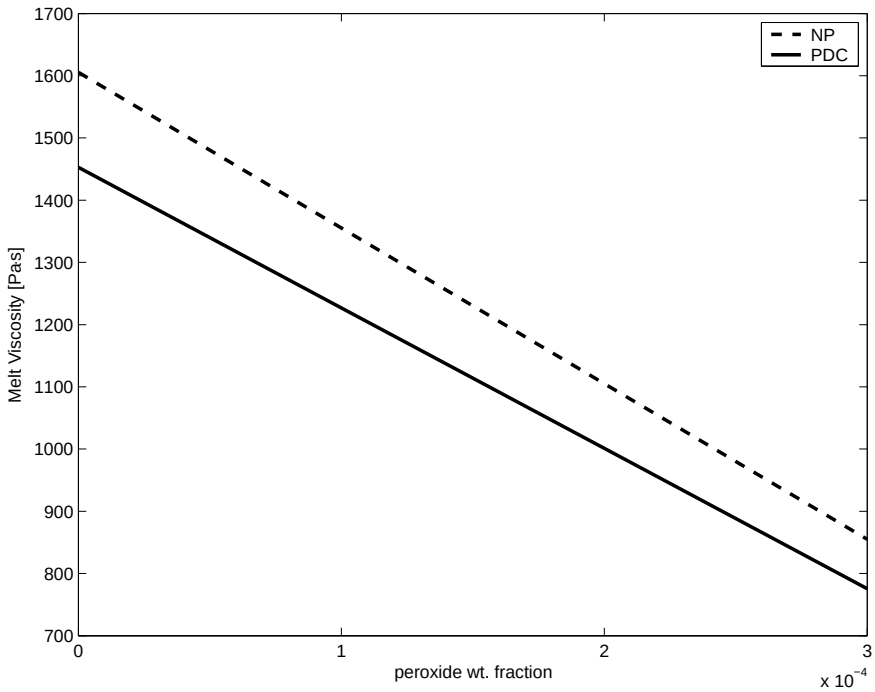

Figure 11.3: Comparison of equations 11.3 and 11.4. Although similar, it can be seen that these curves are for different materials.

ments (Figures 11.6, 11.8, 11.10, 11.12, & 11.14) indicate that the controller successfully tracked the set point change with less overshoot. Figures 11.6 and 11.8 illustrate the closed loop system in a suitable range, however Figure 11.10 illustrates the system response under unfavorable conditions. In this case, the peroxide mixture feeder was not able to track the controller inputs until a feed rate of approximately one fifth of a pound per hour had been reached. Due to this, there is an additional delay before the peroxide enters the system, as can be seen in the figure. In spite of feeder issue, the controller compensates and brings the system to the set point.

The controller is able to deal with other inaccuracy well; Figures 11.12 and 11.14 show that suitable control was achieved in spite of the fact that the non-linear gain function was for $2.98mL/s$ and $2.33rps$ and the operating conditions for the runs were $2.98mL/s$ and $2.98rps$ (recall that the gain function was determined at $2.98mL/s$ and $2.33rps$, Equation 11.3).

Peak and rise times were computed for all the open loop tests as well as all the closed loop figures. The open loop results are in Table 11.2, and those for the closed loop tests are contained in Table 6 11.3. These were computed by normalizing the response curves. The signals were then sampled to determine the peak time and the rise time, which was computed as the time necessary for the signal to go from 10% to 90% of the normalized target value. Some of the results are erratic. Immediately it is evident that the closed loop conditions beginning without peroxide addition generally exhibit longer peak times. This is due to the fact that the material feeders cannot smoothly ramp up the signal from no feed to a small value. The smallest value at which the feeders can reasonably feed material is on the order of a fifth of a pound per hour. Therefore there is

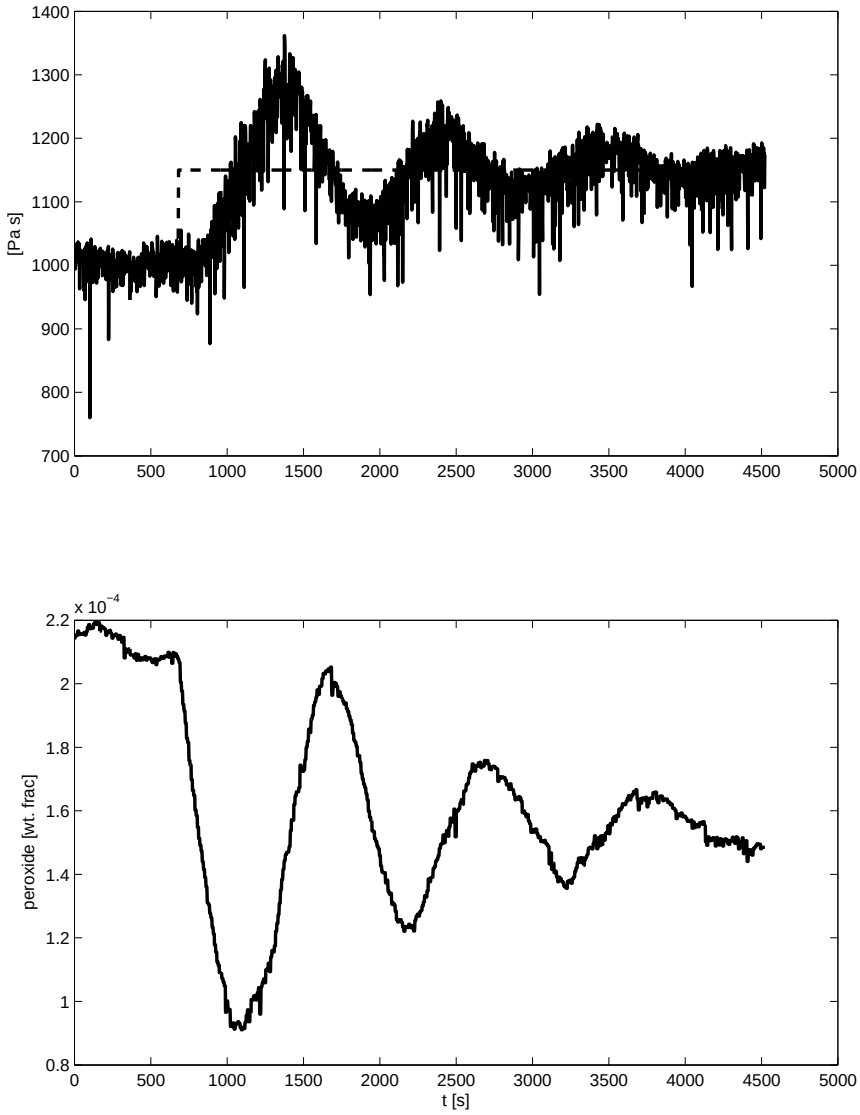

Figure 11.4: Closed loop tracking of extrudate viscosity set point. The operating conditions are $2.98mL/s$ and $2.33rps$. The controller is using the parameters of $K_c = 0.11$ and $K_i = 0.18min$. The appropriate shape factors and delay times were used in the Smith predictor.

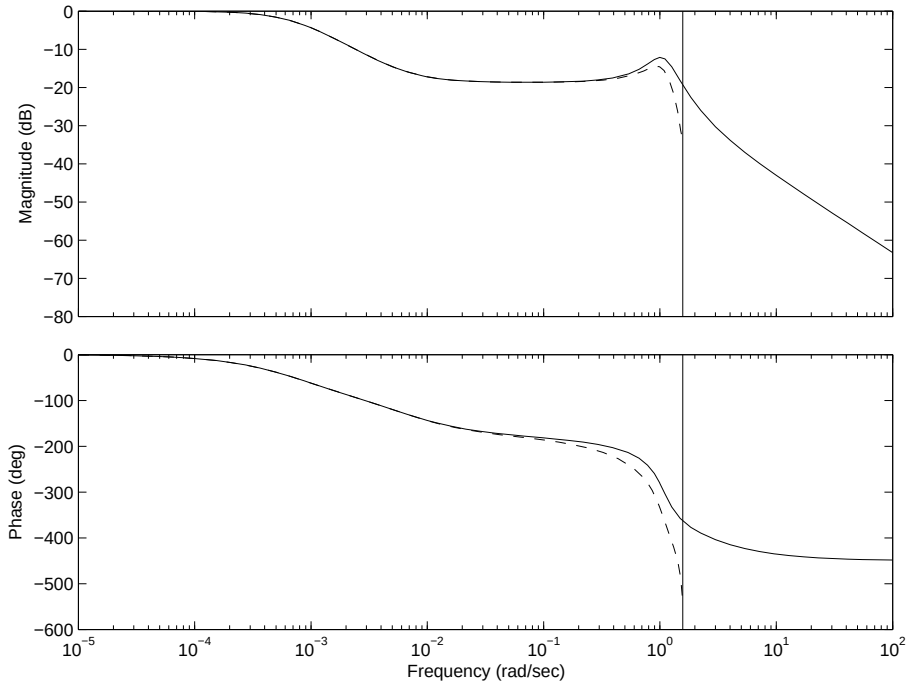

Figure 11.5: Bode plot for figure 11.4.

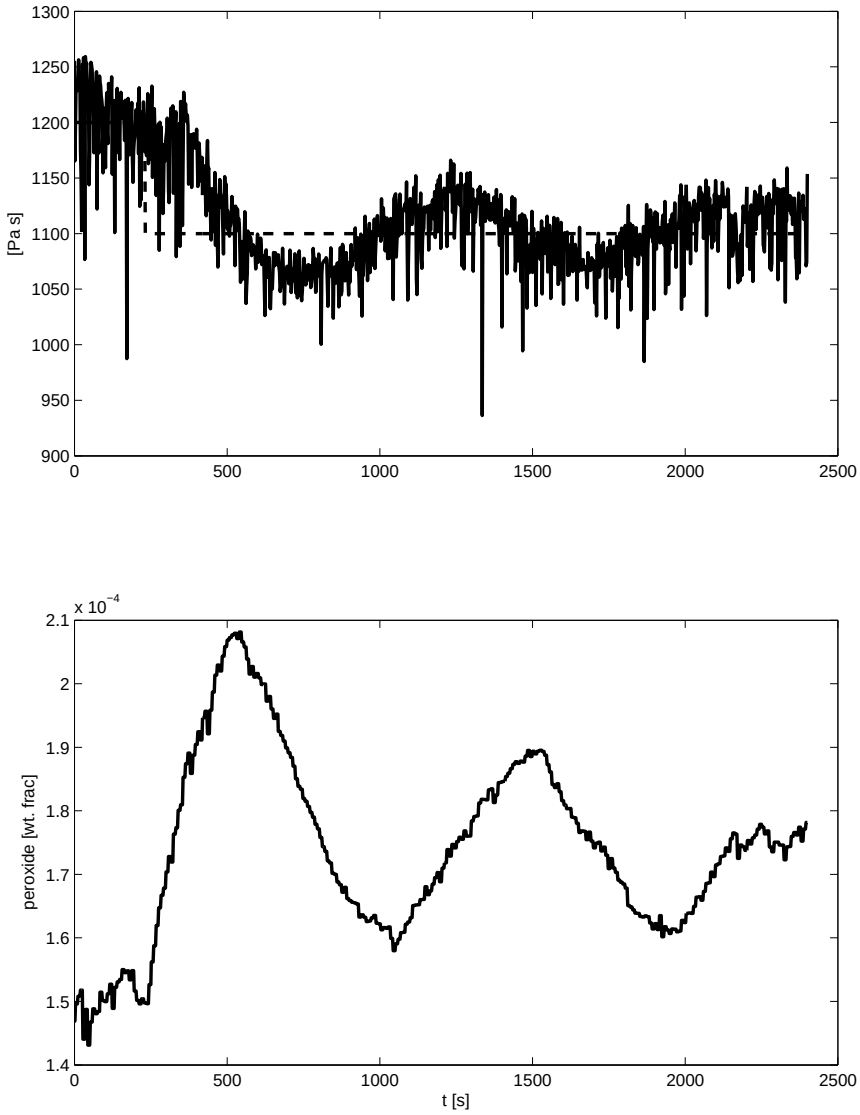

Figure 11.6: Closed loop tracking of extrudate viscosity set point. The operating conditions are $2.98mL/s$ and $2.33rps$. The controller is using the parameters of $K_c = 0.1$ and $K_i = 0.18min$. The appropriate shape factors and delay times were used in the Smith predictor.

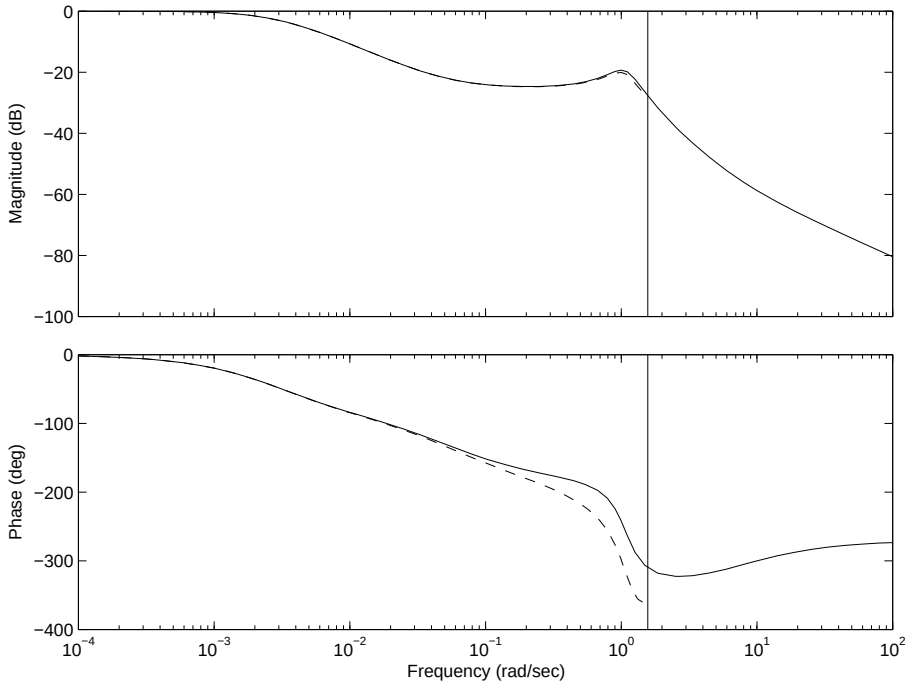

Figure 11.7: Bode plot for figure 11.6.

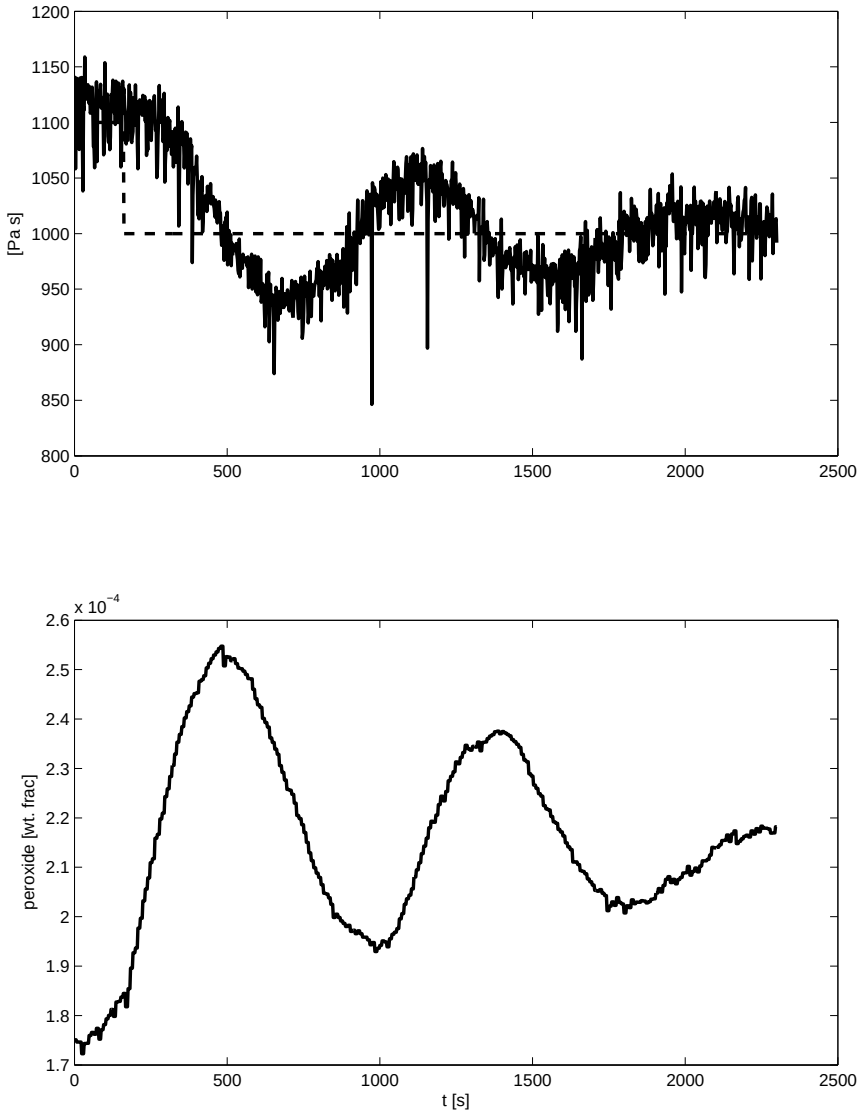

Figure 11.8: Closed loop tracking of extrudate viscosity set point. The operating conditions are $2.98mL/s$ and $2.33rps$. The controller is using the parameters of $K_c = 0.1$ and $K_i = 0.18min$. The appropriate shape factors and delay times were used in the Smith predictor.

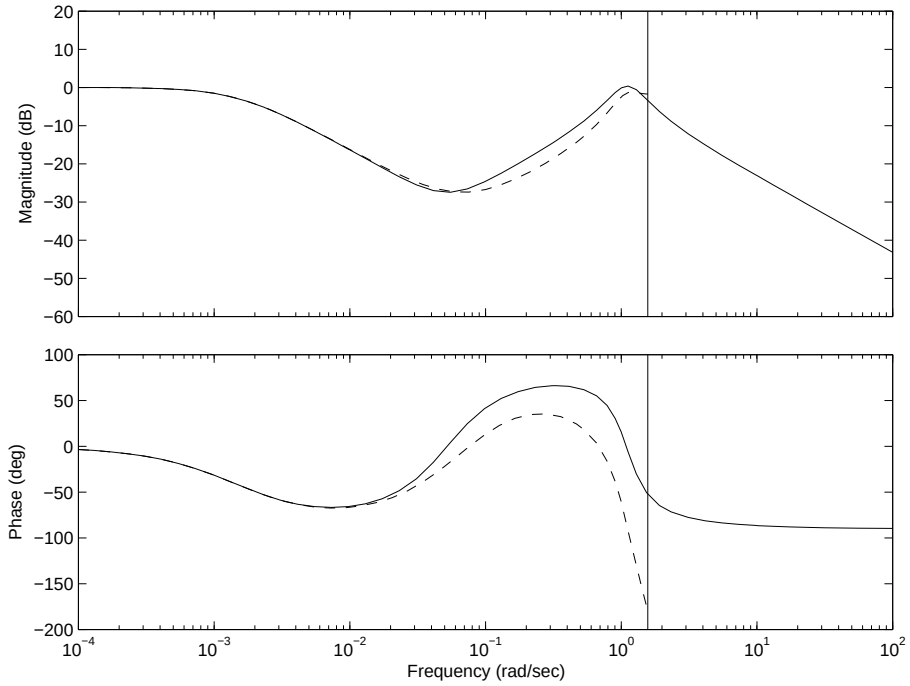

Figure 11.9: Bode plot for figure 11.8.

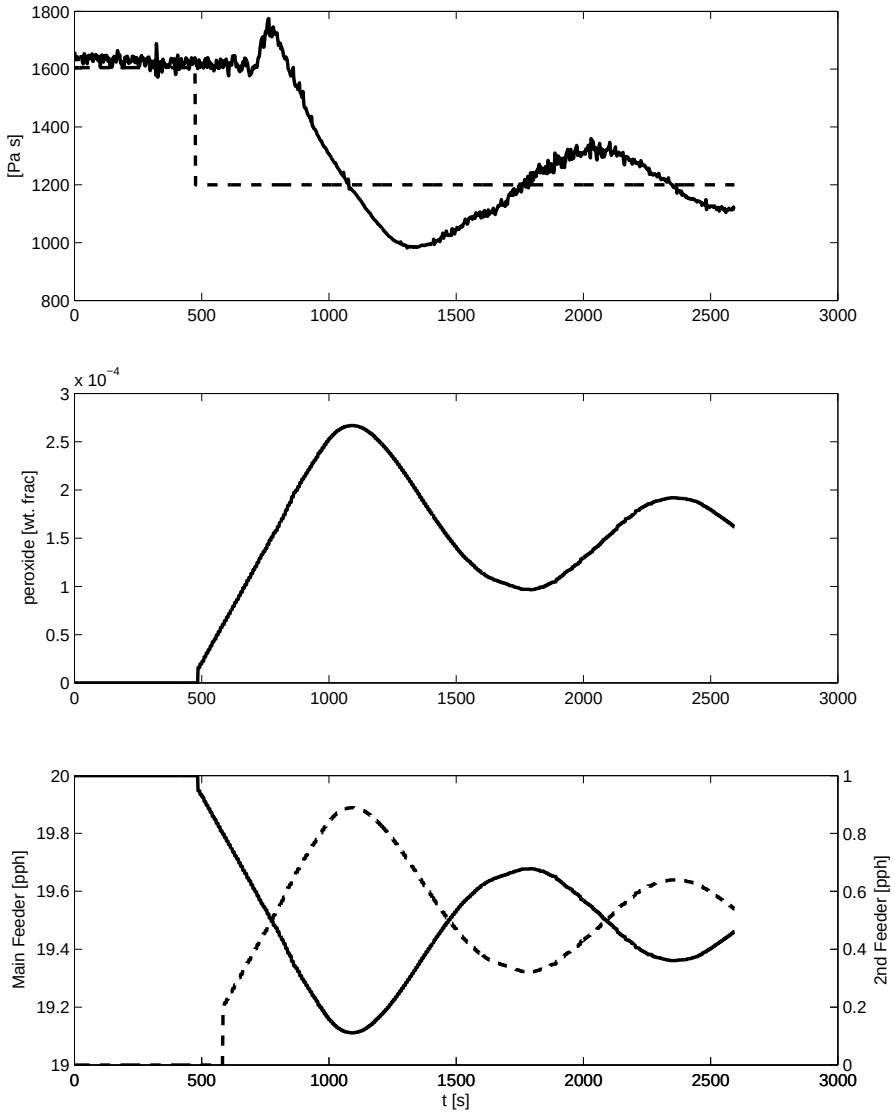

Figure 11.10: Closed loop tracking of extrudate viscosity set point. The operating conditions are $2.98mL/s$ and $2.33rps$. The controller is using the parameters of $Kc = 0.1$ and $\mathrm{Ki} = 0.18min$. The appropriate shape factors and delay times were used in the Smith predictor.

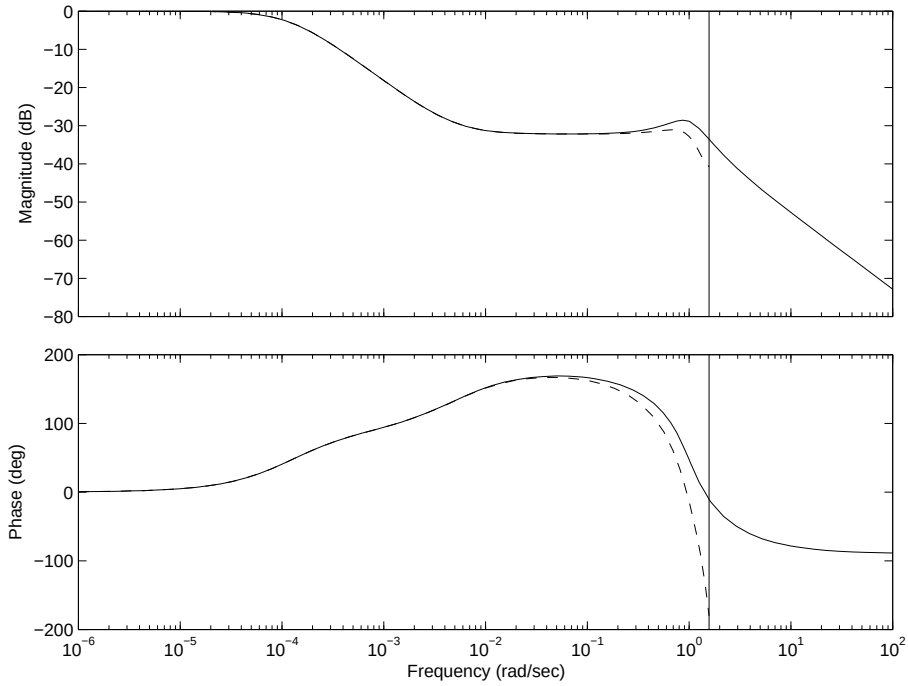

Figure 11.11: Bode plot for figure 11.10.

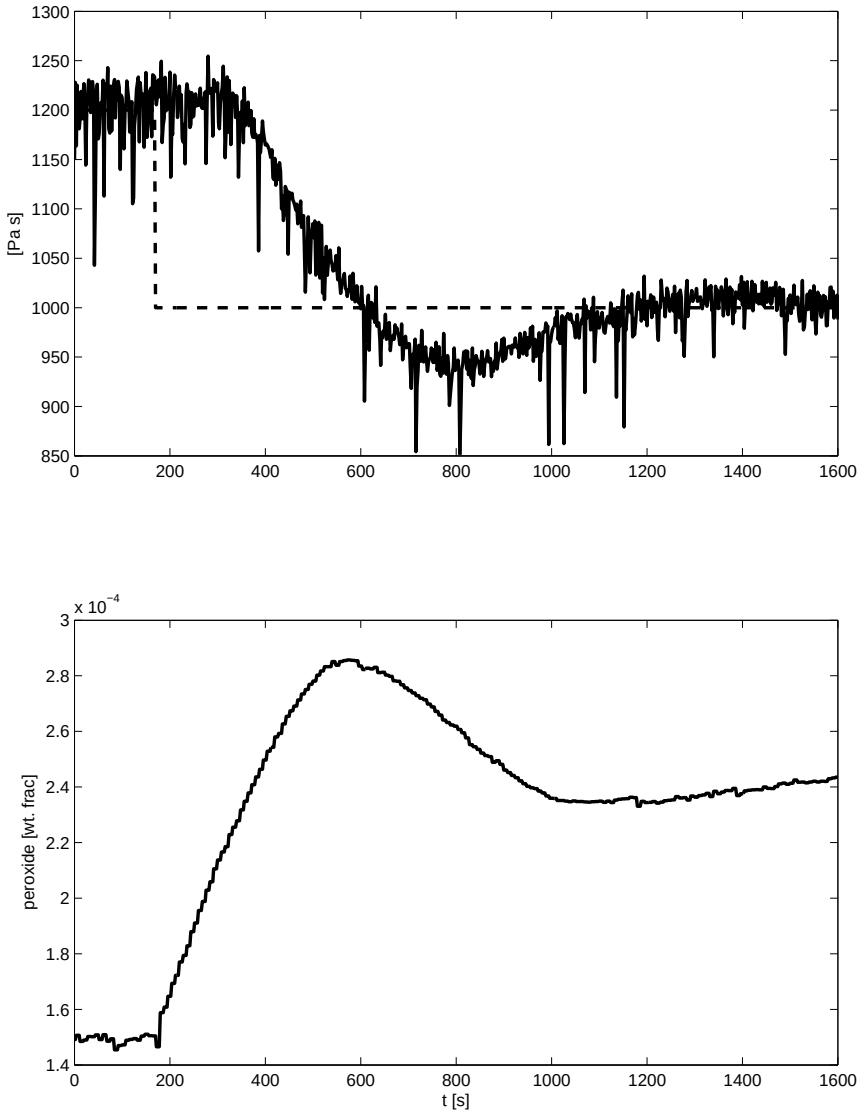

Figure 11.12: Closed loop tracking of extrudate viscosity set point. The operating conditions are $2.98mL/s$ and $2.98rps$. The controller is using the parameters of $K_c = 0.1$ and $K_i = 0.18min$. The appropriate shape factors and delay times were used in the Smith predictor.

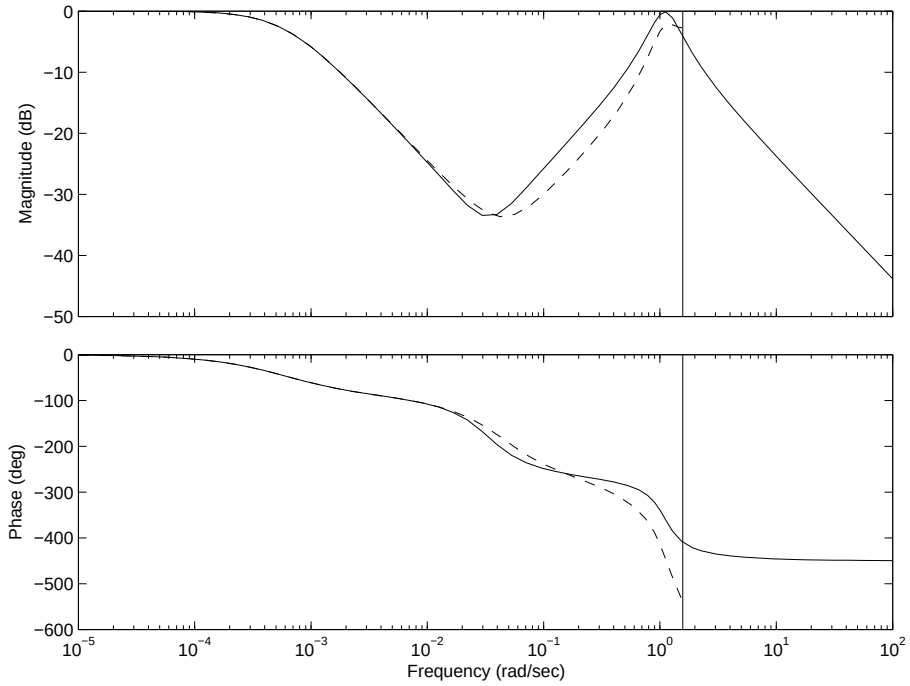

Figure 11.13: Bode plot for figure 11.12.

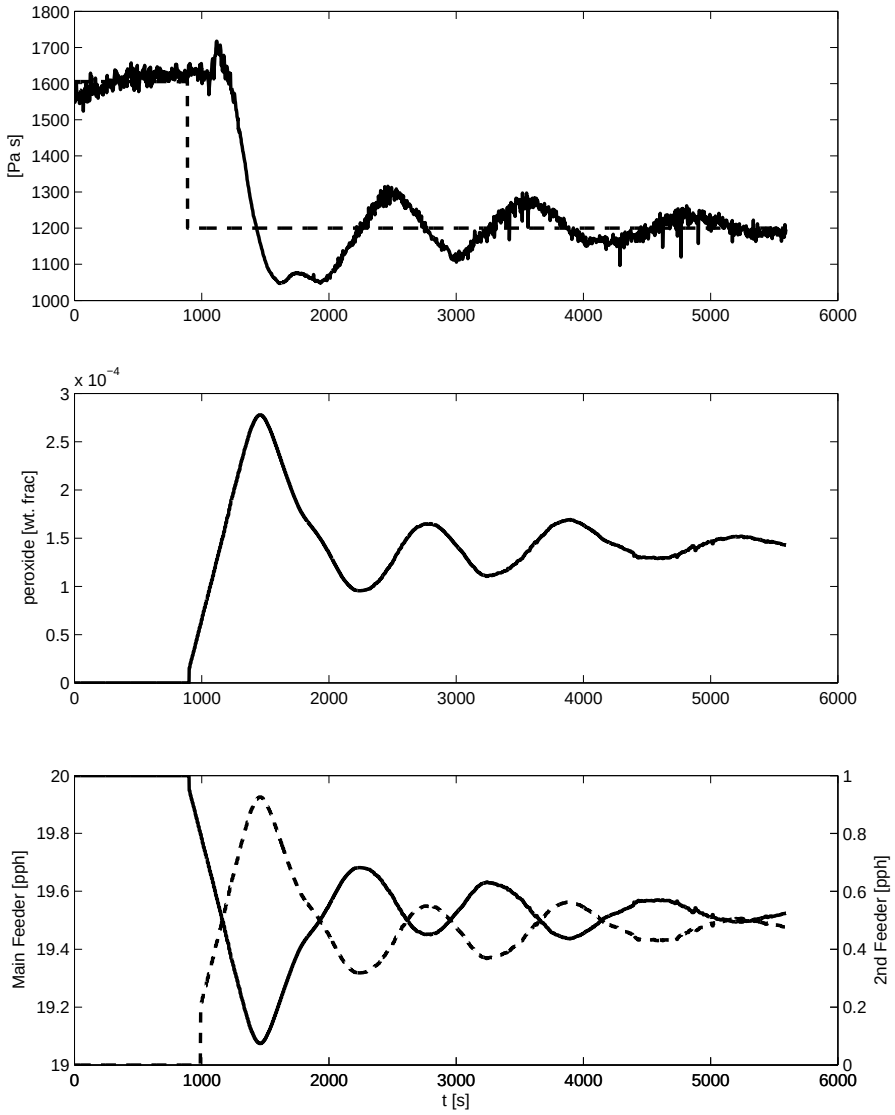

Figure 11.14: Closed loop tracking of extrudate viscosity set point. The operating conditions are $2.98mL/s$ and $2.98rps$. The controller is using the parameters of $Kc = 0.1$ and $Ki = 0.18min$. The appropriate shape factors and delay times were used in the Smith predictor.

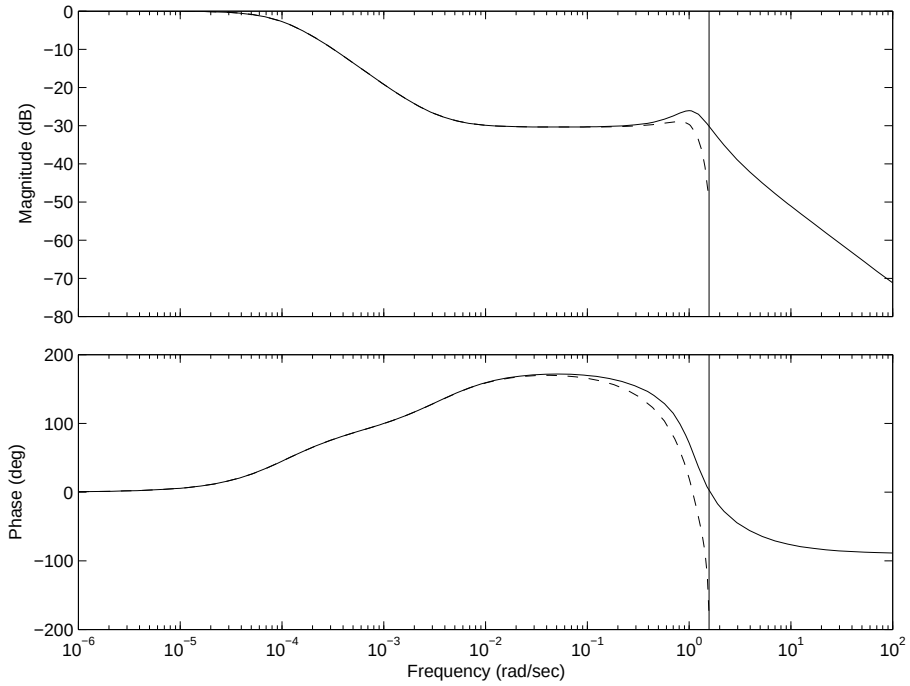

Figure 11.15: Bode plot for figure 11.14.

a delay under such conditions for closed loop control examples. An area where the signals may lead to confusion is the peak that exists immediately before the melt viscosity begins to change after a step is applied, such as in Figure 11.1. This peak must be a sensor measurement problem. The explanation is that the material is already pure feed. It is not possible for the viscosity to increase from addition of peroxide, which the sensor indicates the viscosity does.

The mean rise time for the open loop step changes (excluding those starting without the peroxide feed) is $279s$ at $2.98mL/s$ and $2.33rps$. The mean rise time represents the mean of the rise time for the open loop experiments within Table 11.2. The mean rise time of the $2.98mL/s$ $2.33rps$ closed loop conditions (including the one starting without the peroxide feed) is $174s$ (Table 11.3). This indicates that at $2.98mL/s$ $2.33rps$ the controller can be faster then the open loop system. When the screw speed is increased to $2.98rps$, the mean rise time is $186s$. This is slower then the closed loop conditions at the previous condition. There are no open loop data at this screw speed and no comparison can be made.

Gain and phase margins were also determined for each test. The open loop gain and phase margins (Table 11.2) indicate that the conditions are stable. The closed loop and phase gain margins (Table 11.3) indicate stability also.

Other experiments to test how well the controller regulates the system were also performed. The first tests involved changing the feed rate while controlling the plant. The first case (Figure 11.16) shows that the 50% increase of throughput to $4.47mL/s$ does not make the system unstable in spite of the use of the $2.98mL/s$ $2.98rps$ parameters for the Smith predictor. The controller still keeps the plant under control. The second test (Figure 11.18) uses the same parameters, and while still at $4.47mL/s$ has a tracking example and a regulation

Operating Condition	Initial Condition (Approx. $Pa \cdot s$, $x10^{-4}$ wt. frac)	Final Condition (Approx. $Pa \cdot s$, $x10^{-4}$ wt. frac)	Peak Time $[s]$	Rise Time $[s]$	Gain Margin $[dB]$ [Freq. s^{-1}]	Phase Margin $[deg.]$ $[rad/s]$
$2.98mL/s$	1100	900	946	306	8.7051	-180
$2.33rps$	2	3			1.1354	0
$2.98mL/s$	1000	1100	698	252	5.5359	-180
$2.33rps$	2.5	2			1.5708	0
$2.98mL/s$	1650	975	376	210	6.6691	-180
$2.33rps$	0	2.5			0.9096	0
$2.98mL/s$	1650	1100	860	508	0.991	133.9453
$2.33rps$	0	2			0.0205	1.2155
Figure 11.1						

Table 11.2: Open loop peak and rise times and gain and phase margins. The Initial and Final Condition columns are for descriptive purposes. The mean rise time for the step changes (excluding those starting without the peroxide feed) is 279s.

Operating Condition	Controller K_c K_i $[min]$	Initial Condition (Approx. $Pa \cdot s$, $x10^{-4}$ wt. frac)	Final Condition (Approx. $Pa \cdot s$, $x10^{-4}$ wt. frac)	Peak Time $[s]$	Rise Time $[s]$	Gain Margin $[dB]$ [Freq. s^{-1}]	Phase Margin $[deg.]$ $[rad/s]$
$2.98mL/s$	0.11	1000	1150	756	184	8.5369	-180
$2.33rps$	0.18	2.2	1.5			.0626	0
Figures 11.4 and 11.5							
$2.98mL/s$	0.1	1200	1100	508	110	17.2886	-180
$2.33rps$	0.18	1.5	1.8			0.1982	0
Figures 11.6 and 11.7							
$2.98mL/s$	0.1	1100	1000	490	184	1.2269	-180
$2.33rps$	0.18	1.8	2.2			1.5708	0
Figures 11.8 and 11.9							
$2.98mL/s$	0.1	1000	900	576	172	11.135	-180
$2.33rps$	0.18	2.2	2.5			0.0865	0
$2.98mL/s$	0.1	1600	1200	862	228	109.1656	-180
$2.33rps$	0.18	0	1.7			1.5708	0
Figures 11.10 and 11.11							
$2.98mL/s$	0.1	1200	1000	630	196	1.376	-180
$2.98rps$	0.18	1.5	2.4			1.5708	0
Figures 11.12 and 11.13							
$2.98mL/s$	0.1	1600	1200	730	176	285.1959	-180
$2.98rps$	0.18	0	1.5			1.5708	0
Figures 11.14 and 11.15							

Table 11.3: A table of the closed loop figures of responses, and the associated peak and rise times and gain and phase margins. The Initial and Final Condition columns are for descriptive purposes. Unless otherwise noted the Smith predictor and delay parameters were appropriate for the operating conditions. The mean rise time of the 2.98 mL/s and 2.33 rps conditions with Kc = 0.10 and Ki = 0.18 min (including the one starting without the peroxide feed) is 174s.

example. In spite of incorrect parameters, the plant does track the set point change. Afterwards, the change of feedrate back to the original $2.98mL/s$ does not perturb the system to instability. This test also indicates that with the wrong Smith and delay parameters the rise time for the system is only 200s. The figures illustrate that there was more noise for at the lower feed rate. It is surmised that the higher specific throughput stabilized the viscosity measurement by increasing the size of the fully filled die section.

The controller was relatively insensitive to the mismatch of Smith predictor parameters. The most important parameter is the delay time, and inspection of Table 8.1 indicates that the delay and shape factor of the viscometer contributed more time delay then the mixing and die regions of the extruder.

In addition to the regulation problem of changing the feed rate, there also exists the issue of changing feed quality. In order to investigate such a case, a dry mixture of 50% NP and 50% Montell SM6100 (SM) was made. This alternate feed stock is a drastically different feed as the SM is much less viscous then the NP. Figure 11.20 shows the ability of the controller to handle the switch to the alternate feed stock and back. This large difference in feed certainly changed the suitability of the non-linear gain function; the other parameters may also have been inadequate. Although it did fluctuate, the viscosity did stay within $\pm 180 Pa \cdot s$. The change in set point did seem to push the system out of balance, but this could not be investigated more due to time constraints. The bode diagram (Figure 11.21) indicated a stability in the system; however it is clear that the viscosity tracking was certainly not as good as the previous examples.

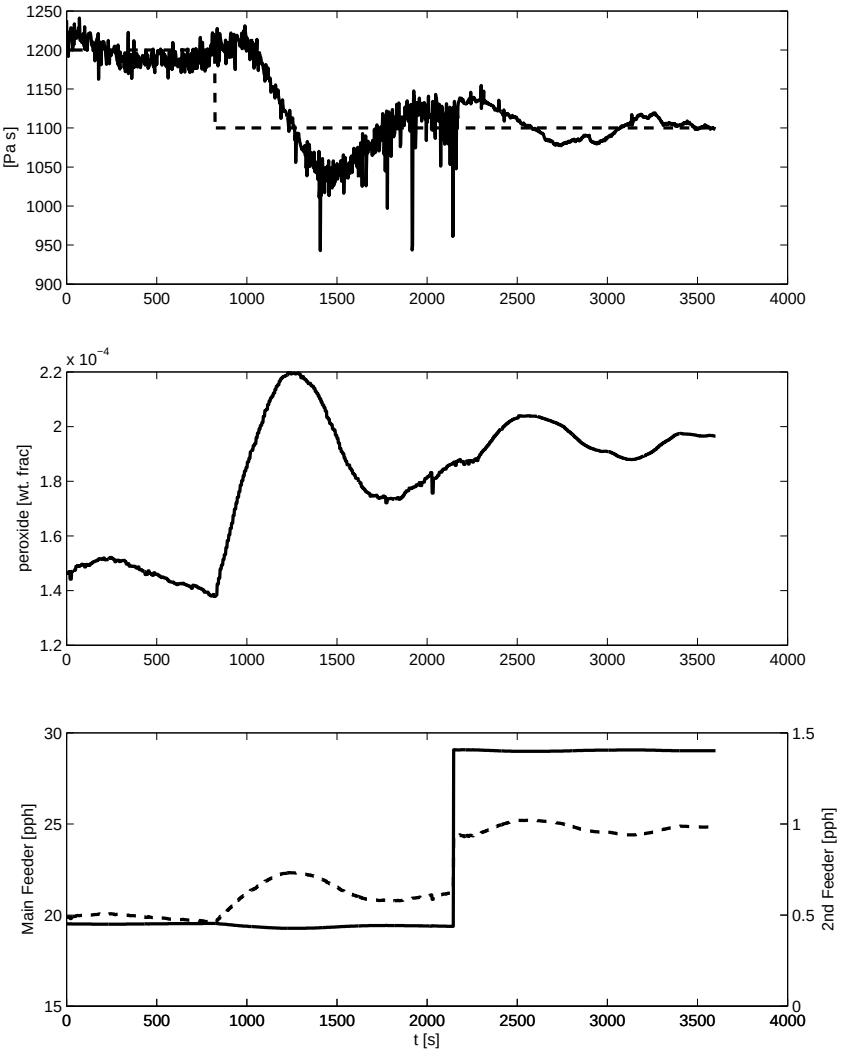

Figure 11.16: Closed loop regulation of extrudate viscosity set point. The controller is using the parameters of $K_c = 0.1$ and $K_i = 0.18min$. The shape factors and delay times for the initial condition were used in the Smith predictor. The operating conditions were initially $2.98mL/s$ and $2.98rps$. The feed rate was then changed to $4.47mL/s$.

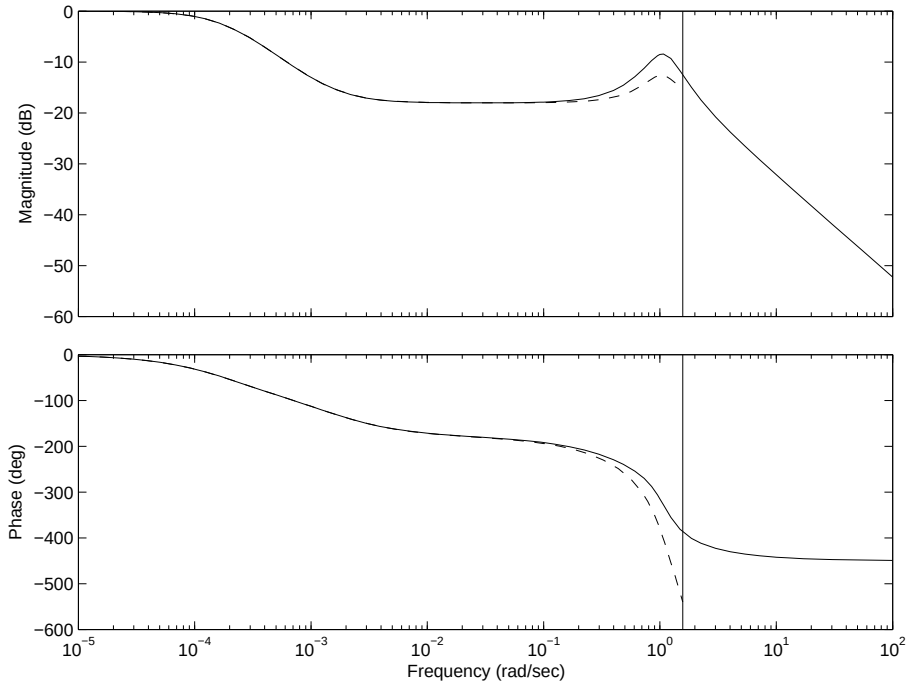

Figure 11.17: Bode plot for figure 11.16.

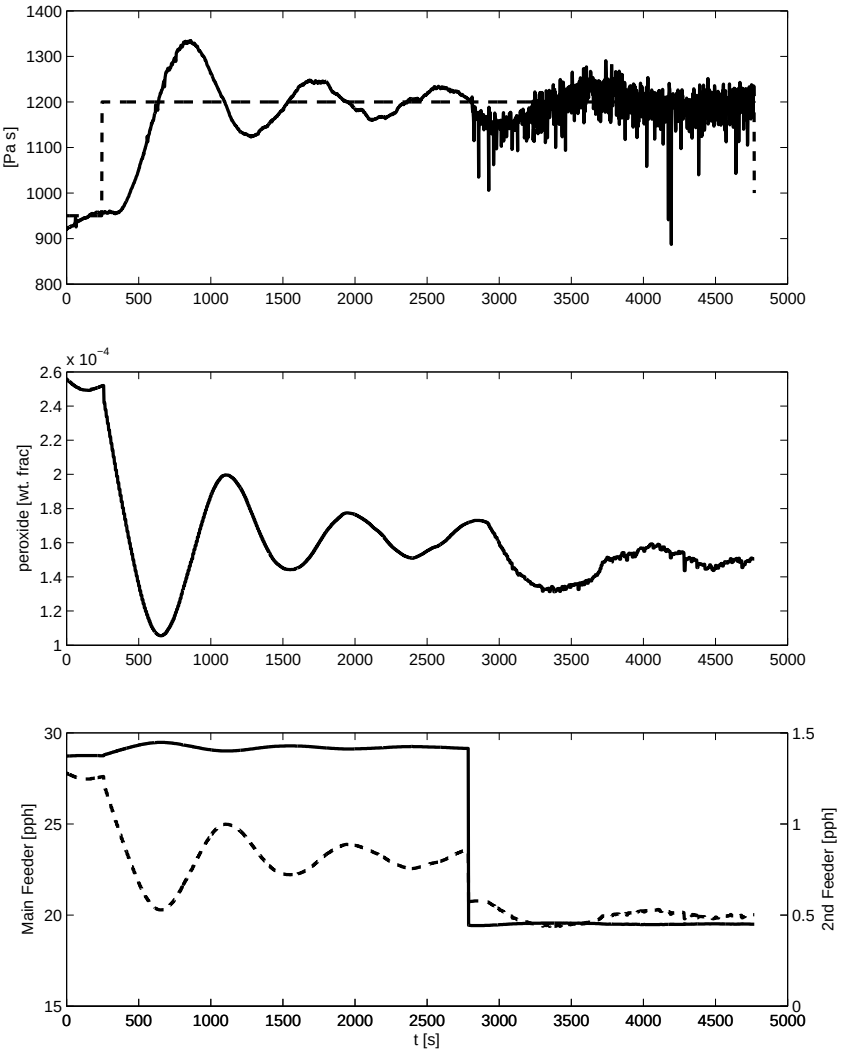

Figure 11.18: Closed loop regulation of extrudate viscosity set point. The controller is using the parameters of $K_c = 0.1$ and $K_i = 0.18min$. The shape factors and delay times for the second condition were used in the Smith predictor. The operating conditions were initially $4.47mL/s$ and $2.98rps$. The feed rate was then changed to $2.98mL/s$.

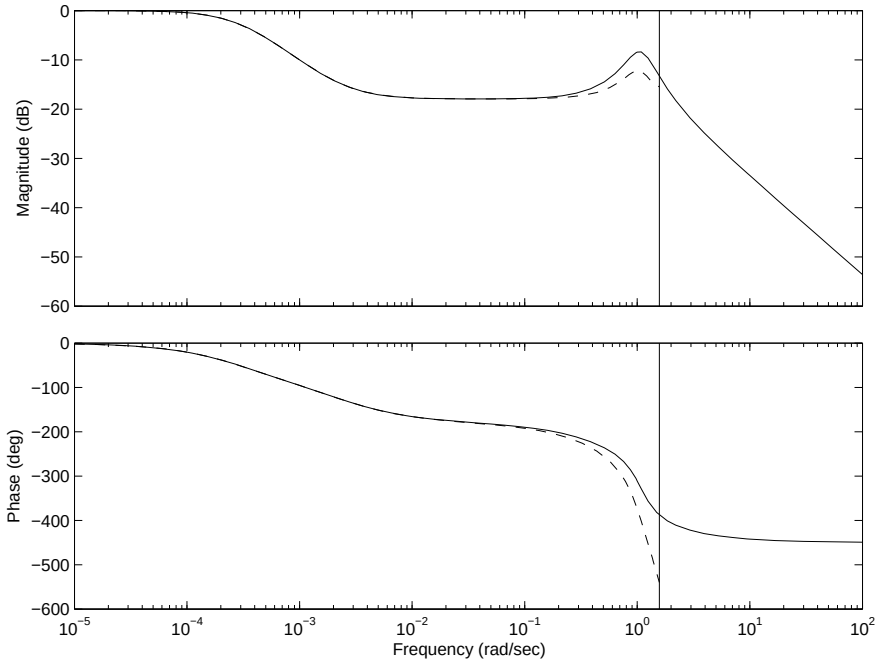

Figure 11.19: Bode plot for figure 11.18.

Figures	Initial Condition	Final Condition
11.16 & 11.17	$2.98mL/s$	$4.47mL/s$
	$2.98rps$	$2.98rps$
11.18 & 11.19	$4.47mL/s$	$2.98mL/s$
	$2.98rps$	$2.98rps$
11.20 & 11.21	NP	50% NP
$2.98mL/s$ & $2.33rps$		50% SM6100

Table 11.4: Closed loop conditions with gross disturbances. All conditions were with $K_c = 0.1$ and $K_i = 0.18min$. The smith predictor parameters were those for $2.98mL/s$ and $2.98rps$ for the first two conditions, and $2.98mL/s$ and $2.33rps$ for the third.

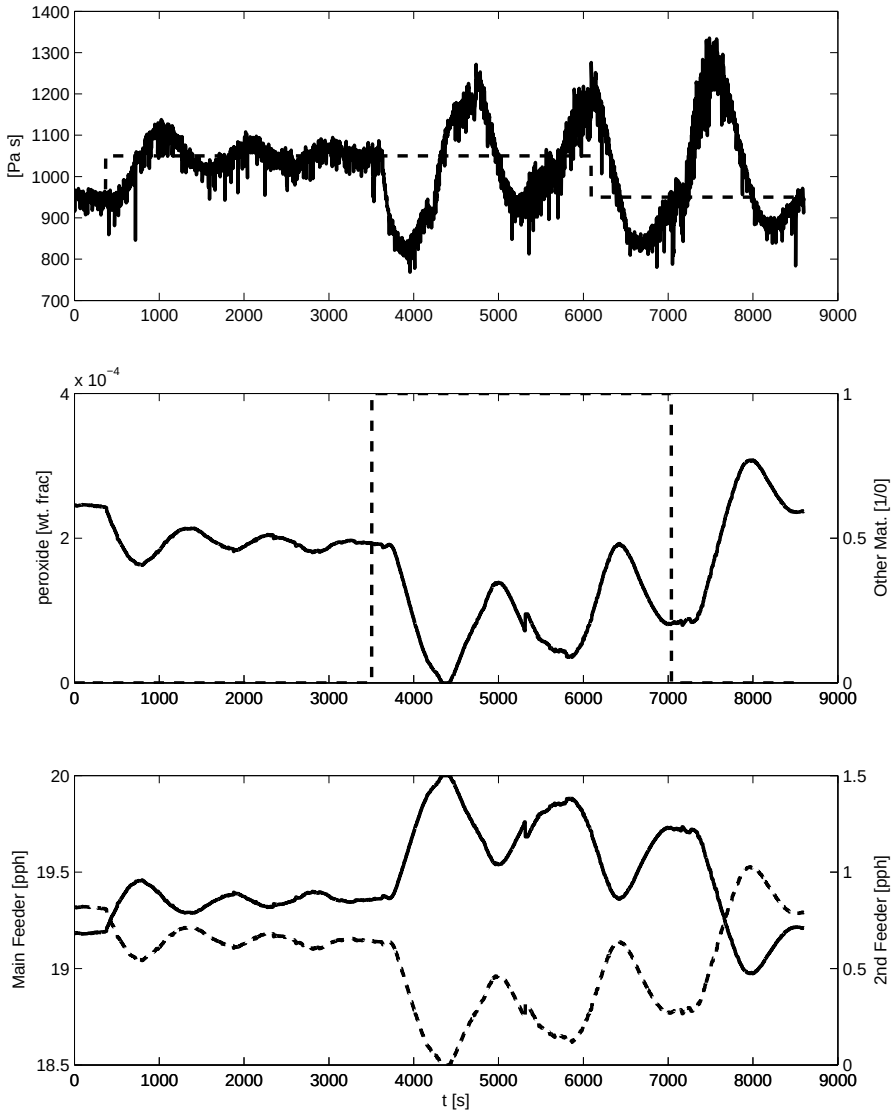

Figure 11.20: Closed loop tracking of extrudate viscosity set point. The operating conditions are $2.98mL/s$ and $2.98rps$. The controller is using the parameters of $Kc = 0.1$ and $Ki = 0.18min$. The appropriate shape factors and delay times were used in the Smith predictor.

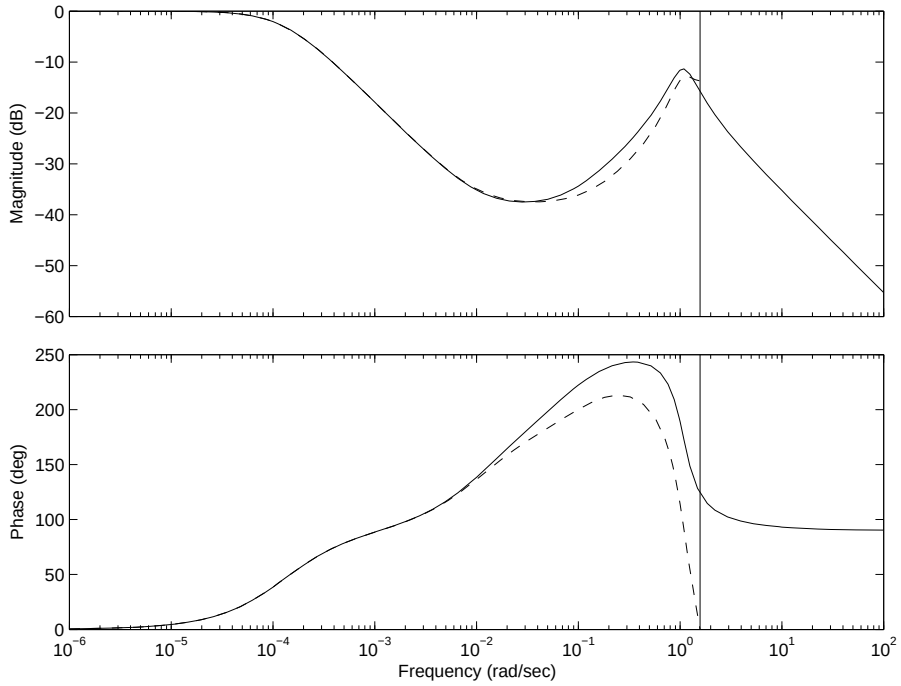

Figure 11.21: Bode plot for figure 11.20.

11.5.1 Improvement of Controller

Some of the closed loop experiments show responses that indicate oscillation in the melt viscosity after the viscosity response has peaked and begun its decay. To improve this response, it would be effective to implement a proportional and integral and derivative (PID) controller. A model plant of similar magnitude poles is selected for the extruder-viscometer.

$$G = \frac{1}{(s+0.1)(s+0.01)(s+0.001)} \tag{11.5}$$

To simulate the response to step inputs, the MatLAB SISO Design tool has been used. The system with a completely effective Smith Predictor has been modeled. Normalized response of the open loop plant to a step input can bee seen in Figure 11.22. The rise time is $2191s$ and the settling time is $3899s$.

Implementing a simple feed back loop with a proportional controller yields the response in Figure 11.23. As expected, there is an offset, and the system does not reach the set point. With a gain, $K = 6.58e-6$, so that the percent overshoot is approximately 10%, the rise time is $213s$, and the settling time is $694s$.

Adding an integrator though a PI controller improves the set point tracking abilities (Figure 11.24) and quickly reduces the offset. However, the PI adds $9s$ to the rise time and $254s$ to the settling time. The controller has a gain, $K = 6.06e-9$, a pole at 0, and a zero at $-9e-4$; the zero is smaller then the smallest plant pole.

Adding the derivative control through a PID controller corrects for the shortcomings of the PI controller, while keeping its advantages (Figure 11.25). The rise time only increases by $1s$. The settling time decreases by $248s$; this almost

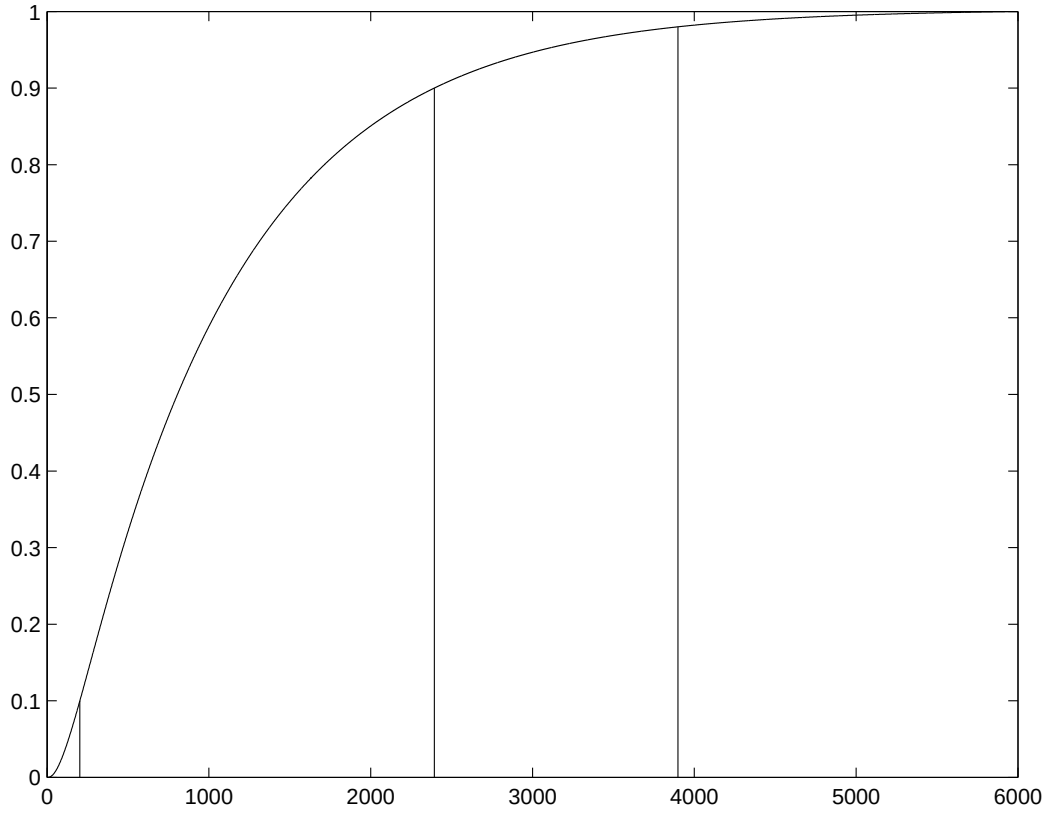

Figure 11.22: Normalized open loop step response. The rise time is $2191s$ and the settling time is $3899s$.

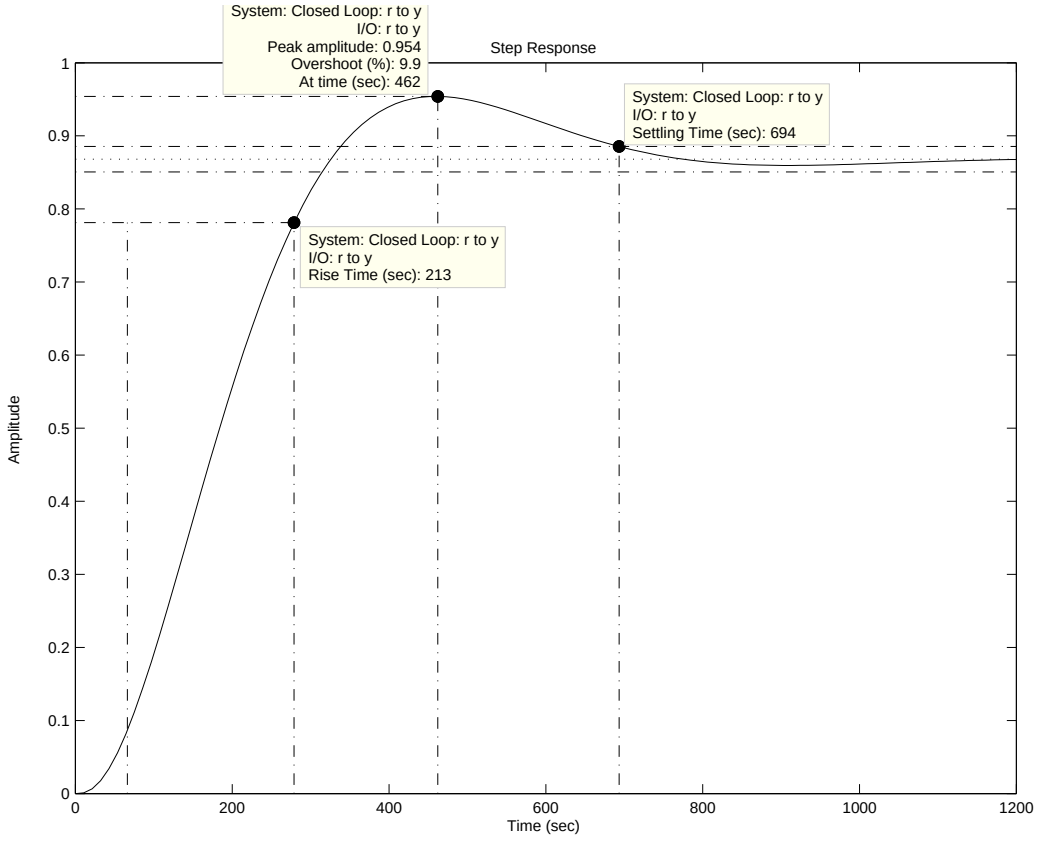

Figure 11.23: Proportional controller step response. The gain, $K = 6.58e - 6$, is set so that the percent overshoot is approximately 10%, the rise time is $213s$, and the settling time is $694s$.

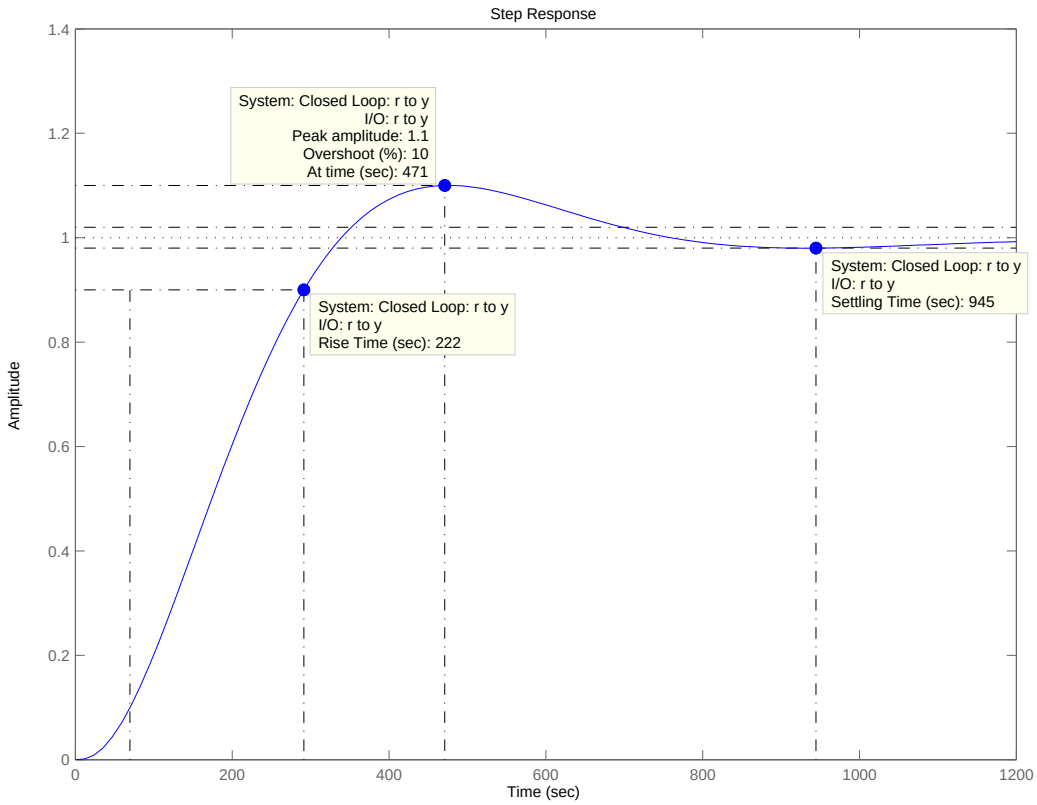

Figure 11.24: Proportional Integral controller step response. The gain, $K = 6.06e-9$, is set so that the percent overshoot is 10%, and the PI controller has no offset The PI adds $9s$ to the rise time and $254s$ to the settling time. The controller has a gain, $K = 6.06e-9$, a pole at 0, and a zero at $-9e-4$.

negates the penalty from adding the integrator. The PID controller is the same as the PI controller with the addition of a zero at -1. This zero is selected to be more negative than the largest pole of the open loop plant.

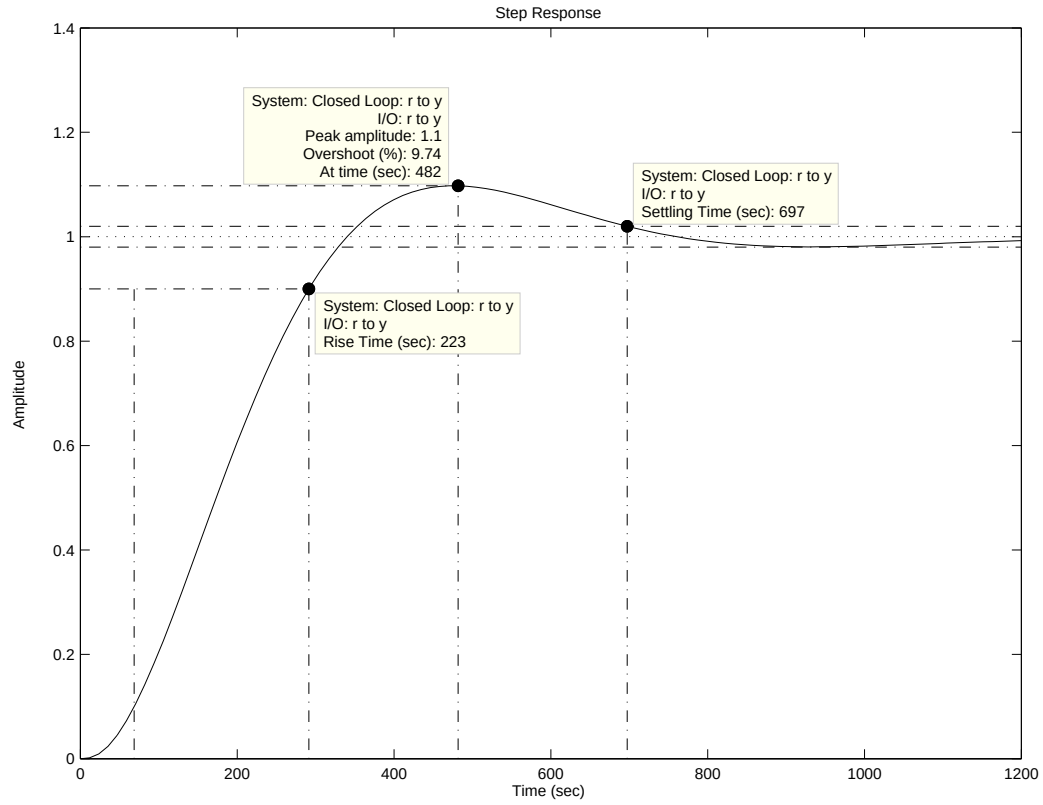

Figure 11.25: Proportional Integral Derivative controller step response. In comparison to the PI controller, the rise time only increases by $1s$, and the settling time decreases by $248s$, which almost equals the penalty from adding the integrator. The PID controller is the same as the PI controller with the addition of a zero at -1.

Wise selection of the location of the zeros and gain for the PID controller. The parameters can be selected to move the closed loop "poles" to negatively larger values, an this would decrease the rise time. The hazard to this is that the

control input could saturate. This would diminish the ability of the controller near these saturation limits.

11.6 Conclusion

The control of the reactive extrusion process was successful. It can be seen that a controller was developed which was insensitive to numerous system parameters such as feed rate and screw speed and still tracked set point changes. Additionally, the smith predictor was developed from data for a different polymer with some material similarities, although with different temperature sensitivities. At given operating condition, it did track a set point changes faster then the open loop system. The controller was able to control the plant in spite of incorrect parameters for the smith predictor. The controller also seemed to keep the viscosity loosely bounded for gross perturbations to feed stock, although it was not well suited for set point tracking with the grossly different feed stock.

Chapter 12

Conclusions

This work was performed to automatically control a reactive extrusion process. It was necessary to characterize the system and design and implement a suitable controller. In order to characterize the system, the work by Gao et al. [14] was expanded upon with additional instrumentation of the extruder. Equation 5.1 was used to determine parameters for the RTD signals found from RTD probes at each filled zone of the extruder. The equation was also used as the basis for the determination of RTD's representing individual screw zones through deconvolution of the signals. This was successful; however, Equation 5.1 was developed for a screw with three filled zones. Due to this, a better model was necessary for description of other geometries or individual zones.

A new kinematic RTD model is described (Equations 8.1 and 8.2). This model allows for the individual description of the zones of the extruder through a shape factor and a delay time. Determination of the parameters is performed by deconvolution of the reflectance probe signals. The deconvolution process allows for the determination of individual zones from probes describing composite regions of the screw. When this model is used in the volume domain, the corresponding RVD description, Equation 8.4 is made. It possesses parameters

that are consistent over a broad range of conditions, and allow for description of the family of curves with one set of parameters. This simplification of the extruder description can make other tasks simpler to analyze. The individual zones of the screw can be described by a consistent volume domain shape factor, c, which describes all the curves. The viscometer's parameters were also determined, however its shape factor were not as consistent as the screw zones. The steady state data used to characterize the extruder dynamics was also used to relate the steady state relationships of the peroxide concentration and the melt viscosity of the extrudate.

Experimental data have shown that the residence distributions can be very similar for two different materials. This is the case for the two polyethylenes, which in spite of having different viscosities have very similar residence distributions, as indicated by their volume domain shape factors. The two polypropylenes did not show this same behavior.

The rheometric analysis of these phenomena have allowed for computation of the Weissenberg number for each polymer studied. The two polymers with similar RVD's, the polyethylenes, also have very similar Weissenberg numbers as a extension of having similar modulus crossover frequencies. Both Weissenberg numbers indicate viscous behavior. However, the Weissenberg numbers calculated for the polypropylenes, which had dissimilar modulus crossover frequencies, indicated more viscous behavior for one, while the other had more elastic behavior.

It is possible that when elastic effects are at a minimum as shown with the Weissenberg numbers, even large differences in viscosity have minimum effect on the residence distributions. On the other hand, when elastic effects are present, even polymers of the same viscosity will show varying distributions. This work

does reinforce the assertion that the residence time distribution is independent of certain material properties for specific cases. However, inspecting the simple viscosity alone will not help explain why different materials have similar residence distributions, while others have different ones. Analysis of the complex viscosity and computation of the Weissenberg number may be a better tool for this comparison. A consequence of this is that visco-elastic properties are very important to the residence distributions.

The control of the reactive extrusion process was successful. It can be seen that a controller was developed which was insensitive to numerous system parameters such as feed rate and screw speed and still tracked set point changes. Additionally, the smith predictor was developed from data for a different polymer with some material similarities, although with different temperature sensitivities. At given operating condition, it did track a set point changes faster then the open loop system. The controller was able to control the plant in spite of incorrect parameters for the smith predictor. The controller also seemed to keep the viscosity loosely bounded for gross perturbations to feed stock, although it was not well suited for set point tracking with the grossly different feed stock.

Chapter 13

Future Work

The work presented suggests two areas of research that should be further studied. They are the effect that material qualities have upon residence distributions, and controlling the reactive extrusion process.

Although four materials were tested with batteries of RTD measurements, insufficient data was available to correlate the Weissenberg number to the measured characteristics of the residence distributions, one being c, the volume domain shape factor. It is suggested that future RTD collections with other materials also use the same screw geometry and extruder, and use the historic operating conditions. This would allow for ready comparison of different materials, and also help determine if functional relationships exist between the Weissenberg number and the RTD. Materials with different crossover frequencies as well as materials of other types of polymers would be very informative.

The work for the control of reactive extrusion should be to expand the ability of the controller over a large range of operating conditions and materials. Currently materials must be tested to determine a gain function relating the peroxide concentration to the melt viscosity. Implementation of the warp time model should allow for prediction of the melt viscosity as a function of operating condi-

tions and peroxide concentration. Otherwise, a comprehensive set of data would be needed to determine functional parameters for a gain function. Additionally, the controller should be implemented and tested in the volume domain to take advantage of the uniformity of the RVD curve. The control software should also be designed to handle changes in transport and measurement delays as a function of operating conditions. the controller should also be expanded from a PI controller to a PID controller. The advantages (Section 11.5.1) of such a change would allow for improved settling time.

Appendix A

Residence Distribution Figures for KF6100

A.1 Residence Time Distribution

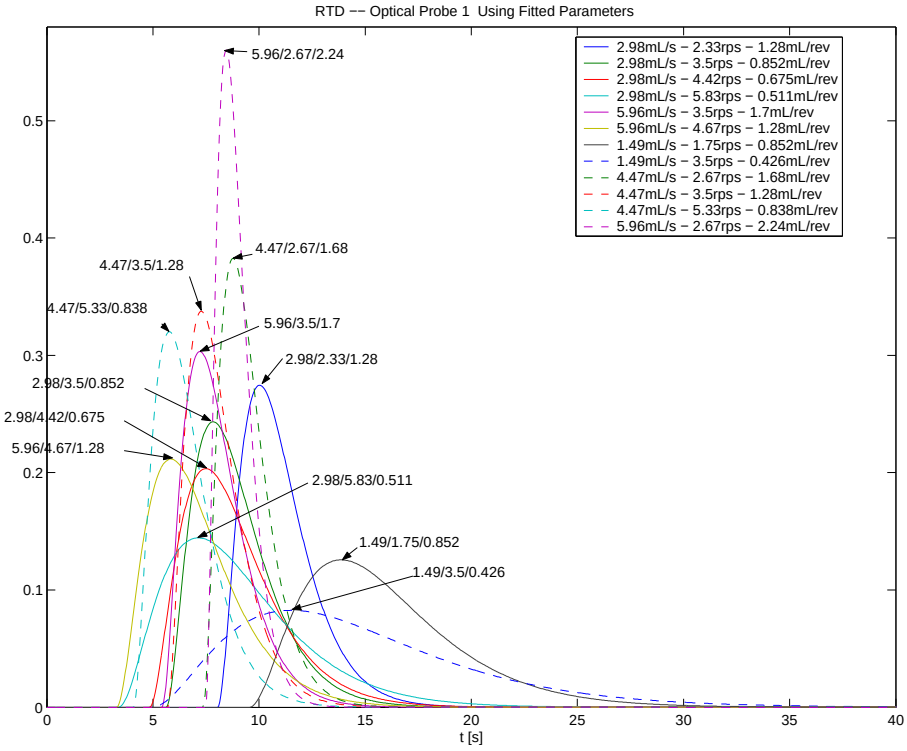

Figure A.1: The residence time distribution for the first reflectance probe.

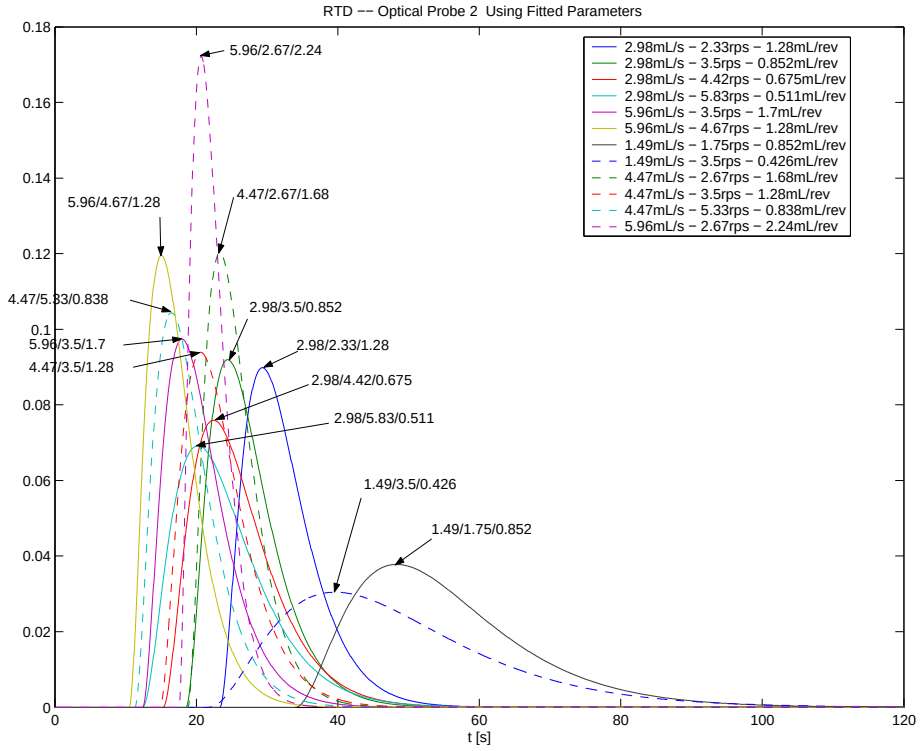

Figure A.2: The residence time distribution for the second reflectance probe.

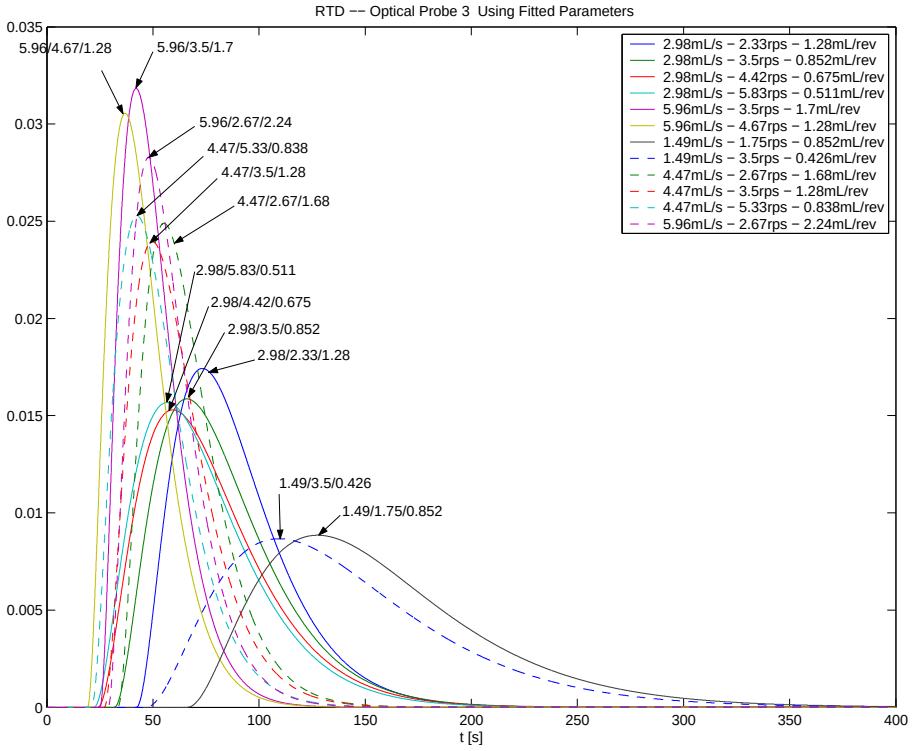

Figure A.3: The residence time distribution for the third reflectance probe.

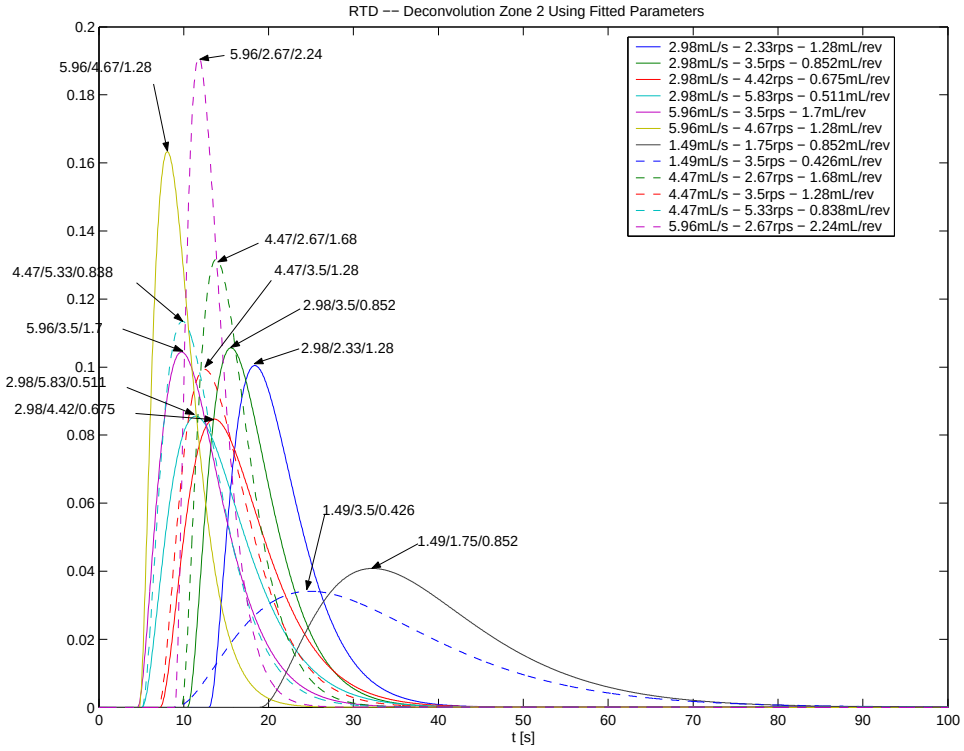

Figure A.4: The residence time distribution for the deconvoluted mixing zone.

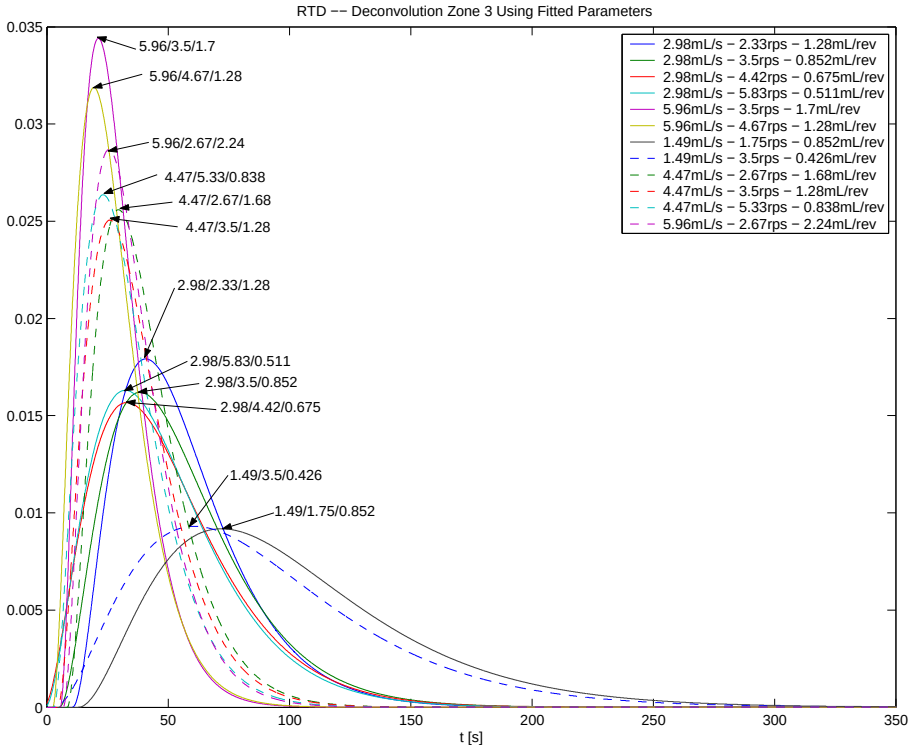

Figure A.5: The residence time distribution for the deconvoluted metering zone.

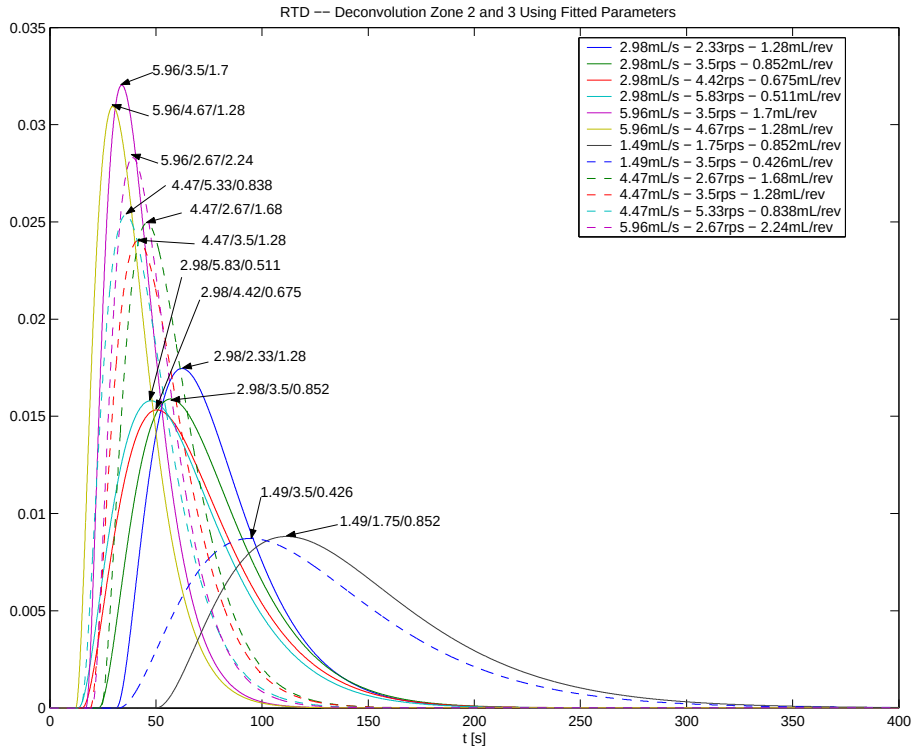

Figure A.6: The residence time distribution for the deconvoluted mixing and metering zones.

A.2 Residence Volume Distribution

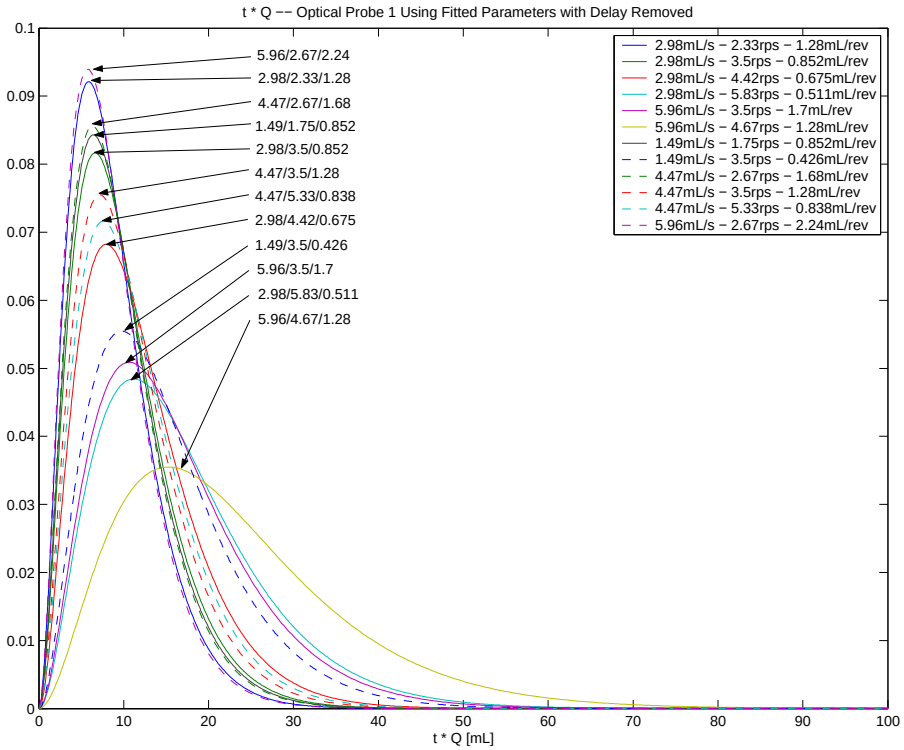

Figure A.7: The residence volume distribution for the first reflectance probe.

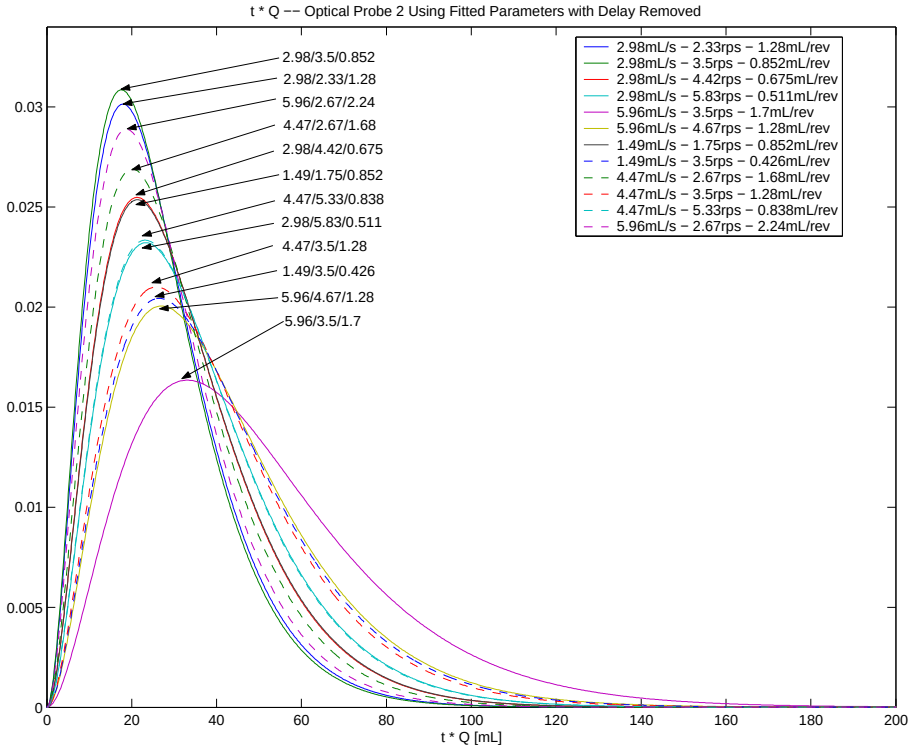

Figure A.8: The residence volume distribution for the second reflectance probe.

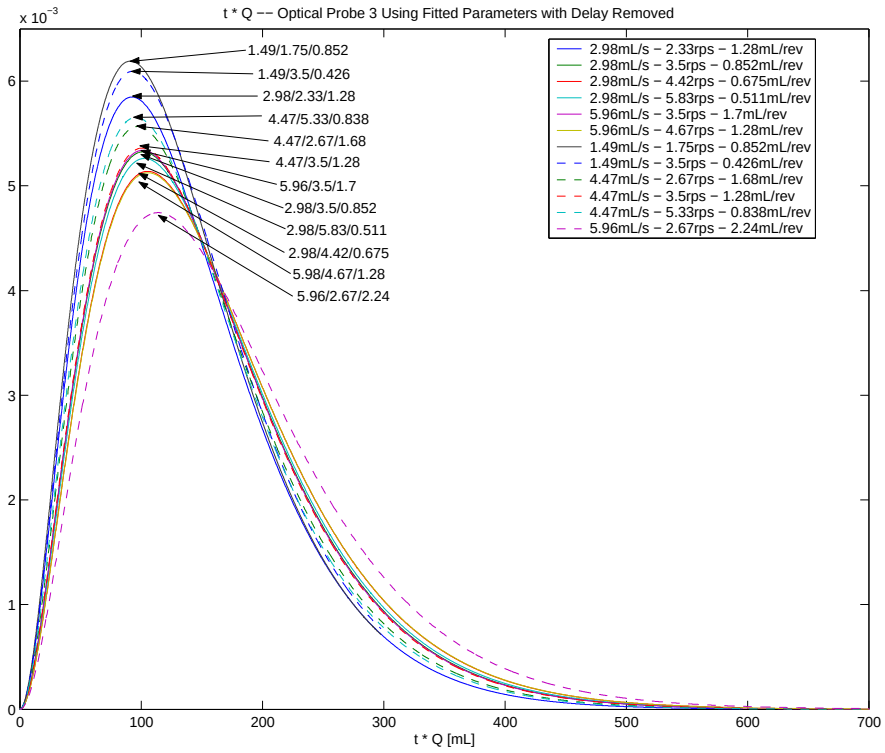

Figure A.9: The residence volume distribution for the third reflectance probe.

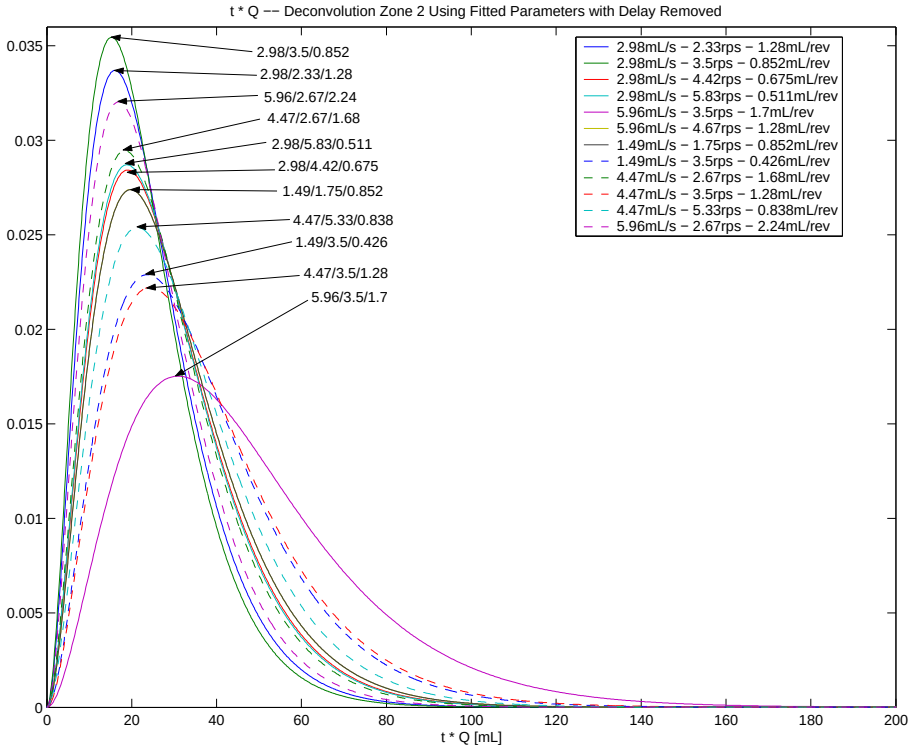

Figure A.10: The residence volume distribution for the deconvoluted mixing zone.

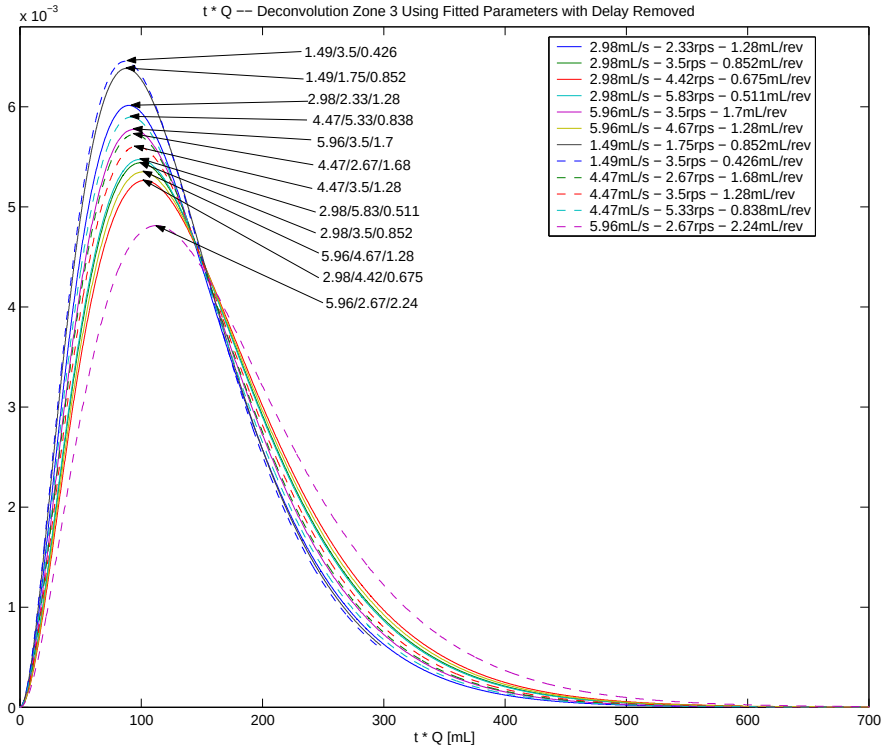

Figure A.11: The residence volume distribution for the deconvoluted metering zone.

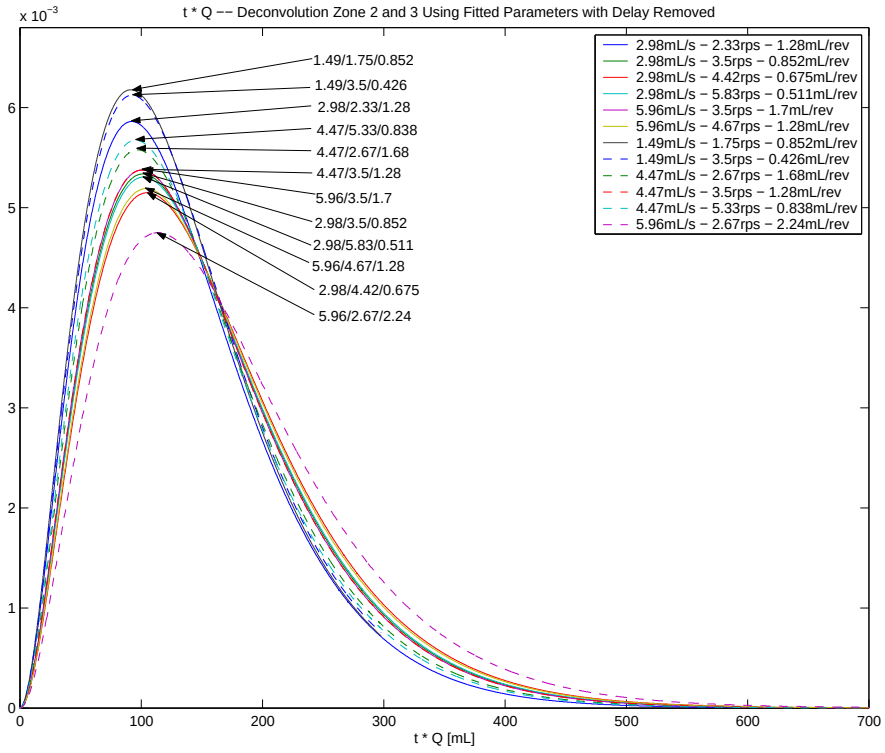

Figure A.12: The residence volume distribution for the deconvoluted mixing and metering zones.

A.3 Residence Rotation Distribution

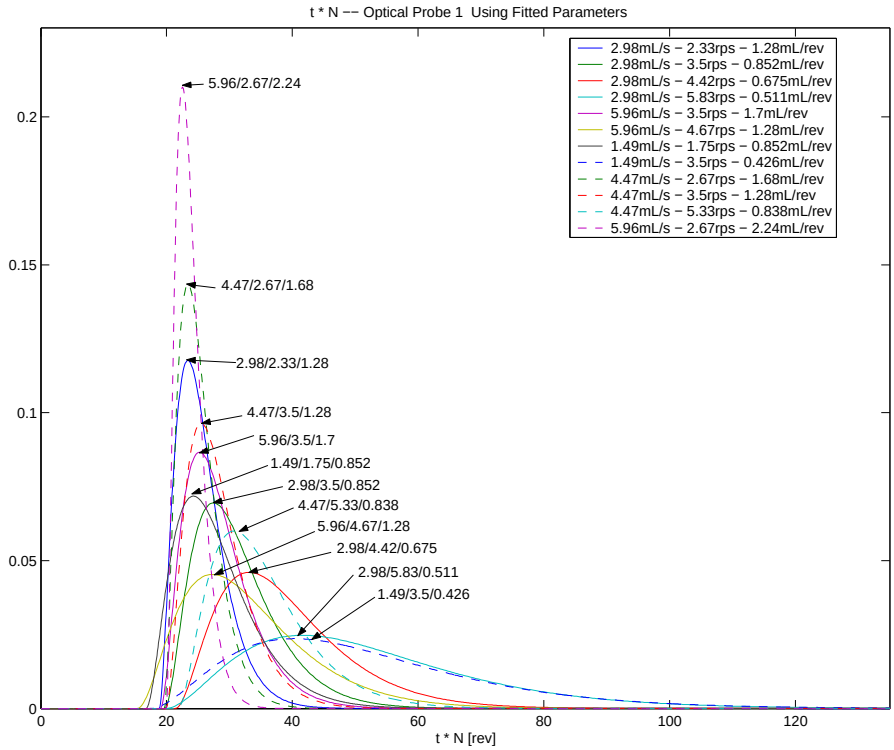

Figure A.13: The residence rotation distribution for the first reflectance probe.

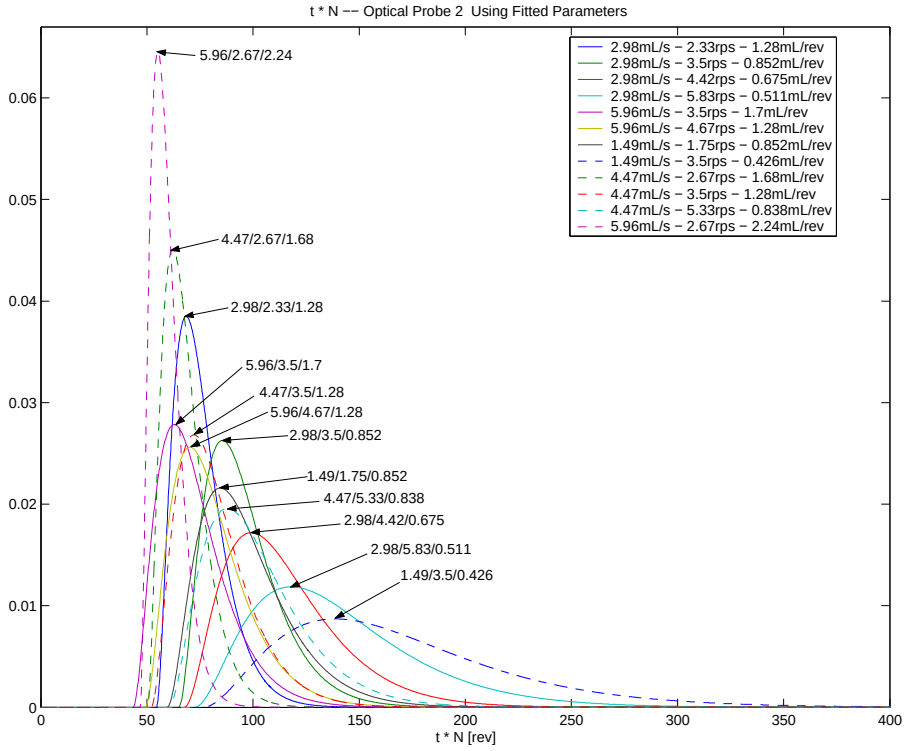

Figure A.14: The residence rotation distribution for the second reflectance probe.

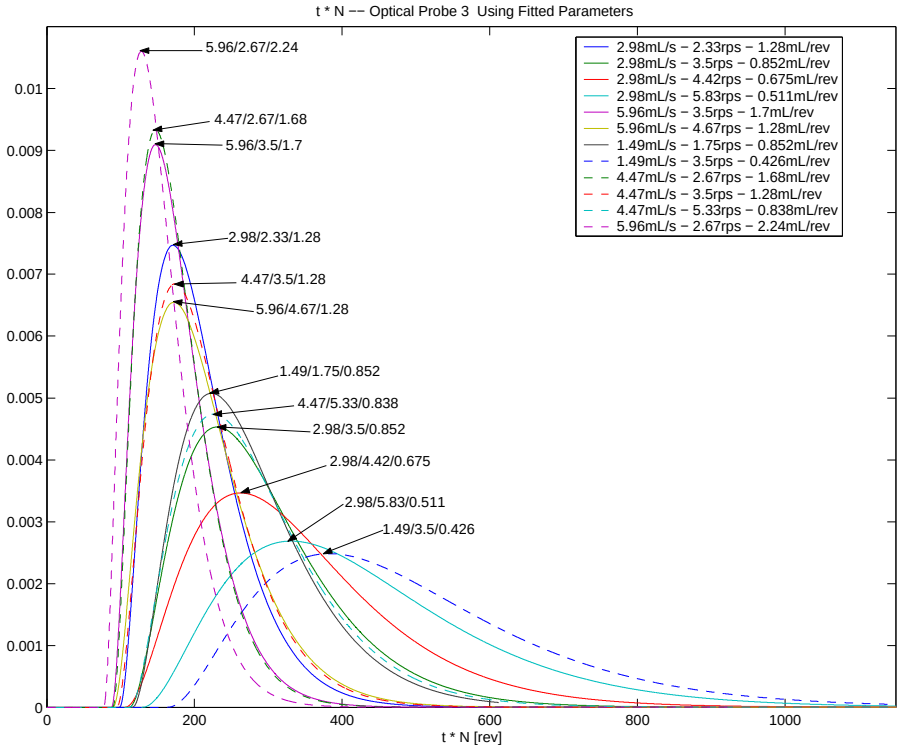

Figure A.15: The residence rotation distribution for the third reflectance probe.

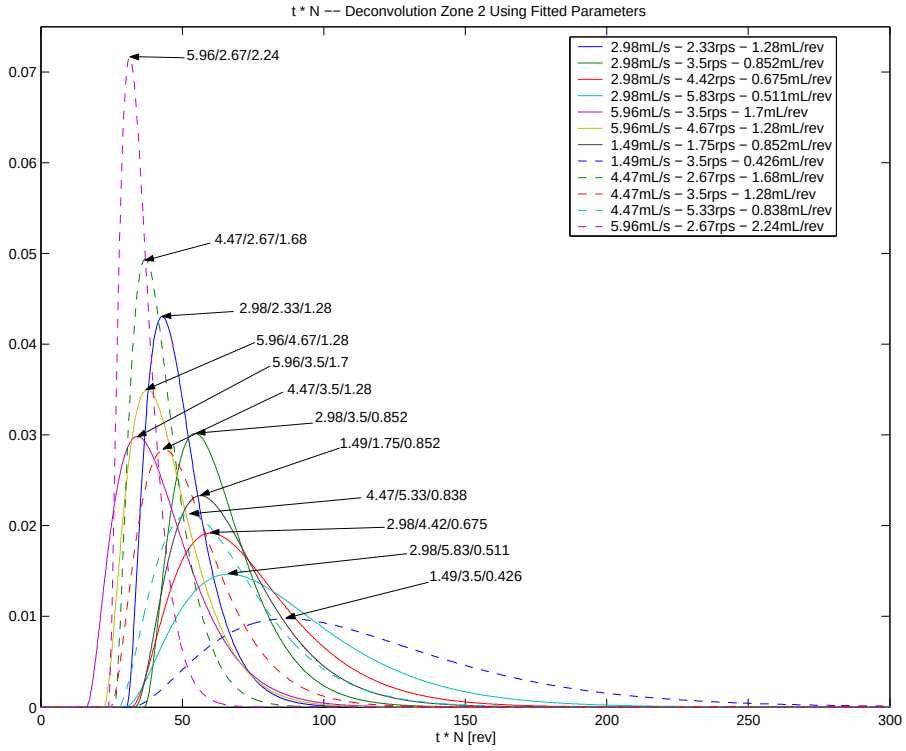

Figure A.16: The residence rotation distribution for the deconvoluted mixing zone.

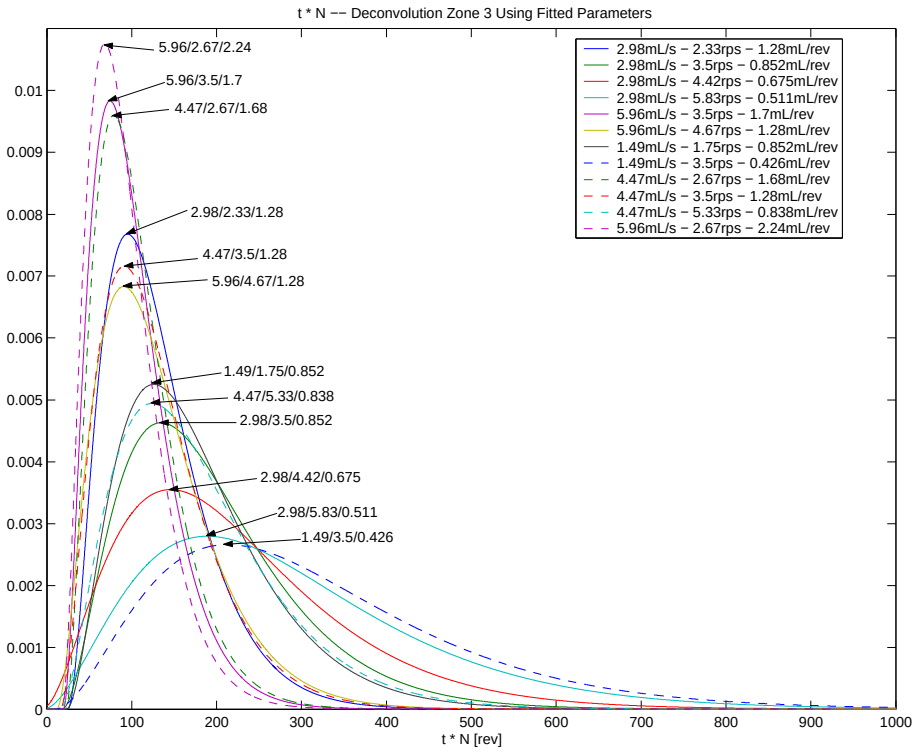

Figure A.17: The residence rotation distribution for the deconvoluted metering zone.

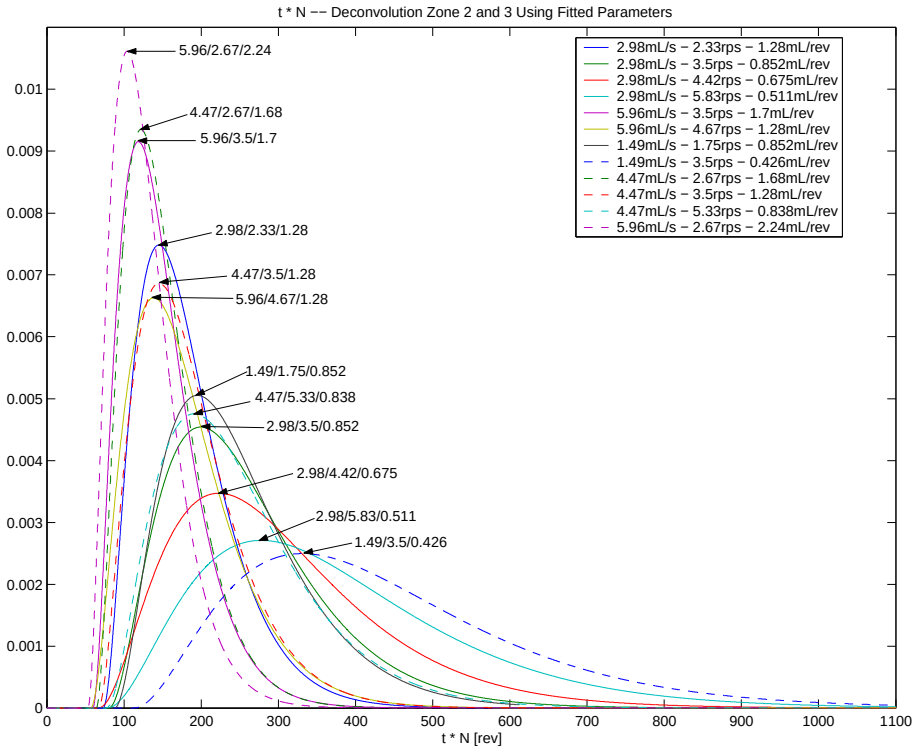

Figure A.18: The residence rotation distribution for the deconvoluted mixing and metering zones.

Appendix B

Steady State Statistical Analysis of Viscosity Data

B.1 Subset Regressions

The following results are the first subset regressions and regression for the statistical analysis of the steady state data. Eighteen cases were used for each analysis. The analysis was for the KF6100 material.

Var's	R^2	R^2_{adj}	C_p	S	t_m Zone2,3 $[s]$	Q/N $[mL/r]$	$[I] \cdot N_m$ $[wt\% \cdot r]$
1	94.0	92.1	4.4	120.80			X
1	91.7	89.2	9.0	141.48	X		
2	94.1	91.7	6.1	124.11	X		X
2	94.1	91.6	6.2	124.57		X	X
3	94.6	91.7	7.0	123.75	X	X	X

Table B.1: As discussed in Section 6.3.1, this table shows the results from the preliminary best subsets regression for viscosity $[Pa \cdot s]$ versus $[I]$, N_m, Q_m, and other variables as noted above.

Var's	R^2	R^2_{adj}	C_p	S	t_m Zone2,3 $[s]$	Q/N $[mL/r]$	$[I] \cdot Q_m$ $[wt\% \cdot mL]$
1	93.1	90.9	4.4	129.68			X
1	91.7	89.2	6.7	141.48	X		
2	93.2	90.4	6.0	133.15	X		X
2	93.2	90.3	6.2	133.82		X	X
3	93.8	90.5	7.0	132.94	X	X	X

Table B.2: As discussed in Section 6.3.1, this table shows the results from the preliminary best subsets regression for viscosity $[Pa \cdot s]$ versus $[I]$, N_m, Q_m, and other variables as noted above.

Var's	R^2	R^2_{adj}	C_p	S	t_m Zone2,3 $[s]$	Q/N $[mL/r]$	$[I] \cdot t_m$ $[wt\% \cdot s]$
1	92.9	90.8	5.8	130.78			X
1	91.7	89.2	8.1	141.48	X		
2	93.8	91.3	6.0	127.15	X		X
2	92.9	90.0	7.8	136.11		X	X
3	94.4	91.3	7.0	127.01	X	X	X

Table B.3: As discussed in Section 6.3.1, this table shows the results from the preliminary best subsets regression for viscosity $[Pa \cdot s]$ versus $[I]$, N_m, Q_m, and other variables as noted above.

Var's	R^2	R^2_{adj}	C_p	S	t_m Zone2,3 $[s]$	Q/N $[mL/r]$	$[I] \cdot Q/N$ $[wt\% \cdot mL/r]$
1	93.8	91.9	4.1	122.24			X
1	91.7	89.2	8.3	141.48	X		
2	94.1	91.6	5.6	124.56	X		X
2	93.8	91.3	6.1	127.05		X	X
3	94.4	91.4	7.0	126.50	X	X	X

Table B.4: As discussed in Section 6.3.1, this table shows the results from the preliminary best subsets regression for viscosity $[Pa \cdot s]$ versus $[I]$, N_m, Q_m, and other variables as noted above.

B.2 Regression Analysis

A regression was performed on the following equation.

$$\eta = -1134 - 17892[I] + 3.08N_m + 11.3Q_m - 19164[I]Q/N \qquad \text{(B.1)}$$

Predictor	Coefficient	s Coeff	t-value	P
Constant	-1134	1748	-0.65	0.528
$[I]$	-17892	10070	-1.78	0.099
N_m	3.084	2.347	1.31	0.212
Q_m	11.277	5.686	1.98	0.069
$[I] \cdot Q/N$	-19164	8416	-2.28	0.040

Table B.5: Regression Analysis Coefficient Significance for Equation B.1. The following values were also determined: $s = 122.2$, $R^2 = 93.8\%$, Adj.$R^2 = 91.9\%$.

Source	DF	SS	MS	F	P
Regression	4	2952937	738234	49.40	0.000
Residual Error	13	194256	14943		
Total	17	3147194			

Table B.6: Preliminary Analysis of Variance

Appendix C

MatLAB Code for System Identification

The code combines data from different runs to create data for estimation and data for validation. The "arxstruc" command is used to determine the best model for the ARX estimation. The ARX model is: A(q) y(t) = B(q) u(t-nk) + e(t). The "arx" command is then used to minimize the model for the selected model orders. Afterwards, a continuous time model is created from the discrete model.

```
%---------------------------
% Actual System ID
% Mark Wetzel provided Code and Assistance
% in this portion of the code
Ts=5;
fs=1/Ts;
for kk=1:5
    % make ident data set and validation data
    switch kk
    case 1
        disp('Q 30 N 210')
        eval(['datai=[data1r5;data2r5;data3r5];'])
```

```
    eval(['datav=[data13r5;data14r5];'])
case 2
    disp('Q 30 N 160')
    eval(['datai=[data5r5;data6r5];'])
    eval(['datav=[data4r5];'])
case 3
    disp('Q 30 N 320')
    eval(['datai=[data8r5;data9r5];'])
    eval(['datav=[data7r5];'])
case 4
    disp('Q 40 N 210')
    eval(['datai=[data11r5;data12r5];'])
    eval(['datav=[data10r5];'])
case 5
    disp(['Q 20 N 210 Not using the data16,',...
     ' it is not good.'])
    eval(['datai=[data17r5;data18r5;data19r5];'])
    eval(['datav=[data15r5];'])
end
% first use 2nd order model and find time delay, Td.
% Use all the data
n_delay_range = 1:floor(360/Ts); % Ts is 5s
io_data=[datai;datav];
V=arxstruc(io_data,io_data,struc(2,1,n_delay_range));
[nn,Vm] = selstruc(V,0);
```

```
n_delay=nn(3);
% Next use the ARX evaluator to compare models
% from 1st to 3rd order,
% with fixed time delay:
V = arxstruc(io_data,io_data,struc(1:3,1:2,n_delay));
[nn,Vm] = selstruc(V,0);
disp(sprintf('ARX Model Selected: Na (poles) = %d, ',...
 'Nb (num) = %d, Ndelay = %d',nn(1),nn(2),nn(3)))
na = nn(1);
n_poles = na;
nb = nn(2);
n_zeros = nb - 1;
n_delay = nn(3);
Td = n_delay*Ts;
disp(sprintf('Time Delay = %.1f sec. at %.2f ',...
 'samples/sec (Ts = %.1fsec)',Td,fs,Ts))
% Na = Number of POLES,
% Nb = Number of Coefficients in the Numerator!
na=3;
nb=1;
n_zeros = nb - 1;
n_poles = na;
disp(' ')
disp(' ')
disp('Final Model Selection Results:')
```

```
disp(' ')
disp(['Discrete ARX Model: Na (Den Poles) = ' num2str(na)',
  Nb ','(Num Coeffs) = ' num2str(nb) ', Sample Delay = '
  num2str(n_delay) ])
nn = [na nb n_delay];
th = arx(io_data,nn,[],Ts);
[num,den]=th2tf(th);
sysd=tf(num,den,Ts);
ysim=lsim(sysd,io_data.u);

% Continuous Time System Model:
% Build the Transfer Function
num_no_delay = num(n_delay+1:n_delay+nb);
% Get # Numerator Coeffs (1, 2, ...)
den_no_delay = den(1:na+1);
% Get # Coefficients = n_poles + 1 (2, 3, ...)
disp(' ')
disp('Discrete Transfer Function (No time delay):')
disp(' ')
sysd_no_delay=tf(num_no_delay,den_no_delay,Ts)
disp(' ')
hd = tf(num_no_delay,den_no_delay,Ts,'Variable','z^-1')
disp(' ')
tf_gain = dcgain(sysd);
disp(' ')
```

```
    disp(['Discrete-Time System DC Gain = ' ...
     num2str(tf_gain,6)])

    % Convert to a continuous-time model so we can do classical
    % systems analysis:
    sysc=d2c(sysd_no_delay,'zoh',Ts);
    disp(' ')
    disp('Selected Model Continuous Transfer Function H(s):')
    disp(' ')
    sysc
    disp(' ')
    num = sysc.num{1};
    den = sysc.den{1};
    A=den;
    B=num;
    tf_gain = dcgain(num,den);
    disp(['Continuous-Time System DC Gain Gp = ' ...
     num2str(tf_gain,6)])
    disp(['Time Delay Td = ' num2str(Td,4) ' seconds'])
    disp(' ')
end
%---------------------------
```

Appendix D

MatLAB Code for Deconvolving Signals.

The code optimizes parameters for functions to approximate the signal that is the deconvolution of on from another.

D.1 Curve Functions

This function is used for a 1^{st} order impulse response. curvefun1.m:

```
%---------------------------
function f=curvefun1(k,yt)
% this program is used with lsqcurvefit to determine the
% constants k ([gain;time delay]) that satisfy this
% model in the code
% delay time is k(2)
% k(1) is shape factor
% a*Heaviside(t-td)*exp(-a*(t-td))
st=yt-k(2);
f = (k(1)*exp(-k(1)*st))';
for m = 1:length(st)
```

```
if st(m) < 0
f(m) = 0;
end
end
%---------------------------
```

This function is used for a 2^{nd} order impulse response. curvefun12.m:

```
%---------------------------
function f=curvefun12(k2,yt,k1)
% this program is used with lsqcurvefit to determine the
% constants k ([gain;time delay]) that satisfy this model
% in the code
% delay time is k?(2)
% k?(1) is shape factor
% t>(td1+td2) => a1*a2*(1/(-a1+a2)*Heaviside(t-td)*exp(-a1*(t-td))
%                      -1/(-a1+a2)*Heaviside(t-td)*exp(-a2*(t-td)))
a1=k1(1);
a2=k2(1);
td=k1(2)+k2(2);
st=yt-td;
f = a1*a2*(1/(-a1+a2)*exp(-a1*st)-1/(-a1+a2)*exp(-a2*st));
for m = 1:length(st)
if st(m) < 0
f(m) = 0;
end
end
```

```
%---------------------------
```

This function is used for a 3^{rd} order impulse response. curvefun123.m:

```
%---------------------------
function f=curvefun123(k3,yt,k1,k2)
% this program is used with lsqcurvefit to determine the
% constants k ([gain;time delay])
% that satisfy this model in the code
% delay time is k?(2)
% k?(1) is shape factor
% a1*a2*a3*(1/(-a1+a2)/(-a1+a3)*Heaviside(t-td)*exp(-a1*(t-td))
% -1/(a3-a2)/(-a1+a2)*Heaviside(t-td)*exp(-a2*(t-td))
% +1/(-a2*a3+a1*a2-a1*a3+a3^2)*Heaviside(t-td)*exp(-a3*(t-td)))

a1=k1(1);
a2=k2(1);
a3=k3(1);
td=k1(2)+k2(2)+k3(2);
st=yt-td;
f = a1*a2*a3*(exp(-a1*st)/(-a1+a2)/(-a1+a3) ...
    -exp(-a2*st)/(a3-a2)/(-a1+a2) ...
    +exp(-a3*st)/(-a2*a3+a1*a2-a1*a3+a3^2));
for m = 1:length(st)
if st(m) < 0
f(m) = 0;
end
```

```
end
%--------------------------
```

This function is used for a 3^{rd} order step response. curvefun123step.m:

```
%--------------------------
function f=curvefun123step(k3,yt,k1,k2)
% This is for a step response for G123 pp19 lab notebook
% this program is used with lsqcurvefit to determine the
% constants k ([gain;time delay])
% that satisfy this model in the code
% delay time is k?(2)
% k?(1) is shape factor
% f(t)=0 t<td

a1=k1(1);
a2=k2(1);
a3=k3(1);
td=k1(2)+k2(2)+k3(2);
st=yt-td;
f = a1*a2*a3*(1/(a1*a2*a3) ...
    -exp(-a1*st)/a1/(a2-a1)/(a3-a1) ...
    +exp(-a2*st)/a2/(a2-a1)/(a3-a2) ...
    -exp(-a3*st)/a3/(a1*a2-a2*a3+a3^2-a3*a1));
for m = 1:length(st)
if st(m) < 0
f(m) = 0;
```

```
end
end
%--------------------------
```

D.2 Deconvolution

From deconvol.m:

```
%--------------------------
%%%%%%%%%%%%%%%%%%%%%%%%%%%%%%%%%%%%%%%%%%%%%%%%
% determine 1st order models for each section
%%%%%%%%%%%%%%%%%%%%%%%%%%%%%%%%%%%%%%%%%%%%%%%%
NN=12;
for nn=1:NN
    eval(['L=length(OP' num2str(nn) '(:,1));']);
    t=0:0.05:0.05*(L-1);
    % determine parameters for 1st order fit
    % to melt section
    switch nn
    case 1
        LB=[0.2;7.5];
        UB=[];
    case 5
        LB=[0.05;6.5];
        UB=[0.4;10];
    case 6
```

```
    LB=[0.3;4.5];
    UB=[];
case 8
    LB=[0.1;5];
    UB=[0.3;10];
case {9,10,11}
    LB=[0.1;5];
    UB=[0.45;10];
otherwise
    LB=[0.05;1];
    UB=[];
end
eval(['K1=lsqcurvefit(''curvefun1'',rtdcons(:,1,nn),t,OP'...
 num2str(nn) '(:,1),LB,UB);']);
% determine parameters for 1st order fit to mix section
eval(['K2=lsqcurvefit(''curvefun12'',(K1+[0.05;5]),t,OP'...
 num2str(nn) '(:,2)'',[],[],[],K1);']);
% determine parameters for 1st order fit to metering section
eval(['K3=lsqcurvefit(''curvefun123'',(K2+[0.05;5]),t,OP'...
 num2str(nn) '(:,3)'',[],[],[],K1,K2);']);
rtdcons_paulfit(:,:,nn)=[K1 K2 K3];
% plot output
y1=curvefun1(K1,t);
y12=curvefun12(K2,t,K1);
y123=curvefun123(K3,t,K1,K2);
```

```
    figure(nn)
    eval(['plot(t,y1,t,y12,t,y123,t,OP' num2str(nn)...
     '(:,1),t,OP' num2str(nn) '(:,2),t,OP'...
     num2str(nn) '(:,3));']);
    legend('1st order model',...
      '2nd order model, different poles and delays',...
          '3rd order model, different poles and delays',...
          'filtered data 1','filtered data 2',...
          'filtered data 3')
    xlabel('t [s]');
    ylabel('Normalized Response')
    Title(['Fit using 1st order models for each zone. Q = '...
      num2str(Q(nn))'; N = ' num2str(N(nn)) '; Date = '...
      num2str(m(nn)) '/' num2str(d(nn))  '/'...
      num2str(y(nn))]);
    orient landscape
    print('-depsc2','-tiff','-r300',['paulfit_q'...
     num2str(Q(nn)) 'n' num2str(N(nn)) 'rtd_m'...
     num2str(m(nn)) 'd' num2str(d(nn)) '.eps'])
    delete(nn)
    clear y1 y12 y123 t L
end
%--------------------------
```

Appendix E

LabVIEW Virtual Instrument

These are images of the LabVIEW virtual instrument used for the closed loop controller.

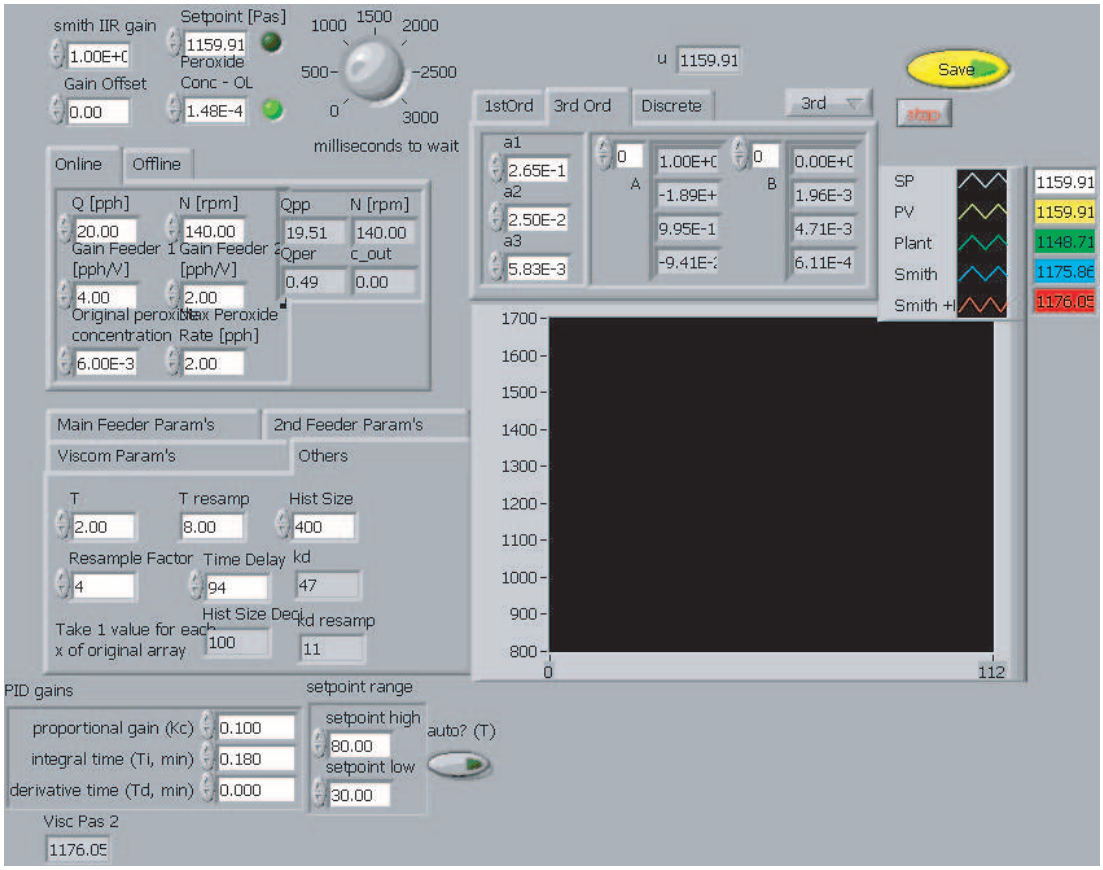

Figure E.1: The LabVIEW virtual instrument front panel.

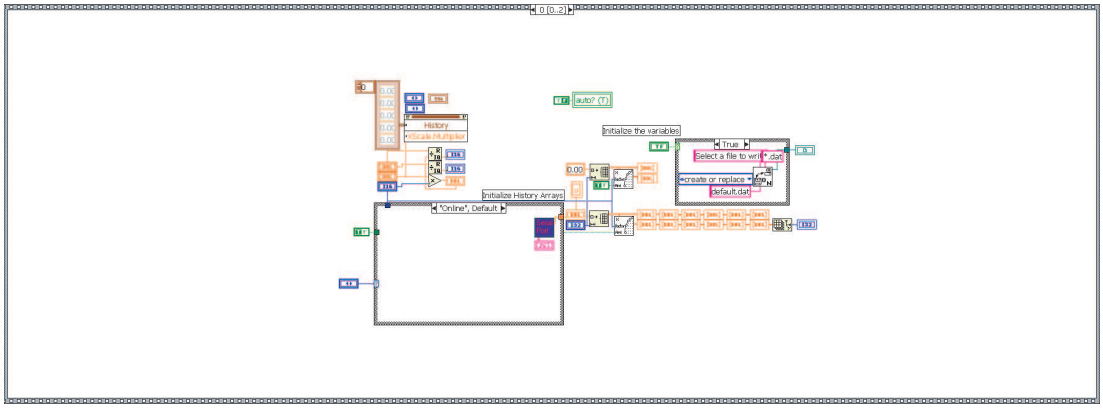

Figure E.2: The LabVIEW virtual instrument back panel initial iteration.

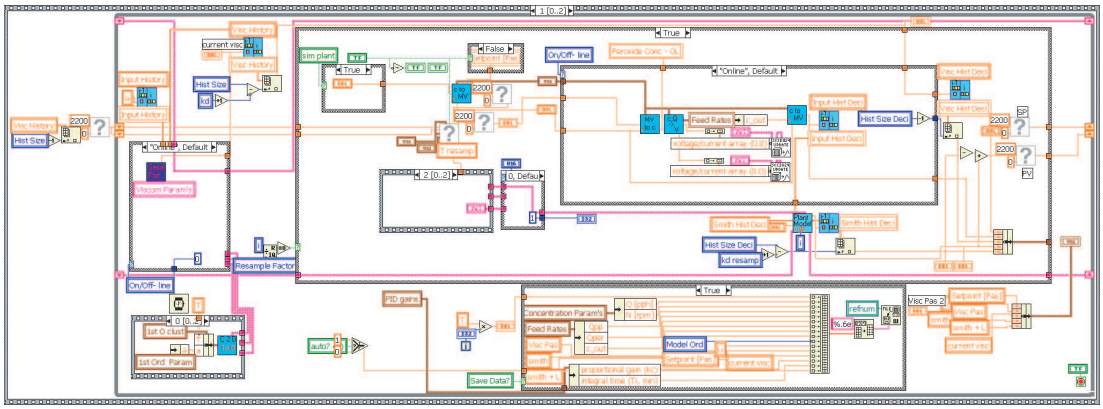

Figure E.3: The LabVIEW virtual instrument back panel general iteration.

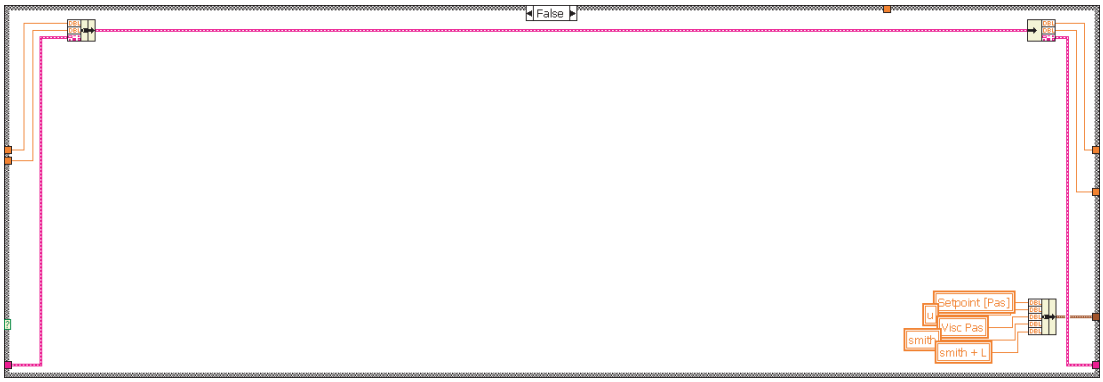

Figure E.4: The LabVIEW virtual instrument back panel general iteration sub-panel.

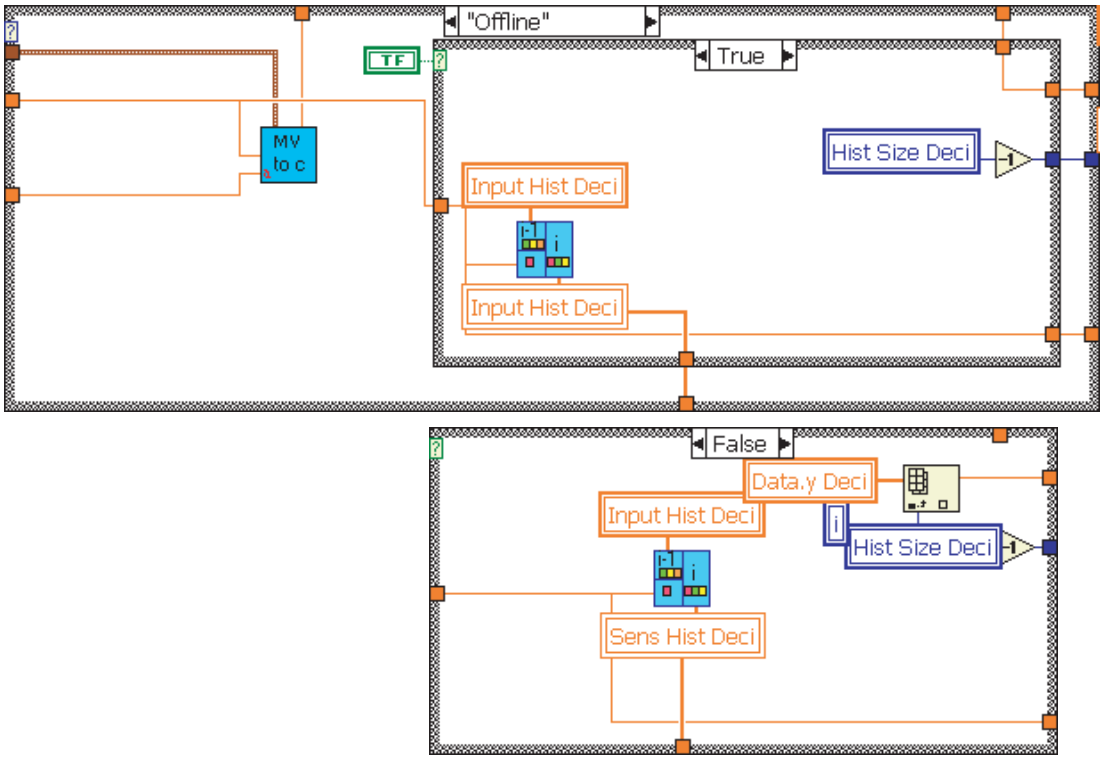

Figure E.5: The LabVIEW virtual instrument back panel general iteration sub-panels.

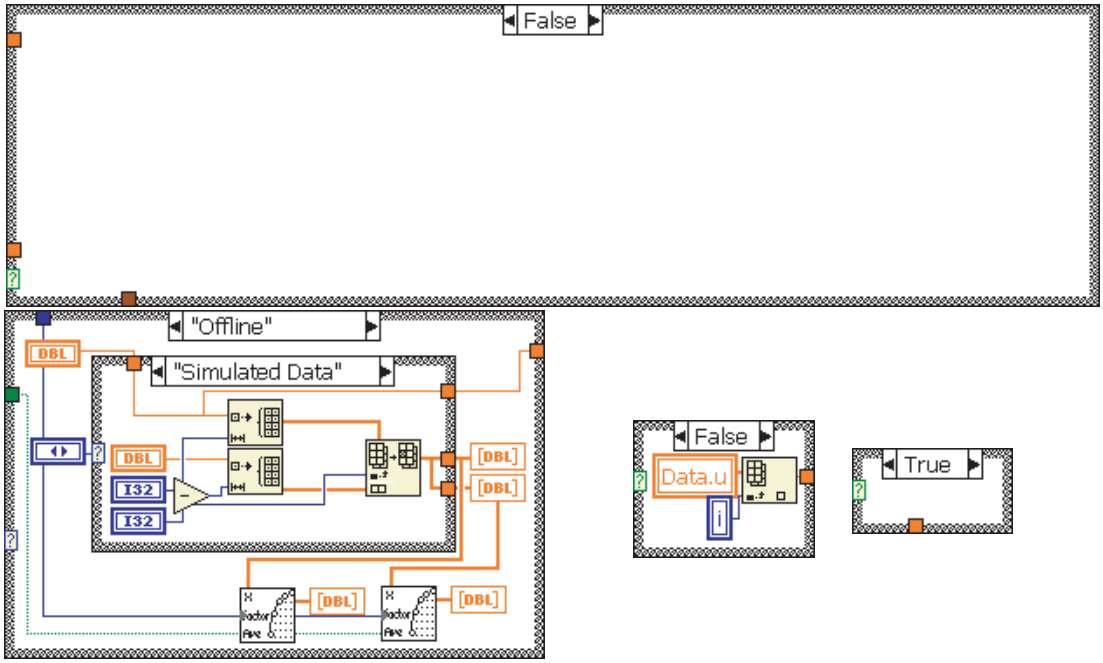

Figure E.6: The LabVIEW virtual instrument back panel general iteration sub-panels.

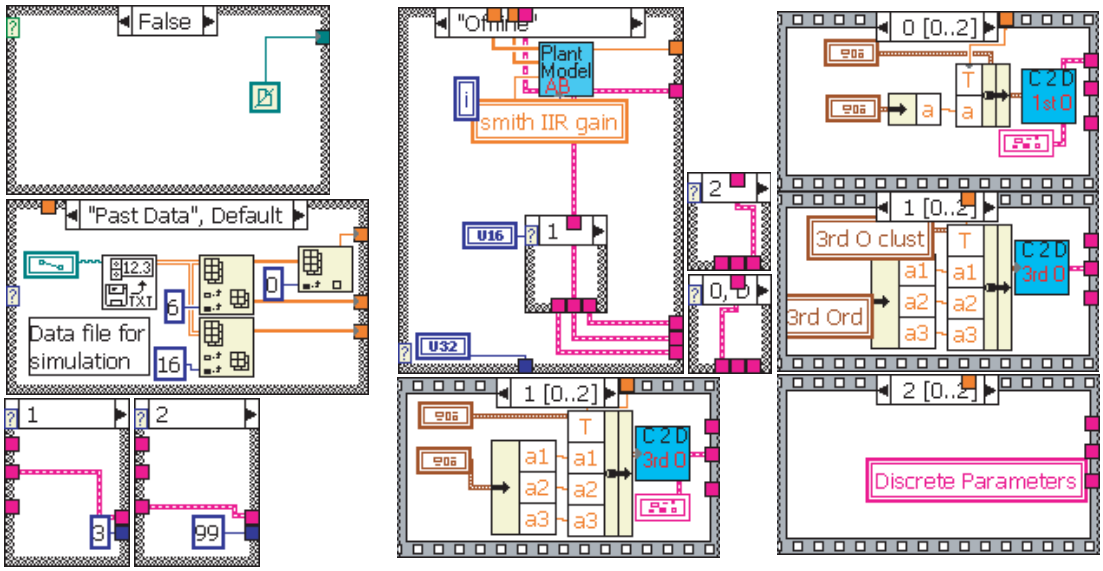

Figure E.7: The LabVIEW virtual instrument back panel general iteration sub-panels.

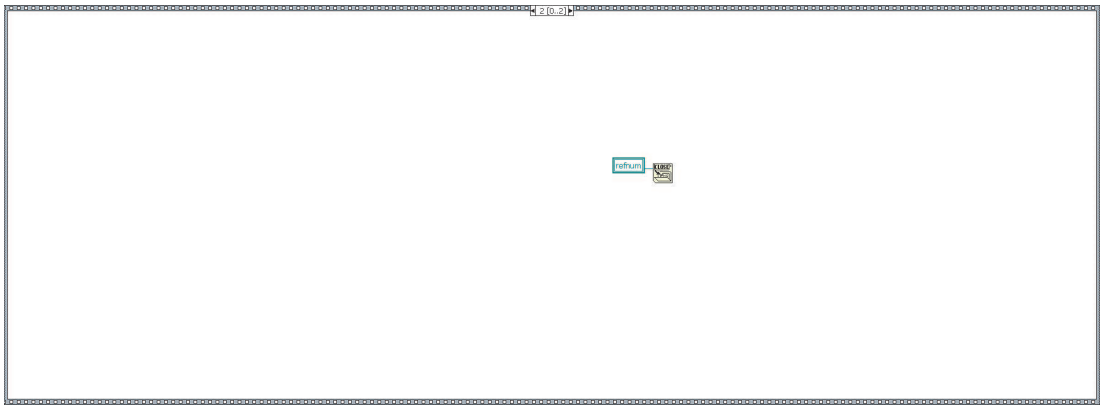

Figure E.8: The LabVIEW virtual instrument back panel final iteration.

Appendix F

Warp Time Simulation Code

F.1 Main Code

The main warp time code, `WarpTime_Solver_0_3.m`:

```
% WarpTime_Solver
% Given, the appropriate Q,N, and I, the solver
% will determine the best
% alpha to match Mn, Mw, Mz
% This program uses WarpTime_0_6.m
% After that it will calculate the Mn, Mw, Mz, and
% viscosity for a multitude of conditions
% This is done using data from PDC_1277


%known conditions
MnMwMz_k = [25165   83593   215343;
            26559   82174   222177;
            27482   85598   188003;
            27591   81814   175959;
```

```
            36876   107580  213375];
Q_k=[20;20;20;20;20];
N_k=[210;140;140;140;140];
I_k=[1.5e-4;0;1.5e-4;2e-4;2.5e-4];
MV_k=[1109 1341 1153 1090 1027];
zone=234;
tc= 5.4;%Luperox 101 1/2 life [s]

% solve for alpha
%  -7.9839e-004
warning off MATLAB:divideByZero
alpha_guess=[-0.0221 -0.0026 -0.0026 -0.0028 -7.8149e-004];
% these are also the results of the optimization.

for ii=1:5
    temp = [Q_k(ii) N_k(ii) I_k(ii) zone tc];
    alpha(ii)=lsqcurvefit(@WarpTime_0_6,alpha_guess(ii),...
     temp,MnMwMz_k(ii),[-3],[0])
end

% Statistical EQ for MV:
% QN=Qpph*456/rho/3600/(Nrpm/60);
% Qm=151.92+85.207*QN;
% MV = x1 + x2*Qm + x3*c*QN + Offset;
```

```
% alpha = -7.8150e-004 is indicative of 20--140
% plot MV vs. I
plot(I_k(2:5),MV_k(2:5));
plot(MnMwMz_k(2:5,1),MV_k(2:5),MnMwMz_k(2:5,2),MV_k(2:5),...
MnMwMz_k(2:5,3),MV_k(2:5));
plot(MnMwMz_k(2:4,3),MV_k(2:4));
% from this graph, MV = 0.0054*Mz + 130.58

% Determine MV's for different c's
c = 0 : 0.1e-4 : 3.1e-4;
II = length(c);
for ii = 4:II
    temp = [20 140 c(ii) 234 tc];
    [tmp_a,tmp_b,tmp_c]=WarpTime_0_6(alpha_guess(3),temp);
    MV(ii) = 0.0054*tmp_c + 130.58;
end



temp = [20 140 1.5e-1 234 tc];
[tmp_a,tmp_b,tmp_c]=WarpTime_0_6(-1,temp)
temp = [20 140 2.5e-1 234 tc];
[tmp_a,tmp_b,tmp_c]=WarpTime_0_6(alpha_guess(3),temp)
```

F.2 Supporting Code

The warp time code, `warpfunc_0_3.m`:

```
%-----------------------------------------
function  [phi_out,x_out,xi_w]=warpfunc_0_3(phi_0,x_0,...
del_t,stretch,alpha,tc,prx_nod)
% A function that returns the distribution for vis breaking of PP
% Based on code from warptime.m
% phi_0     := original concentraion distribution, it has four
%              rows for I, Q0,Q1, Q2
% x_0       := initial position array
% del_t     := amount of time to warp and mix
% stretch   := type of stretching: 'lin', 'exp'
% alpha     := stretching constant

if strcmp(stretch,'lin')
    str=1;
else
    str=2;
end
x = x_0;
tr = [1 0];
R = 0;
N=length(x_0); % number of nodes
t_step=del_t;
t_total=del_t;
t_warp(1,:)=zeros(1,N);
for i=2:(ceil(t_total/t_step)+1)
```

```
   t_warp(i,:)=t_step*(i-1)*ones(1,N);
   [theta_w,xi_w]=tx2thxi(t_warp(i,1),0.5,alpha,1,tc);
%    x(i,:)=x(i-1,:)*xi_w;
   x(i,:)=x(1,:)*xi_w;
%    x(1,N)
%    x(2,N)
%    xi_w/2
   for ii=1:4 %ii=1 means peroxide, ii>1 means Q
% j='warpfunc'
       [theta_temp, phitemp] = ode15s(...
        @finitediffdiffus_PRX_0_3,...
        [0 theta_w],phi_0(ii,:),[],x(i,:),...
        R,tr,prx_nod,ii,xi_w);
       phi(ii,:) = phitemp(size(phitemp,1),:);
       clear phitemp
   end
end

% Remake Vectors
i=length(x(:,1));
phi_out = phi;
x_out = x(i,:);
%-----------------------------------------
```

The warp time code, `WarpTime_0_6.m`:

```
%-----------------------------------------
```

```
function [Mn, Mw, Mz] = WarpTime_0_6(alpha,QNPerox_conczonetc);
% Function for determining the distribution
% Initial Parameters
% Prop's of materials
I_0 = 2.9266;   % page 10 Notebook 2
Q0_0 = 130.8491;    % from MolMoments.m
Q1_0 = 1.5992e5;
Q2_0 = 1.2920e9;
Q_0=[I_0; Q0_0; Q1_0; Q2_0];
%% tc = 1;             % characteristic time

% Operating Condition parameters
%% Q = 30;             % pph
%% N = 210;            % rpm
% Calculation of Alpha factor for stretching
% Circumference is 0.03m
% Velocity of screw tip is pi*D*N/60
%% alpha=-pi*0.03*N/60;
Q=QNPerox_conczonetc(1);
N=QNPerox_conczonetc(2);
Perox_conc=QNPerox_conczonetc(3);
zone=QNPerox_conczonetc(4);
tc=QNPerox_conczonetc(5);

% make initial distribition
```

```
% variable grid, half the distribution see p 13 notebook13
nodes=200;
[phi_o,x_o,prx_nod]=vargrid(Q_0,Perox_conc,nodes);

t = PDC1277t_res(Q,N,zone);
% up to here works.

% Apply Residence Time To Warp Time Calculation
[phi, x, xi_w]=warpfunc_0_3(phi_o,x_o,t,'lin',alpha,tc,prx_nod);
% plot(x_o,phi_o,x,phi)
% j='warptime_0_6'
Q=varmean_03(phi,x,xi_w);

Q=mean(phi,2); % Q0 is Q(2), etc. because Q(0) is I
% max(x)
% Q-(1-Perox_conc)*Q_0
m_0 = 42.08; %C3H6
Q_0 = Q(2);
Q_1 = Q(3);
Q_2 = Q(4);
Q_3=2 * Q_2/(Q_1*Q_0) * (2*Q_2*Q_0-Q_1^2);
MnMwMz(1) = m_0 * Q_1/Q_0;
MnMwMz(2) = m_0 * Q_2/Q_1;
MnMwMz(3) = m_0 * Q_3/Q_2;
Mn = MnMwMz(1);
```

```
Mw = MnMwMz(2);
Mz = MnMwMz(3);
%-----------------------------------------
```

The warp time code, `varmean_03.m`:

```
%-----------------------------------------
function Q = varmean_03(phi,x,xi_w)
% function to calculate averages from variable grid
nodes = length(x);xi_w
%determine differences, and then multiply by concentration,
% then divide by
%xi_w sort of Trapezoidal rule.

for ii= 1 : (nodes-1)
    h(ii) = x(ii+1)-x(ii);
end

% determine avg phi for a pair of nodes using linear
% approximation.
% each row of phi is a different species
for ii=1 : (nodes-1)
    avg_phi(:,ii) = ( phi(:,ii+1) + phi(:,ii) ) / 2;
end

% for jj = 1 : 4
%     Q(jj) = mean( h .* avg_phi(jj,:) );
```

```
% end


for jj=1:4
    Q(jj) = sum(h .* avg_phi(jj,:)) / (xi_w/2);
end
%-----------------------------------------
```

The warp time code, `tx2thxi.m`:

```
%-----------------------------------------
function [theta,xi]=tx2thxi(t,x,alpha,type,tc)
%type=1 constant stretching
%type=2 exponential stretching
%type=3 logarythmic stretching
if type<4 & type>0
    if type<2 %type 1
        theta=(exp(2*alpha*t)-1)/(2*alpha*tc);
        xi=x*exp(alpha*t);
    elseif type<3 %type 2
        xi=x*exp(1)/exp(exp(t));
        syms th;
        S=exp(2*exp(th));
        theta=subs(int(S,th,0,t)/(tc*exp(2)));
    else %type 3
        xi=x*(t^(-t))*exp(t);
        syms th;
        S=th^(2*th)/exp(2*th);
```

```
        N=150;
        tht=linspace(0,t,N);
        th=tht(1);
        thti(1)=subs(S);
        theta=0;
        for i=2:150
            th=tht(i);
            thti(i)=subs(S);
            theta=theta+tht(2)*(thti(i)+thti(i-1))/2;
        end
        theta=theta/tc;

        %int function does not work.
    end
end
%-----------------------------------------
```

The warp time code, `finitediffdiffus_PRX_0_3.m`:

```
%-----------------------------------------
function dphidtau=finitediffdiffus_PRX_0_3(tau,phi,...
x,R,tr,prx_nod,ii,xi_w)
% reflective BC's, no flux at boundaries.
% for irregular grid
% Assume infinite reaction plane, so peroxide does not exist
% where there is Q, and vice-versa
% ii=1 means peroxide
```

```
% tr1=tr(1);


% tr2=tr(2);


% tr1=tc/td
% tr2=tc/tr
nodes=max(size(phi));
N=nodes;
dphidtau=zeros(N,1);
dxi=1/(N-1);
if prx_nod ~= 0
    switch ii
    case 1 % Peroxide
        phi((prx_nod+1):nodes) = zeros(1,(nodes-prx_nod));
    otherwise % Q_x
        phi(1:prx_nod) = zeros(1,prx_nod);
    end
end
% j='finitediff'
for ii=1:N-1 % The index is one higher then the actual index.
    h(ii) = x(ii+1) - x(ii);
end
h(N) = xi_w - x(N);
h_0=h(N);
```

```
dphidtau(1,1)=((phi(2)-phi(1))/h(1)) * (h(1)+h_0)/2;
for i=2:(N-1)
    dphidtau(i,1)=((phi(i+1)-phi(i))/h(i) - ...
     (phi(i)-phi(i-1))/h(i-1)) * (h(i)+h(i-1))/2;
end
dphidtau(N,1)=( -(phi(N)-phi(N-1))/h(N-1) ) * (h(N)+h(N-1))/2;
if prx_nod ~= 0
    switch ii
    case 1 % Peroxide
        dphidtau((prx_nod+1):nodes,1) = zeros(1,(nodes-prx_nod))';
    otherwise % Q_x
        dphidtau(1:prx_nod,1) = zeros(1,prx_nod)';
    end
end
%-----------------------------------------
```

The warp time code, `vargrid.m`:

```
%-----------------------------------------
function [phi_o,x_o,prx_nod]=vargrid(Q_0,Perox_conc,nodes)
% make initial distribition
% variable grid, half the distribution see p 13 notebook13
I_0 = Q_0(1);
Q0_0 = Q_0(2);
Q1_0 = Q_0(3);
Q2_0 = Q_0(4);
if Perox_conc == 0
```

```
    x_o = 0 : (1/nodes) : (nodes-1)*(1/nodes);
    phi_o(1,:)=zeros(1,nodes);
    for ii = 2:4
        phi_o(ii,:) = Q_0(ii) .* ones(1,nodes);
    end
    prx_nod = 0;
else
    prx_cutoff = 0.5 * Perox_conc;
    nodes_I = 0.4 * nodes;
    nodes_Q = nodes - nodes_I;
    for ii = 1:nodes_I
        h_i(ii) = log(2 + nodes_I - ii);
    end
    h_i = h_i / sum(h_i) * prx_cutoff;
    for ii = 1:nodes_Q
        h_q(ii) = log(ii+1);
    end
    h_q = h_q / sum(h_q) * (0.5 - prx_cutoff);
    h = [h_i h_q];
    x_o(1) = 0;
    for ii = 2:nodes
        x_o(ii) = x_o(ii-1)+h(ii);
    end
    prx_nod = nodes_I;
    phi_o = zeros(4,nodes);
```

```
    phi_o(1,1:prx_nod) = I_0 * ones(1,prx_nod);
    phi_o(2,(prx_nod+1):nodes) = Q0_0 * ones(1,(nodes-prx_nod));
    phi_o(3,(prx_nod+1):nodes) = Q1_0 * ones(1,(nodes-prx_nod));
    phi_o(4,(prx_nod+1):nodes) = Q2_0 * ones(1,(nodes-prx_nod));
end
%-----------------------------------------
```

BIBLIOGRAPHY

[1] Gregory Walsh, David Bigio, Jun Gao, and Paul Elkouss. Viscosity regulation for polymer extruders. In *SPE ANTEC Papers*, 2000.

[2] M. Costin, P. Taylor, and J. Wright. On the dynamics and control of a plasticating extruder. *SPE ANTEC Papers*, 22(17):1095–1106, Mid-December 1982.

[3] A. Pabedinskas, W.R. Cluett, and S.T. Balke. Process control for polypropylene degradation during reactive extrusion. *Polymer Engineering and Science*, 29(15):993–1003, Mid-August 1989. ISSN 0032-3888.

[4] A. Pabedinskas and W.R. Cluett. Controller design and performance analysis for a reactive extrusion process. *Polymer Engineering and Science*, 34(7): 585–597, Mid-April 1994. ISSN 0032-3888.

[5] T.O. Broadhead, W.I. Patterson, and J.M. Dealy. Closed loop viscosity control of reactive extrusion with an in-line reometer. *Polymer Engineering and Science*, 36(23):2840–2851, Mid-December 1996.

[6] Costas Tzoganakis, J. Vlachopoulos, and A. E. Hamielec. Production of controlled-rheology polypropylene resins by peroxide promoted degradation during extrusion. *Polymer Engineering and Science*, 28(3):170–180, Mid-February 1988. ISSN 0032-3888.

[7] A. Pabedinskas, W.R. Cluett, and S.T. Balke. Modeling of polypropylene degradation during reactive extrusion with implications for process control. *Polymer Engineering and Science*, 34(7):598–612, Mid-April 1994. ISSN 0032-3888.

[8] P. V. Danckwerts. Continuous flow systems distribution of residence time. *Chemical Engineering Science*, 2, 1953.

[9] M. Wetzel, C. Shih, and U. Sundararaj. In *SPE ANTEC Papers*, volume 3, page 3707, 1997.

[10] J.P. Puaux, G. Bozga, and A. Ainser. Residence time distribution in a corotating twin-screw extruder. *Chemical Engineering Science*, 55(9):1641–1651, May 2000.

[11] Glenn E. Gasner, David Bigio, and Charles Marks. A new approach to analyzing residence time and mixing in a co-rotating twin screw extruder. *Polymer Engineering and Science*, 39(2):286–298, February 1999. ISSN 0032-3888.

[12] Jun Gao, David Bigio, Gregory Walsh, and Mark Wetzel. Residence time analysis for twin screw extruders. In *SPE ANTEC Papers*, 1999.

[13] Paul Elkouss, David Bigio, Gregory Walsh, and Paul Andersen. Mean residence time characterization in co-rotating twin screw extruder: Screw configuration comparison. In *SPE ANTEC Papers*, 2000.

[14] Jun Gao, Gregory Walsh, David Bigio, Robert Briber., and Mark Wetzel. Mean residence time analysis for twin screw extruders. *Polymer Engineering and Science*, 40(1):227–237, 2000.

[15] Jun Gao, Gregory Walsh, David Bigio, Robert Briber., and Mark Wetzel. Residence-time distribution model for twin-screw extruders. *AICHe Journal*, 45(12):2541–2549, 1999.

[16] Paul F. Elkouss. Pressure drag flow equilibrium model : a physics based approach to determining filled volumes within a corotating twin screw extruder. Master's thesis, University of Maryland, 2000.

[17] David Strutt, Costas Tzoganakis, and Thomas A. Duever. Mixing analysis of reactive polymer flow in a single-screw extruder channel, April 2000. ISSN 0032-3888.

[18] F. Berzin, B. Vergnes, P. Dufossé, and L. Delamare. Modeling of peroxide initiated controlled degradation of polypropylene in a twin screw extruder. *Polymer Engineering and Science*, 40(2):344–356, February 2000.

[19] J.M. Ottino. *The Kinematics of Mixing: Stretching, Chaos, and Transport*. Cambridge University Press, 1989.

[20] J. Gao. *Control of Polymer Extruders*. PhD thesis, University of Maryland, 2000.

[21] *Minitab Documentation*. Minitab Inc., 2000.

[22] R. Gendron, L. E. Daigneault, J. Tatibout, and M.M. Dumoulin. Residence time distribution in extruders determined by in-line ultrasonic measurements. *Advances in Polymer Technology*, 15, 1996.

[23] T. Chen, W. I. Patterson, and J. M. Dealy. On-line measurement of residence time distribution in a twin screw extruder. In *International Polymer Processing X*, volume 1, page 3, 1995.

[24] C. W. Macosko. *Rheology: Principles, Measurements & Applications*. Wiley-VCH Publishers, 1994.

[25] J. M. Dealy and K. F.Wissbrun. *Melt Rheology and its Role in Plastics Processing: Theory and Applications*. Van Nostrand Reinhold, 1990.

[26] Fernando Muzzio, Jeffrey Zalc, and Paul Elkouss. In *Personal communications*, 1997.

Index

Berzin et al. [2000], 9, 14, 219

Broadhead et al. [1996], 2, 3, 14, 15, 217

Chen et al. [1995], 96, 219

Costin et al. [1982], 2, 12, 15, 217

Danckwerts [1953], 5, 76, 218

Dealy and F.Wissbrun [1990], 109, 220

Elkouss et al. [2000], 6, 7, 96, 218

Elkouss [2000], 7, 14, 219

Gao et al. [1999], 6, 14, 30, 37, 64, 218

Gao et al. [2000], 6, 7, 64, 77, 96, 158, 218

Gao [2000], 12, 15, 29, 219

Gasner et al. [1999], 6, 14, 218

Gendron et al. [1996], 78, 219

Macosko [1994], 103, 219

Muzzio et al. [1997], 111, 220

Ottino [1989], 10, 111, 219

Pabedinskas and Cluett [1994], 2, 3, 13, 15, 217

Pabedinskas et al. [1989], 2, 13, 15, 217

Pabedinskas et al. [1994], 2, 9, 14, 217

Puaux et al. [2000], 5, 14, 218

Strutt et al. [2000], 8, 14, 219

Tzoganakis et al. [1988], 2, 8, 9, 12, 14, 109, 117, 217

Walsh et al. [2000], 1–3, 9, 11, 12, 14, 15, 62, 77, 217

Wetzel et al. [1997], 5, 78, 218

min [2000], 41, 219

Controller

PID, 152

Gain

Function, 126, 127

RRD

Transforms, 65

RTD

3^{rd} Order Model, 65, 67

n^{th} Order Model, 64

First Order Model, 64

Model, 30

RVD

n^{th} Order Model, 65

Transforms, 65

System Identification

MatLAB Code, 186

Warp Time Model

Derivation, 112

Stretching, 111